Provenance of sediments in the Faroe-Shetland Basin: Characterisation of possible source components in Southeast Greenland

KRISTINE THRANE AND NYNKE KEULEN

Geological Survey of Denmark and Greenland, Øster Voldgade 10, 1350 København

*Corresponding author: kt@geus.dk, +4538142050

Abstract

Previous studies provide conflicting predictions concerning the source of the sediment deposited in the Faroese and British sectors of the Faroe-Shetland Basin. Some studies suggested that the sediment was derived from the UK margin, while other studies point to a Greenlandic source. To test this, we investigated samples from Southeast Greenland between Kangerlussuaq and Timmiarmiut, to assess this area as a source region. U-Pb ages of detrital zircons, compositional data of the heavy mineral suite and garnets have been obtained from stream sediment and till samples. The radiometric age pattern of the zircons change from north to south, with a dominant age range from 2900-2700 Ma. The overall age signature for Southeast Greenland is thus markedly different from that of the samples from the drill cores in the Faroese and British sector, making it unlikely that this part of Greenland was the source for the sediment in the Faroe-Shetland basin. An alternative source exists in central East and North-East Greenland where suitable-aged source rocks with similar metamorphic history are known to occur. This potential source is more compatible with pollen records and sediment transport directions.

Faroe Islands Exploration Conference: Proceedings of 4th Conference.
Annales Societatis Scientiarum Færoensis Supplementum LXIV.

Introduction

Palaeogeographic reconstructions of the North Atlantic region at the end of the Mesozoic show that the pre-drift position of the Faroe Islands was located near the Greenlandic coast east of the area between Kangerlussuaq and Kap Gustav Holm in Greenland (Figure 1). During the Cretaceous, a number of basins formed in the North Atlantic region south of the Faroe Islands (e.g. Knott *et al.*, 1993). Field studies in the Kangerlussuaq area, where Cretaceous and Early Tertiary sediments outcrop in basins, indicate that Greenland played a role as a sediment supplier during the opening of the Northern Atlantic (Larsen, 1996, Larsen *et al.*, 2005; Nøhr-Hansen *et al.*, 2006)). Larsen (1996) suggested that large amounts of sediment bypassed the area that is currently outcropping near Kangerlussuaq and were deposited in basins southeast of that area.

A key issue for hydrocarbon exploration in the Faroese region is the understanding of sediment dispersal patterns and depositional systems in the Faroe-Shetland Basin prior to continental breakup in the Late Palaeocene to Early Eocene. Identification of sediment provenance is crucial for this goal. Location of the source areas places important constraints on sediment transport pathways and intrabasinal sand body distribution. Furthermore, the nature of the sediment source has important implications for the porosity and permeability characteristics of the deposited

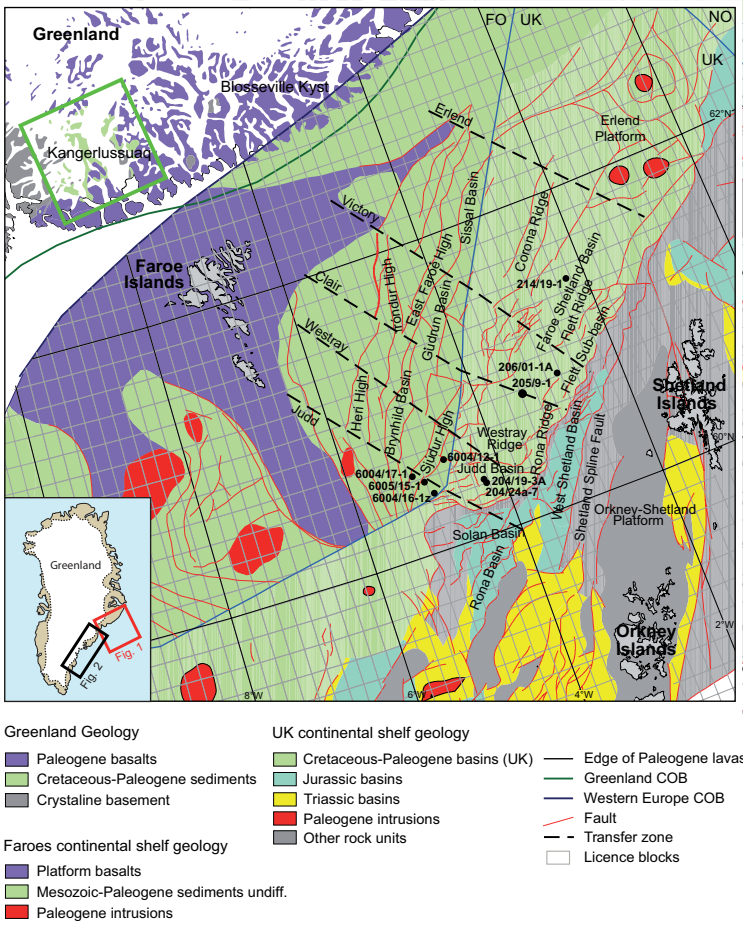

Figure 1
Overview map of East Greenland and the Faroe-Shetland region depicting the geographical position of the areas prior to the onset of seafloor spreading in the Late Palaeocene-Early Eocene. The positions of the Faroese and the British wells are shown (modified from Larsen *et al.*, 2005). The sample area in the Kangerlussuaq basin discussed in Figure 9 is show with a green box.

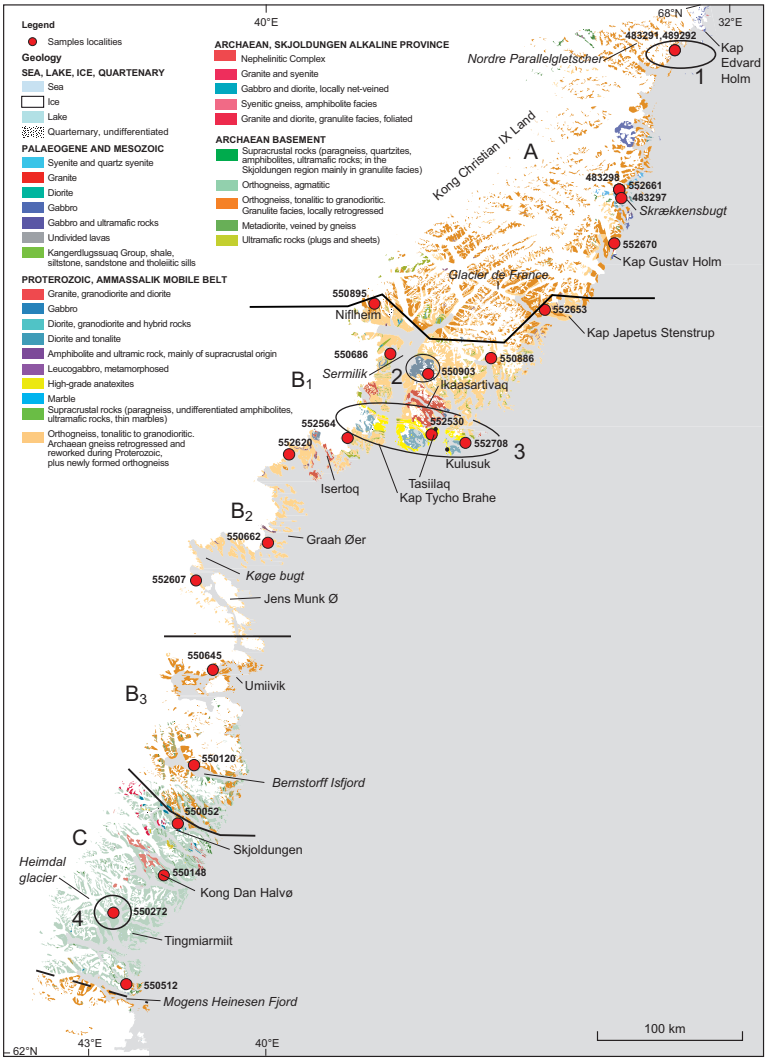

Figure 2
Geological map of South-east Greenland with sample localities of the sediment samples. The map is modified by T.F.D. Nielsen (pers. comm. 2010) after the three original 1:500 000 scale maps produced by the Geological Survey of Greenland (now Geological Survey of Denmark and Greenland, GEUS): Skjoldungen (Escher 1990), Kangerlussuaq (Myers *et al.*, 1988) and Sydgrønland (2nd edition, Garde, 2007). Division of the basement rocks in orthogneisses A, B1-B3, and C and sample areas 1-4, where orthogneisses are not the major rock type, are discussed in the text. (1) metasedimentary rocks, (2) Unnamed diorite intrusion, (3) Ammasslik Intrusive Complex, and (4) area with intensive retrogression.

sediments. Identified variations in source might also be used to establish correlation frameworks (at both local and regional scales) and can provide a basis for discrimination of individual sand bodies.

Frei *et al.* (2005a, b) demonstrated that the sedimentary successions from the British part of the Faroe-Shetland Basin and from the Kangerlussuaq area (East Greenland) have distinct, different signatures with respect to detrital U-Pb zircon age distributions and heavy mineral suite composition. The detrital zircon age distribution and the bulk rock geochemistry of the sedimentary successions drilled in the Faroese sector have been investigated by Frei and Knudsen (2008). The results from the UK and the Faroese sector are very similar. However, the full potential of the results and a reconstruction of the sediment supply history to the Faroe-Shetland basin are only realised if the provenance sensitive signatures in all possible source areas are sufficiently well constrained.

Determination of the provenance sensitive signatures is especially difficult for the East Greenlandic source, where the major part of the potential source area is covered by the Inland Ice and is not amenable to sampling. In this project we constrain the provenance signatures of the potential sediment source areas south of Kangerlussuaq. These data will significantly contribute to our understanding of the provenance characteristics of the southeast Greenland source and may give new information on provenance changes across major structural lineaments identified in the area (Karson and Brooks 1999). It will, therefore, make a significant contribution to a more coherent framework for the interpretation of the sediment supply history to the Faroe-Shetland basin and the correlation of sediment units across the basin based on sedimentary provenance characteristics.

Materials

We processed 4 tillite samples and 19 stream sediment samples from streams that drain basement rocks in Southeast Greenland between 62-68°N (Fig. 2). A stream sediment sample is a volume of recently deposited sediment from a minor stream with a local catchment area. Sand in stream sediment samples is related to the local bedrock geology in an area, while reworking of glacial material and the change in composition of the sand due to sedimentary processes only plays a minor role (Kalsbeek *et al.*, 1974). Thus, as long as streams do not directly drain moraine deposits, their sediments are a good way to describe the local geology.

Methods

Zircon provenance by LA-SF-ICPMS

Zircons from the stream sediment samples were separated using the Wilfley table. The zircons were handpicked and mounted in epoxy and polished to expose a central cross section of each grain. Pictures were taken of the different samples in a scanning electron microscope such that the individual grains can be located and identified. Prior to loading the mount into the instrument, it is cleaned with ethanol to remove surface Pb contamination.

All U-Pb age determinations reported in this study were done at GEUS in Copenhagen, Denmark. The analyses were done in situ using a ThermoScientific Element2 Sector Field Inductively Coupled Plasma Mass Spectrometer (SF-ICP-MS) coupled to a New Wave Research®/ Merchantek® UP213 laser ablation unit that is equipped with a frequency quintupled ND-YAG laser (wavelength of 213 nm). The methods applied essentially follow those of Gerdes and Zeh (2006) and Frei and Gerdes (2009).

All data were acquired using a 30 μm diameter single spot and an ablation time of 30 s. The depth of the ablation craters is approximately 15-20 μm. It is primarily the cores, which are analysed, but if the zircons have large rims, these can also be analysed. The GJ-1 zircon (Jackson *et al.*, 2004) was used as primary standard. Samples were analysed in sequences where an initial six standards are followed by ten samples, then three standards, followed by ten samples, three standards, etc.

The raw data was corrected for instrumental mass bias and laser-induced U-Pb fractionation through normalization to the GJ-1 zircon using our in-house software ZIRCHRON. Data evaluation and presentation is done in Excel spread sheets and take advantage of IsoplotEx v. 3.0 (Ludwig, 1999) and AgeDisplay (Sircombe, 2004).

Modal heavy mineral analysis by Computer-controlled scanning electron microscopy (CCSEM)

The sediment samples were washed and sieved to obtain the 45-500 micrometer fraction. A heavy mineral separate of the sample was collected by putting the sample through bromoform (ρ = 2.9 g/cm^3). Approximately 1 g of heavy mineral concentrate was mounted in epoxy resin. The mounts were subsequently polished, and coated with carbon to ensure their conductivity. CCSEM analysis uses a Philips XL40 Scanning electron

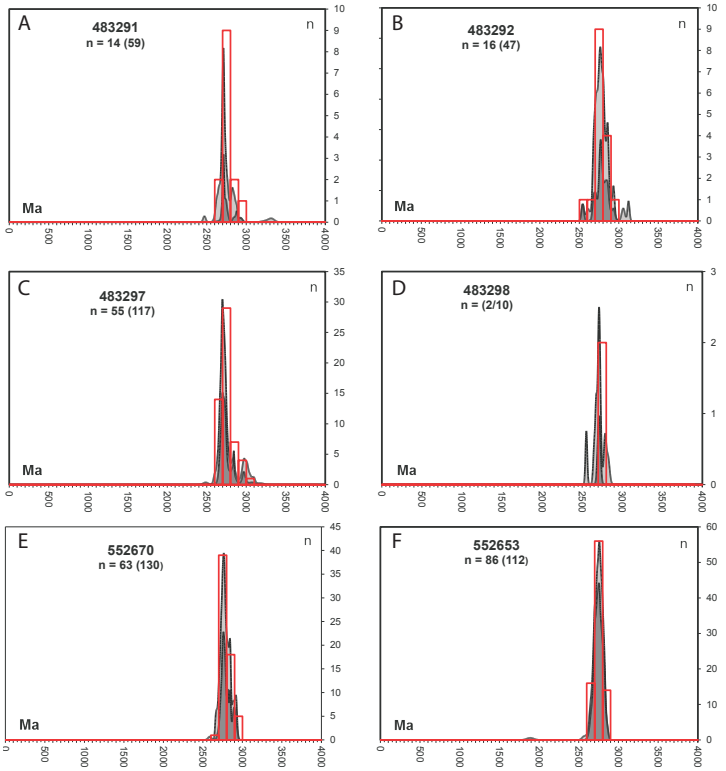

Figure 3
Age probability diagrams and histograms for detrital zircons. Dark grey: concordant zircon ages; light grey: all zircon ages (note that the light grey patterns in the background are partly masked by the dark grey patterns in the foreground). The histograms display the numbers of concordant zircons in 100 Ma intervals. N is the number of dated zircons: n= 30 (80) means that 30 out of a total of 80 zircon grains yielded concordant ages.

Microscope equipped with two energy dispersive X-ray detectors: a Thermo Nanotrace 30 mm^2 window and a Pioneer Voyager 2.7 10 mm^2 window Si(Li) detector. The tungsten filament of the SEM is operated with an acceleration voltage of 17 kV, a filament current of typically 50–70 µA. The Noran System SIX software package automatically collects X-ray spectra, grain size and morphology of all particles and recalculates the data following the Proza (ϕρZ) data correction and the filtering quantification technique. Commonly, 800–1200 grains were measured in approximately three-four hours. The chemical data are further reduced using a software package developed at GEUS that is connected to a mineral library database for automatic mineral classification and data storage. See Keulen *et al.* (2008, 2012) for details of the technique.

The mineral classification is purely based on chemical composition of the measured grains. There are no further petrological investigations involved in the classification. The density of the used heavy liquid is 2.9 g/cm^3, which removes quartz and feldspars, but keeps minerals like hornblende (3-3.4 g/cm^3), dolomite (2.9 g/cm^3), white mica (ca. 2.9 g/cm^3), which are not heavy minerals *sensu stricto*. In this study, however, all analysed minerals, except quartz and feldspars, will be referred to as heavy minerals. For the aluminous garnets in the metamorphic and igneous rocks a classification based on 7 groups defining rock types and metamorphic conditions has been used (Keulen and Heijboer, 2011; Keulen *et al.*, 2012).

The amount of water in the crystal lattice cannot be determined with an energy dispersive X-ray detectors (thus not with CCSEM) since light elements, like O, cannot be analysed accurately and very light elements, like H, are not detected

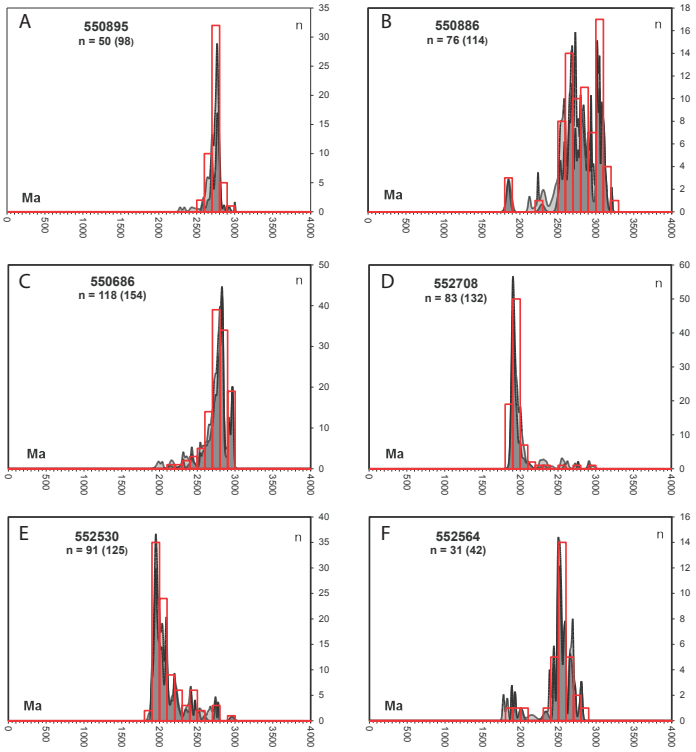

Figure 4
Age probability diagrams and histograms for detrital zircons. Dark grey: concordant zircon ages; light grey: all zircon ages (note that the light grey patterns in the background are partly masked by the dark grey patterns in the foreground). The histograms display the numbers of concordant zircons in 100 Ma intervals. N is the number of dated zircons: n=30 (80) means that 30 out of a total of 80 zircon grains yielded concordant ages.

at all. Therefore, the presence of water in the crystal structure cannot be determined. Since analyses are standardless, the software automatically recalculates the obtained concentrations to 100%; hence, it is not possible to observe that certain elements were missing in the analysis. The analyses are thus semi-quantitative. As a result it is not possible to distinguish between pyroxenes and hornblendes. A large compositional overlap exists between the two minerals, when the water in hornblende crystal lattice is not taken into account. Therefore, the mineral classification scheme lists both minerals together: clino-amphibole/pyroxene and ortho-amphibole/pyroxene, or clino-pyrobole and ortho-pyrobole for short. For the same reasons, no distinction can be made between magnetite and hematite; between sillimanite, andalusite and kyanite, or between rutile, brookite and anatase.

Results

Zircon provenance by LA-SF-ICPMS

The results are depicted in probability density distribution plots, using an arbitrarily chosen filter criteria, where all data between that are 90-110% concordant are plotted together with a dark grey colour in the histograms, whereas all data more than 10% discordant are plotted with a light grey colour. The two patterns mostly follow each other, but where they do not, we only refer to the concordant ages. The results are described from north to south. Where not specified, the analyses concern stream sediment samples. Two stream sediment samples (552661 and 550903) had no zircons.

483291 and 483292 (Figure 3a, b) are tillite samples, collected between Kap Edvard Holm and the Nordre Parallelgletscher (Kong Christian IX Land). The samples were small and not many zircons were retrieved from these samples. The concordant fraction yielded ages between 3000

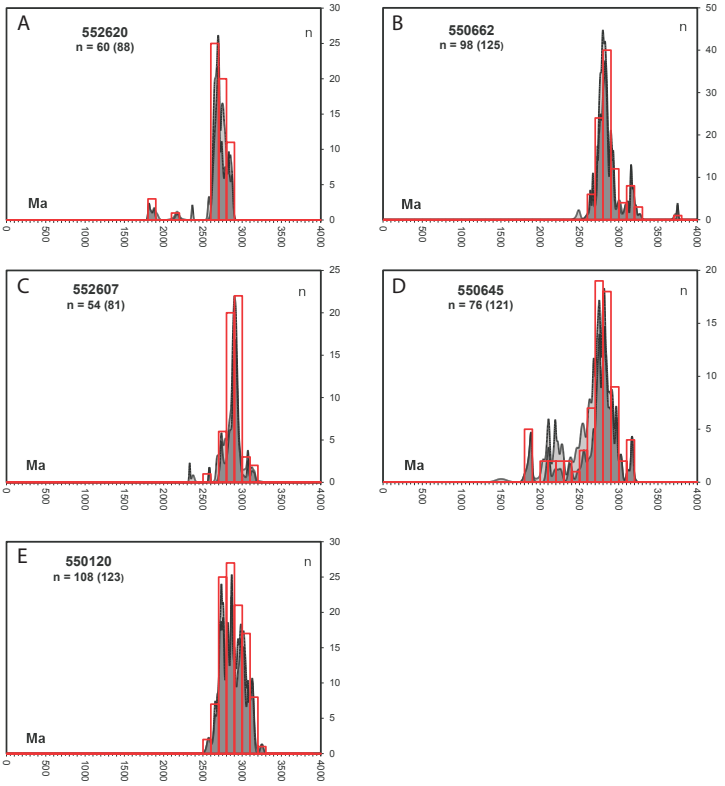

Figure 5
Age probability diagrams and histograms for detrital zircons. Dark grey: concordant zircon ages; light grey: all zircon ages (note that the light grey patterns in the background are partly masked by the dark grey patterns in the foreground). The histograms display the numbers of concordant zircons in 100 Ma intervals. N is the number of dated zircons: n=30 (80) means that 30 out of a total of 80 zircon grains yielded concordant ages.

and 2500 Ma with the main peak at approximately 2700 and 2770 Ma, respectively.

483297 and 483298 (Figure 3c, d) are tillite samples collected in the Skrækkensbugt area. These samples were also small, but where sample 483297 contained a relatively large amount of zircons, 483298 only had 10 grains. Sample 483297 yielded ages between 3100 and 2600 Ma with a prominent peak at 2700 Ma. Sample 483298 also had the main peak at 2700 Ma, despite much fewer analyses.

552670 (Figure 3e) was collected at Kap Gustav Holm and sample **552653** (Figure 3f) was collected further south, at Kap Japetus Stenstrup. Both samples are dominated by one very large peak at 2750 Ma, but whereas sample 552670 has some smaller and older peaks at 2900 and 2850 Ma, the detrital zircon pattern from 552653 yields one large unimodal population.

550895 (Figure 4a) was from the Niflheim area. The zircon population shows the same age range as the previous samples ranging from approximately 3000 to 2500 Ma. The detrital zircon pattern yields the largest peak at c. 2775 Ma with a smaller one at 2700 Ma.

550886 (Figure 4b) was collected along the coast, north of the Sermiligaaq fjord. This sample yields a much larger range of ages than seen in the previous samples. The bulk of the zircon ages fall between 3200 and 2450 Ma. This is the only sample in the northern part of the area that yields ages older than 3000 Ma. This age range is characterized by many different peaks of similar sizes; however, the three most dominant ages are 3100-3000 Ma and c. 2800 Ma and c. 2700 Ma. In addition, the sample also has a small zircon population of 1850 Ma ages, which is not seen in the previous samples.

550686 (Figure 4c) from the north-western part of Sermilik Fjord is dominated by a large peak

at 2820 Ma and by a smaller, but still significant peak at 2975 Ma. The zircon pattern yields a tail of ages from 2820 Ma down to 2100 Ma.

552708 and 552530 (Figure 4d, e) are both from the Ammassalik Intrusive Complex area. These samples are in contrast to the former dominated by Palaeoproterozoic peaks, and they only have minor occurrences of Archaean grains. The main peak in sample 552708 is at 1900 Ma and in sample 552530 it is at 1950 Ma. The age range spans from 3000 to 1850 Ma.

552564 (Figure 4f) was collected west of Kap Tycho Brahe, in the close vicinity to a proposed suture zone. The zircon pattern is very different from any other samples and yield ages which have not previously been recognized in the area. The ages range from 2850 to 1850, with the most dominant peak around 2500 Ma and a couple of smaller peaks at 2650 and 2600 Ma.

552620 (Figure 5a) was collected near Ikertivaq. The zircon pattern is dominated by ages from 2900 to 2600 Ma with the most prominent peak at 2700 Ma. A small Palaeoproterozoic peak at 1900-1800 Ma is also present.

550662 (Figure 5b) was collected in the area of Graah Øer. From this point and southwards we enter an area with prominent amount of Meso- and even Palaeoarchaean zircon grains. The ages in this sample range from 3300 to 2550 Ma and in addition there is a minor occurrence of zircons with age of 3750 Ma.

552607 (Figure 5c) was collected in the Køge Bugt region. The ages range from 3200 to 2550 Ma, with the dominating peak at 2900 Ma.

550645 (Figure 5d) was collected at Umiivik. The detrital age pattern spans a large range of ages from 3200 to 1800 Ma. The pattern is dominated by two almost equally large peaks at 2820 and 2750 Ma. In addition there is pronounced peaks around both 3150 and 1900 Ma, just as ages between 3000 and 2850 occurs in high number. This is the only sample in the southern part of the region in where Palaeoproterozoic zircons are found.

550120 (Figure 5e) was from the northern coast of Bernstorff Isfjord. The bulk of the ages are between 3150 and 2700 Ma, while the full spectrum range from 3250 to 2550 Ma. There are several peaks, the most dominant ones being between 3050-2950, around 2850 and between 2775 and 2700 Ma.

550052, 550148 and 550272 (Figure 6a, b, c) are from the agmatitic orthogneiss area in Skjoldungen, Kong Dan Halvø and by Heimdal glacier, respectively. The detrital zircon pattern from these three samples has similar characteristics. They are all dominated by a large peak between 2800 and 2700 Ma. In some of the plots the peak is broad, but in others very narrow. In all three samples there are few younger ages and the youngest are around 2500-2400Ma. All samples also contain older populations of zircons, but to varying extent. In sample 550552 there is a significant amount of older grains with the oldest being around 3300 Ma. Sample 550148 only have a minor amount of older grains with the oldest being 3150 Ma. Sample 550272 has the largest range of old ages with the oldest being 3650 Ma.

550512 (Figure 6d) was collected north of Mogens Heinesen Fjord. The sample is similar to the samples in the previous group, as it is dominated by a large peak between 2800 and 2700 Ma, with minor younger grains, but the difference is that it has almost no zircons older than 2950 Ma.

Modal heavy mineral analysis by CCSEM

The results for the modal heavy mineral analysis on the same samples as discussed above are shown in Figure 7. Garnet composition analysis was performed on samples with more than 10 aluminous garnets (Figure 8). Since clino-pyroxene/clino-amphibole is the main heavy mineral in the region, an attempt to further classify these minerals was made, based on their major and minor element contents. To do so, Ca-Mg and Si-Al element scatter plots of all samples were plotted. The different minerals show up as clusters in these plots. Of the individual clusters, the Fe, K, and Na concentrations were also taken in account.

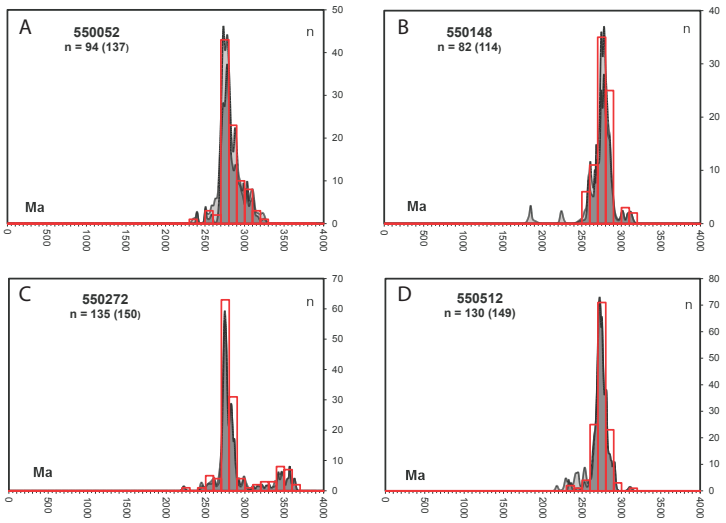

Figure 6
Age probability diagrams and histograms for detrital zircons. Dark grey: concordant zircon ages; light grey: all zircon ages (note that the light grey patterns in the background are partly masked by the dark grey patterns in the foreground). The histograms display the numbers of concordant zircons in 100 Ma intervals. N is the number of dated zircons: n=30 (80) means that 30 out of a total of 80 zircon grains yielded concordant ages.

These seven elements together were in most cases enough to determine the pyroxene or amphibole species.

483291 and **483292** have garnet as their major heavy mineral. Clino-pyroxene/clino-amphibole, biotite and ortho-pyroxene/ortho-amphibole are common. Less abundant are sillimanite-kyanite, muscovite, epidote and ilmenite-Ti-magnetite (Figure 7). The clino-pyroxene/clino-amphibole in these samples probably has an augite composition. The garnets in these samples were derived from felsic rocks that recrystallised at high to intermediate metamorphic grade (Figure 8).

483297, **483298**, **552661** and **552670** show a very similar heavy mineral suite: clino-pyroxene/clino-amphibole, ortho-pyroxene/ortho-amphibole, Ti-magnetite and biotite are the most common minerals (Figure 7).Iron-oxide (probably magnetite) is found abundantly as well. The clino-pyroxene/clino-amphibole minerals in the four samples are probably hornblende (of edenite-hastingsite composition) and augite or diopside-augite. The ortho-pyroxene/ortho-amphibole in samples 483297 and 483298 might possibly be. The retrograde mineral epidote was observed, especially in sample 552670.

552653, **550895**, **550686** and **550886** yield abundant garnets that mainly are derived from intermediate to mafic composition rocks that were metamorphosed at intermediate temperature conditions (Figure 8). Sample 550686 additionally has garnets that were derived from a more felsic rock. The latter three samples yield more garnet, dark mica and white mica than the previous four samples (Figure 7). Some sillimanite-kyanite was observed in sample 550686. Investigations of the clino-pyroxene/clino-amphibole minerals seem to indicate a strong presence of hornblende (mainly hastingsite, some of more kærsutite and edenite compositions) and some augite-diopside.

550903 is derived from a stream dewatering the large body of diorite and tonalite. Ortho-pyroxene/ortho-amphibolite is the most common heavy mineral in this sample, but clino-pyroxene/clino-amphibole occurs abundantly as well. The ortho-pyroxene/ortho-amphibolite is probably pigeonite.

552708 and **552530** yield abundant garnet, biotite and some sillimanite-kyanite in their heavy mineral suite. Ortho-pyroxene/ortho-amphibole is more abundant than clino-pyroxene/clino-amphibole. Pigeonite might be present in sample 552708. The garnet distribution for these two samples shows clearly that the samples were derived

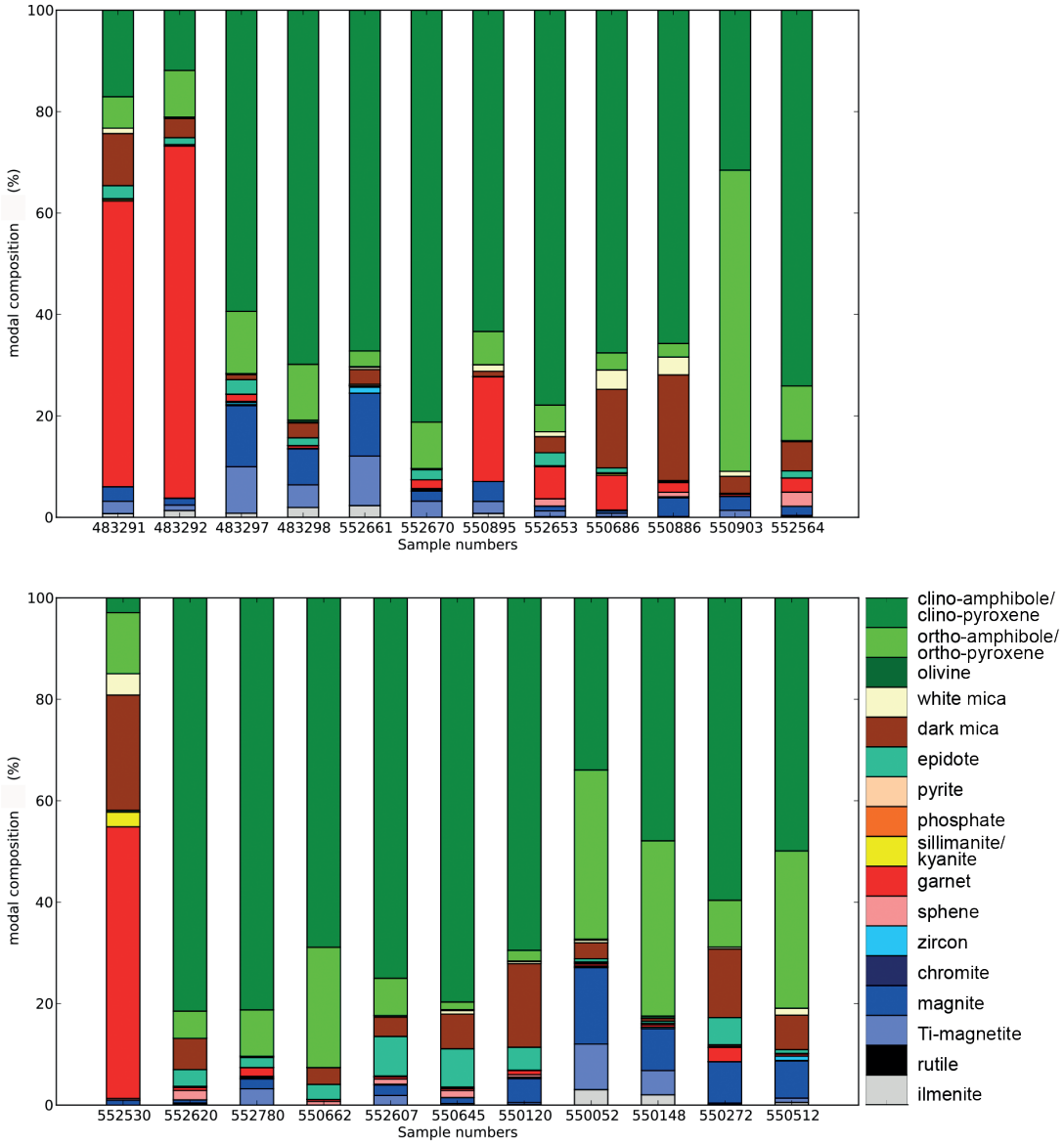

Figure 7

Modal heavy mineral suite for the analysed samples from South-East Greenland in stacked columns. The modal composition of the data is shown as frequency percentage and represent the results for 800-1200 grains. Samples are shown from north to south. The division of the area in different orthogneisses and areas with different main rock types is indicated with A, B1, B2, B3, C, 1-4 , see Figure 2 for localities.

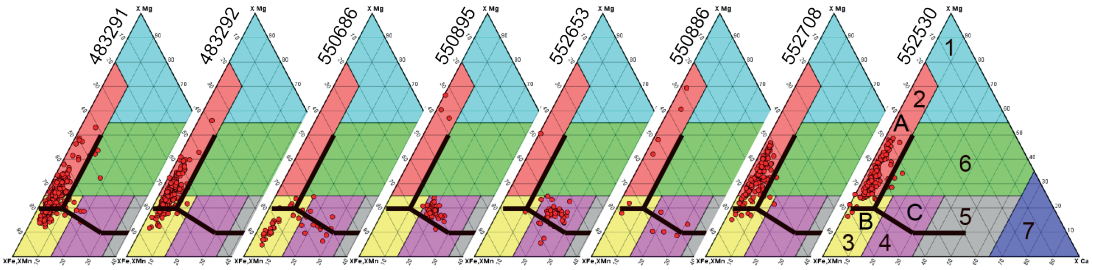

Figure 8
Ternary diagrams showing analyses of garnet grains from the Greenlandic western coast. Garnets are plotted by their end-member compositions pyrope (X_{Mg}), almandine+spessartine (X_{FeMn}) and grossular (X_{Ca}). The garnets were divided into seven groups after Keulen and Heijboer 2011 (colour fields). Garnets in group 1 include kimberlitic garnets and other garnets that suffered from ultra-high pressure metamorphism. Garnets in group 2 are mainly felsic granulites. Group 3 comprises mainly felsic amphibolite facies rocks. Group 4 consists of a) garnet amphibolites, generally formed at lower pressure conditions, or b) felsic amphibolite facies rocks that either have a more Ca-rich or more intermediate composition, or c) felsic rocks that underwent eclogite facies metamorphism, or d) charnockitic rocks. Group 5 includes intermediate and mafic amphibolites, and intermediate and mafic eclogites that were formed under relatively low temperature. Group 6 comprises most garnet amphibolites, mafic granulites and higher temperature mafic eclogites. Garnets derived from calc-silicates and anorthositic rocks plot in group 7. The alternative division into three groups, A, B, C after Morton *et al.* (2004) is shown as well in thick lines. Sample localities are indicated in Figure 2.

from rocks with a felsic composition (Figure 8). Most of the garnets in sample 552730 were derived from a felsic rock metamorphosed at high temperature conditions, while sample 552708 also has a small component of garnet formed at intermediate metamorphic temperatures.

552564, **552620**, **550662**, and **552607** consists of a heavy mineral suite of mainly clino-pyroxene/clino-amphibole, and ortho-pyroxene/ortho-amphibole, biotite, epidote, sphene and garnet also have been observed (Figure 7). Hastingsite hornblende, locally with a more edenite-hornblende composition seems to be the common most clino-pyroxene/clino-amphibole.

550645 and **550120** have a heavy mineral suite that is dominated by clino-pyroxene/clino-amphibole; the samples show epidote and biotite, and some sphene, garnet, muscovite, ortho-pyroxene/ortho-amphibole, epidote and biotite (Figure 7). The clino-pyroxene/clino-amphibole minerals in these two samples mainly seem to be hastingsite hornblende with a little augite in the samples. In sample 5504645, the hornblende composition ranges so broadly that some of the minerals are of tremolite composition. Locally augite was observed.

550052, 550148 and 550512 yielded a heavy mineral suite that consists of roughly similar portions of clino-pyroxene/clino-amphibole and ortho-pyroxene/ortho-amphibole, a large fraction of Ti-magnetite, some biotite, ilmenite, and some minor amounts of garnet, muscovite and epidote (Figure 7). Clino-pyroxene/clino-amphibole and ortho-pyroxene/ortho-amphibole probably have a pigeonite and augite composition and the samples yield abundant iron-oxide, probably magnetite. Sample 550512 shows less ortho-pyroxene, magnetite, and Ti-magnetite, and more hornblende and biotite.

550272 resembles 550120 with mainly

clino-pyroxene/clino-amphibole and common ortho-pyroxene/ortho-amphibole, biotite, epidote and garnet (Figure 7). The clino-pyroxene/clino-amphibole seems to consist of mainly hastingsite-edenite hornblende, and some augite. The garnets in this sample were derived from a felsic rock type that has been metamorphosed under high-temperature conditions, while some garnets are derived from a calc-silicate rock (Figure 8).

Discussion

Provenance characteristics of the Eastern Greenlandic basement between 62° and 68° N.

The age pattern changes from north to south commensurate with ages of the basement rocks, with an overall dominant age range from 2900-2700 Ma. Some samples contain older ages: a single sample yields ages up to 3700 Ma, and several samples have significant amounts of 3200-3000 Ma ages. Other samples contain younger Archaean ages down to 2500 Ma. Most samples do not contain Proterozoic zircons except the two samples collected in the Palaeoproterozoic Ammassalik Intrusive Complex area which yield age patterns dominated by 1950-1900 Ma zircons, in good agreement with the intrusion age (Nutman *et al*. 2008).

Even though the age pattern and the heavy mineral suite composition of the different samples are relatively similar, there are still differences, which make it possible to divide the basement of Southeast Greenland into various zones, as indicated in Figure 2. The zones will be characterized below.

Orthogneiss A (Figure 2): These seven most northern orthogneisses all yield a very similar age pattern, dominated by ages between 2800 and 2700 Ma. In most of these samples, the total age range goes from 2900 to 2600 Ma. None of the samples have any concordant Proterozoic ages, and only one sample yield few ages around 3100-3000 Ma.

The heavy mineral assemblage of this orthogneiss includes ortho-pyroxene, clino-pyroxene, Ti-magnetite and magnetite, which suggests that peak metamorphic temperatures were at granulite facies conditions. The high metamorphic conditions are well visible in the heavy mineral suite of the felsic Al-rich rocks in the northern part of the study area (marked with 1 in Figure 2). Here, garnets are the major part of the heavy mineral suite and those have a composition that agrees with metamorphic peak conditions at high temperatures (Figure 8). Augite, biotite, ilmenite, Ti-magnetite and minor sillimanite-kyanite in these samples are further witnesses of high temperature metamorphism.

Orthogneiss B (Figure 2): The area is a much more complex area than the previous. Whereas area A is dominated by Archaean granulite facies orthogneisses, area B, which covers subareas B1-B3, is dominated by Archaean amphibolite facies orthogneisses, which have undergone strong deformation and probably subduction during the Palaeoproterozoic. Palaeoproterozoic intrusions are numerous. Therefore, the detrital age pattern is very subjective to where the sample is collected and consequently the age patterns vary a lot. In general, the patterns are still dominated by Archaean ages, but several of the samples have input of Palaeoproterozoic ages between 2000 to 1850 Ma. In most samples, these Palaeoproterozoic peaks are small, but two samples collected within the Ammassalik Intrusive Complex is, not surprisingly, dominated by the Palaeoproterozoic ages. Apart from the Palaeoproterozoic ages this area is also characterized by having several samples with a significant amount of older Archaean ages between 3250 to 3000 Ma, which is not seen in area A. One sample, 552564, is differently from the rest. The main peak is around 2500 Ma, which is an uncommon age in this region. The sample is taken near a potentially large shear zone, which has not been studied in any detail.

The more complex nature of orthogneiss B is reflected in their heavy mineral suite, based on which the area has been divided into three different zones. All three zones have amphibolite facies peak metamorphic temperatures, but variations in

their heavy mineral assemblage. Hornblende, biotite and sphene are observed in nearly all samples. Orthogneiss B1 (Figure 2) has clino-pyroxene, garnet, muscovite, and Ti-magnetite as characteristic heavy mineral suite. Orthogneiss B2 (Figure 2) yields ortho-amphibole/ortho-pyroxene and Ti-magnetite. Orthogneiss B3 has been indicated as retrogressed from granulite facies according to Escher (1990). Chadwick *et al.* (1989), however, describe the gneiss as amphibolite facies. The heavy mineral suite does not give much evidence for granulite facies relict minerals. Apart from hornblende, biotite and sphene, the peak metamorphic assemblage, consists of clino-pyroxene, muscovite and garnet, which is typical for amphibolite facies conditions. However, it is important to emphasize that we only have 2 samples from this area.

Some of the clino-pyroxene in the samples from Orthogneiss B1 are richer in Na than usual augite (ca. 4 wt%), which does indicates a composition between omphacite and augite. Omphacite is indicative for high-pressure during metamorphism. The hornblende in the samples derived from Orthogneiss B2 is rather rich in aluminium and mainly of a hastingsite composition. The amount of Al in hornblende increases with increasing pressure (Ernst and Liu, 1998). Thus here as well as in orthogneiss B1, slightly higher pressures during metamorphism might have occurred.

The samples collected from the Ammassalik Intrusive Complex and associated high-grade anatexite sediments bear evidence of metamorphism at high temperatures (Nutman *et al*., 2008). Even though the surrounding orthogneisses might not have reached metamorphic conditions higher than amphibolite facies, higher temperatures seemed to have occurred related to the large intrusions in the Ammassalik area.

In the area of orthogneiss B, a large post-tectonic, Palaeoproterozoic intrusive body of diorite and tonalite has been sampled (marked 2 in Figure 2), which is a major source for the orthopyroxene in sample 550903.

Orthogneiss C (Fig. 2): Covers the area of the Skjoldungen region. All the samples from this area are very similar and the age patterns in all the samples are dominated by 2800 to 2700 Ma ages. The age patterns are very similar to the pattern of area A in the very northern part of the area, as basically all the Palaeoproterozoic ages are lacking here. The difference is that in this area, there are still occurrences of older Archaean grains in some of the samples, with ages up to 3250 Ma. The exception is sample 550272, which has ages ranging all the way up to 3650 Ma, with a small but distinct population between 3600 and 3400 Ma. Zircons older than 3400 Ma have not yet been reported from the Skjoldungen Region, and in general, very few ages between 3600 and 3400 Ma have been reported from Greenland. Orthogneiss C has a high temperature mineral assemblage including orthopyroxene, clinopyroxene, magnetite and Ti-magnetite, which indicate that temperatures might have been up to granulite facies conditions. Other common minerals are ilmenite, biotite, muscovite and garnet. The assemblage is distinctive by its high amount of ortho-pyroxene. Escher (1990) indicated granulite facies for the northern half of the area covered by orthogneiss C and amphibolite facies for the southern half. A temperature gradient in the gneisses might exist from north to south, visible in the decreasing amount of orthopyroxene, magnetite and Ti-magnetite. Kolb *et al.* (2013) on the other hand, interpret the whole area as granulite facies rocks. Sample 550272 (indicated with 4 on Figure 2) yields a more intense retrogression from granulite facies to amphibolite facies than in the other three samples from the orthogneiss C. Its mineral assemblage resembles orthogneiss B3.

Comparison of the Faroe-Shetland Basin with the Kangerlussuaq region and other source regions

The overall age pattern and geochemical signature for Southeast and East Greenland is markedly different from that of the samples from the drill core in the Faroese sector of the Faroe-Shetland Basin (Frei and Knudsen 2008; Weibel and Knudsen

2008), making it unlikely that this part of Greenland was the source for sedimentary detritus in the Faroe sector.

The wells of the Faroese sector are very close to some of the wells in the UK sector of the Faroe-Shetland Basin (Figure 1), whereas others are up to 100 km away. Frei *et al.* (2005b) and Frei and Knudsen (2008) analysed zircons from samples from wells in both sectors, and despite the distance, the age patterns from all the wells are very similar. Both sectors are dominated by a large Archaean peak around 2800-2700 Ma and only very few ages above 3000 Ma. In addition, they both have a significant broad range of Palaeo-, Meso- and even early Neoproterozoic ages, ranging approximately from 1900 to 900 Ma, and, lastly, they have a peak around 500-400 Ma.

Whitham *et al.* (2004) and Frei *et al.* (2005b) analysed zircons from the Cretaceous, Palaeocene and Eocene sedimentary successions from the Kangerlussuaq region to evaluate whether this sediment could be the source for the Faroe-Shetland basin. The average Kangerlussuaq signature is very similar to the pattern from the Faroe-Shetland Basin sediments, however, there is one important difference; the Kangerlussuaq sediments have a significant zircon population of 3250 to 3000 Ma grains. This population does not occur in the Faroe-Shetland Basin. Instead, this age population has been documented in this study to exist in Southeast Greenland, both in the Skjoldungen area and in the Tasiilaq region.

The large Palaeo- to Neoproterozoic age population, as well as the Caledonian peak present in the Kangerlussuaq Signature, does not occur in Southeast Greenland, but instead these ages are present to the north in Central Greenland in large and widespread Neoproterozoic basins e.g. the Smallefjord group, the Krummedal Supracrustals and the Eleonore Bay Supergroup (Kalsbeek *et al.*, 2000; Strachan *et al.*, 1995; Watt and Thrane, 2001). We, therefore, suggest that the sediments in the Kangerlussuaq region must have been sourced both from the north, given the range of Palaeoproterozoic to Neoproterozoic zircons, and from the south where we have several occurrences of 3250 to 3000 Ma zircons. Furthermore, due to the large amount of zircons older than 3000 Ma in the Kangerlussuaq region, this area cannot be the source of the sedimentary detritus in the Faroe-Shetland Basin.

In Central East Greenland, north of Kangerlussuaq, the detrital zircon pattern matches well with the Faroe-Shetland Basin (Cawood *et al.*, 2007, Kalsbeek *et al.*, 2000, Rehnström *et al.*, 2010), no zircons older than 3000 Ma are present here. Due to the large area covered by thick Palaeogene flood basalts, just north of Kangerlussuaq, it is not possible to determine where the signature changes from the Kangerlussuaq Signature to the Central East Greenland Signature, nor is any alternative pathways visible, but they could easily have been present in the Palaeocene.

The garnet classification of Morton *et al.* (2004) was superimposed to the garnet ternary diagrams (Figure 8), such that our results for Southeast Greenland can be compared to the results of Morton *et al.* (2005a) and Frei *et al.* (2005a) for garnets from wells in the UK sector of the Faroe-Shetland Basin and from Kangerlussuaq (Figure 9). They divide their garnets into three groups A; low Ca, high Mg, group B: low Mg, variable Ca and Fe, and group C: high Mg and high Ca. Garnet from Kangerlussuaq are characterised by three different groups: high X_{Fe}+X_{Mn} garnets, iron-rich garnets with a high X_{Mg} of up to 50%, and slightly more Ca-rich garnets that straddle the boundary between garnet fields B and C and plot in garnet group 4 (see Figure 8, 9). Garnets from wells in the Faroe-Shetland basin show the same three groups, but are much richer in iron-rich garnets with a high X_{Mg} and only yielded a few grains with high X_{Fe}+X_{Mn}. The Kangerlussuaq area is therefore an unlikely source of these well sediments. We prefer the garnet division of Keulen & Heijboer (2011), as this division is more strongly based on different rock compositions and metamorphic temperatures than Morton et al. (2004)'s

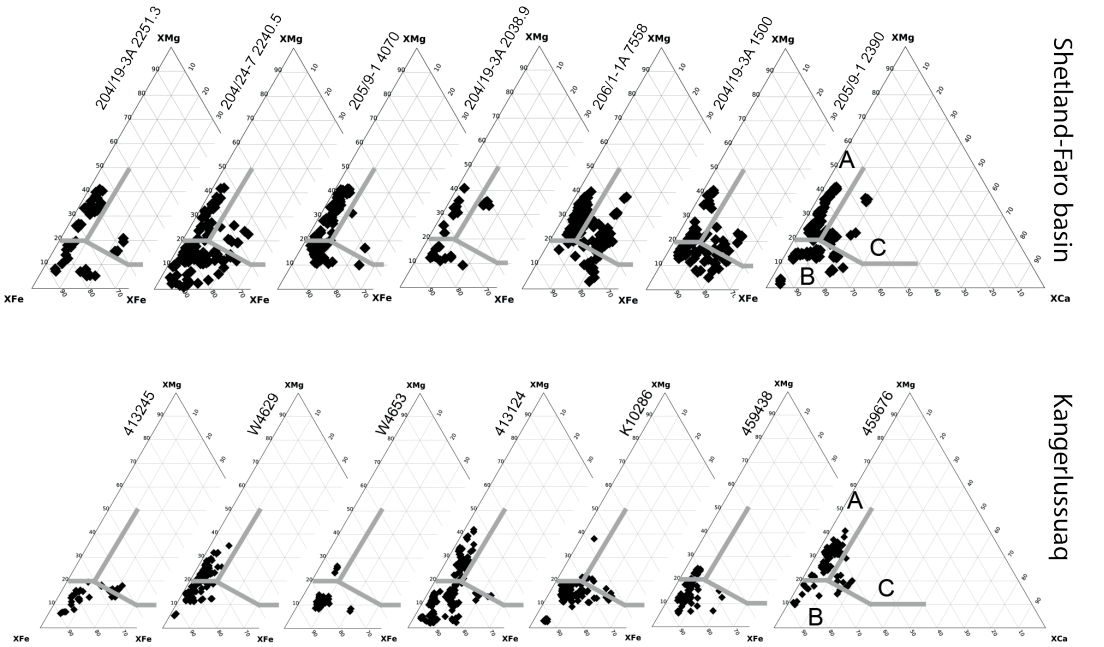

Figure 9

Ternary diagrams showing garnet grains from wells in the Faro-Shetland Basin and from Kangerlussuaq of representative samples analysed by Frei *et al.* 2005a. See Figure 1 for localities. Garnets are plotted by their end-member compositions pyrope (X_{Mg}), almandine+spessartine (X_{FeMn}) and grossular (X_{Ca}). Garnet classification into three groups A, B, and C after Morton *et al.* (2004).

classification. However, as we do not have the raw data from Morton et al. (2004)'s study, we cannot superimpose the Keulen & Heijboer (2011) garnet classification applied Figure 8 to their data in Figure 9.

Our study shows that high X_{Mg} garnets are found in the tillites just south of Kangerlussuaq (samples 483291 and 483292) and in the metasedimentary rocks associated with the Ammassalik Intrusive Complex area. These are the type of garnets found in wells from the Faroe-Shetland basin, but not in the sediment in Kangerlussuaq. The orthogneiss however, which makes up the larger part of the area, is poor in garnets and mainly yields Mg-poor garnets (Figure 8). The basement south of Kangerlussuaq is therefore unlikely to be the only source or even the source of the sediments in Kangerlussuaq and Southeast Greenland is unlikely to be the only source for the sediments in the Faroe-Shetland basin.

Hardly any garnet compositional data is available from Eastern Greenland (but see Morton *et al.*, 2005b; 2005c) and no such data on the Krummedal Supracrustals and the Eleonora Bay Supergroup is, to our knowledge, available in the public domain. Morton *et al.* (2005b) show that samples from Geographical Society Ø and Hold with Hope (Eastern Greenland) yield high X_{Mg} garnets; the sediment source of these samples is unknown, but likely to be placed in East Greenland. Samples with similar high X_{Mg} garnets have been observed in the western part of the Vøring

basin, north of the Faroe-Shetland basin (Morton *et al.*, 2005b; 2005c). High X_{Mg} garnets (garnet group 2 (Keulen and Heijboer, 2011) or type A garnets (Morton *et al.*, 2004)) are characteristic for felsic high-grade metamorphosed rocks. Gilotti *et al.* (2008) and Henriksen and Higgins (1976) describe the Krummedal Supracrustal sequence as such rocks, whereas the major part of the Eleonore Bay Supergroup sediments only underwent low to intermediate grade metamorphism. The Krummedal Supracrustals are therefore a likely source area for the Faroe-Shetland basin sediment, based on both their characteristic age pattern and their garnet composition. A source in Central East Greenland agrees with other studies on pollen records and sediment transport directions (Larsen *et al.*, 2005; Jolley and Morton, 2007).

However, central East Greenland is not the only area with this very characteristic age pattern and a high-grade metamorphic event in the history of the rocks. The same pattern is found in northern Scotland, parts of Scandinavia, Svalbard and Siberia (Cawood *et al.*, 2007 and reference therein). These regions have shared a common history and, therefore, have the same detrital age pattern (Watt and Thrane, 2001). Most of the mentioned areas are made up of Archaean cratons of similar age, and large packages of sediment were deposited between ca. 1000 and 950 Ma (Johansson *et al.*, 2000; Watt and Thrane, 2001; Cawood *et al.*, 2007; Be'eri-Shlevin *et al.*, 2011). The sediments were dominated by zircons populations of Palaeoproterozoic to Mesoproterozoic ages. The Grenville orogenic belt of the Laurentian margin is the most likely source for the majority of the detritus. The sediment was transported to the north along the Laurentian and the East Greenlandic margin, where it was deposited. After deposition, metamorphism, anatexis and granite emplacement occurred during the amalgamation and break up of Rodinia around 950-870 Ma and again during the Caledonian Orogeny around 450-430 Ma.

Conclusion

It has been suggested that the sediment of the Faroe-Shetland Basin was sourced from the UK margin, since the detrital zircon age patterns from the Faroe-Shetland Basin did not match with sediment samples from the Kangerlussuaq region, East Greenland (Frei and Knudsen, 2008).

However, several other potential source areas with similar detrital age patterns exists, e.g. Central East Greenland, Svalbard, (Scandinavia) and Siberia, which all share a similar history and hence a similar age pattern signature, it is not possible to discriminate the different sources on the basis of zircon data.

Frei and co-workers use samples from the Kangerlussuaq area as a proxy for the Greenlandic source in the Faroe region, but the Greenlandic source for the Faroese sediments cannot be defined based on the properties of the Kangerlussuaq area only.

A source in Central East Greenland, where suitable-aged felsic source rocks that underwent intermediate to high-temperature metamorphism are known to occur, would be more compatible with other studies pointing to an East Greenlandic source, such as heavy mineral analyses, pollen records and sediment transport directions (Larsen *et al.*, 2005; Jolley and Morton, 2007).

Acknowledgements

Mojagan Alaei, Fiorella Aguilera, Michael Nielsen and Jørgen Kystol (GEUS) are all thanked for help with the lab work, with everything from preparing the samples to carrying out part of the analyses. The work presented in this volume was funded by SINDRI and GEUS and the samples were collected by GEUS.

References

Be'eri-Shlevin, Y, Gee, D., Claesson, S., Ladenberger, A., Majka, J., Kirkland, C., Robinson, P. & Frei, D. 2011. Provenance of Neoproterozoic sediments in the Särv nappes (Middle Allochton) of the Scandinavian Caledonides: LA-ICP-MS and SIMS U-Pb dating of detrital zircons. *Precambrian Research* 187: 181-200.

Cawood, P., Nemchin, A.A., Strachan, R., Prave, T. and Krabbendam, M. 2007. Sedimentary basin and detrital zircons record along East Laurentia and Baltica during assembly and breakup of Rodinia. *Journal of the Geological Society, London* 164: 257-275.

Chadwick, B., Dawes, P.R., Escher, J.C., Friend, C.R.L., Hall, R.P. Kalsbeek, F., Nielsen, T.F.D., Nutman, A.P., Soper, N.J. and Vasudev, V.N. 1989. The Proterozoic mobile belt in the Ammassalik region, South-East Greenland (Ammassalik mobile belt): an introduction and re-appraisal. *In:* Kalsbeek, F.: Geology of the Ammassalik region, South-East Greenland. *Rapport Grønlands Geologiske Undersøgelse*: 146, 5-12.

Escher, J.C. 1990. Geological map of Greenland, 1:500 000, Skjoldungen, Sheet 14. Copenhagen: Grønlands Geologiske Undersøgelse.

Ernst, W.G. & Liu, J. 1998. Experimental phase-equilibrium study of Al- and Ti-contents of calcic amphibole in MORB—A semiquantitative thermobarometer. *American Mineralogist* 83:, 952–969.

Frei, D., Frei, M. Klünder, M.H., Rasmussen, T. and Knudsen, C. 2005a. Heavy mineral characteristics of Cretaceous-Eocene sandstones in the Kangerlussuaq Basin, East Greenland – results from CCSEM. *In*: Frei, D., Frei, M. and Knudsen, C. (eds.): Linking the Faroese area and Greenland: an innovative, integrated provenance study. *Danmarks og Grønlands Geologiske Undersøgelse Rapport* 2005/54: 77-92.

Frei, D. and Gerdes, A. 2009. Precise and accurate in-situ zircon U-Pb dating with high sample throughput by automated La-SF-ICP-MS. *Chemical Geology* 261: 261-270.

Frei, D. and Knudsen, C. 2008. Understanding sedimentary provenance in the Faroe-Shetland basin: constraints from detrital zircon geochronology. *In*: Frei, D., Weibel, R. and Knudsen, C. (eds.): Provenance of sediments in the Faroese-Shetland basin: Integration of wells in the Faroese sector. *Danmarks og Grønlands Geologiske Undersøgelse Rapport* 2008/21: 11-33.

Frei, D., Rasmussen, T., Frei, M., Knudsen, C., Larsen, M. and Whitham, A.G. 2005b. Heavy mineral characteristics of Cretaceous-Eocene sandstones in the Kangerlussuaq Basin, East Greenland – results from CCSEM. *In*: Frei, D., Frei, M. and Knudsen, C. (eds.): Linking the Faroese area and Greenland: an innovative, integrated provenance study. *Danmarks og Grønlands Geologiske Undersøgelse Rapport* 2005/54: 93-105.

Garde, A.A., 2007. Geological map of Greenland, 1:500 000, Sydgrønland, Sheet 1. Copenhagen: Geological Survey of Denmark and Greenland.

Gerdes, A., Zeh, A., 2006. Combined U-Pb and Hf isotope LA-(MC)-ICP-MS analyses of detrital zircons: comparison with SHRIMP and new constrains for the provenance and age of an Armorican metasediment in Central Germany. *Earth and Planetary Science Letters* 249, 47–61.

Gilotti, J.A., Jones, K.A. and Elvevold, S. 2008. Caledonian metamorphic patterns in Greenland. *In*: Higgins, A.K., Gilotti, J.A. and Smith, M.P. *The Greenland Caledonides. Evolution of the Northeast Margin of Laurentia*. Geological Society of America Memoir 202: 201-226.

Henriksen, N. and Higgins, A.K. 1976. East Greenland Caledonian fold belt. *In*: Escher, A. and Watt, W.S. *Geology of Greenland*. Copenhagen 182-247.

Johansson, A., Larionov, A.N., Tebenkov, A.M., Gee, D.G., Whitehouse, M. J. and Vestin, J. 2000. Grenville magmatism of western and central Nordaustlandet, northeastern Svalbard. Transactions of the Royal Society of Edinburgh, Earth Sciences 90: 221-254.

Jolley, D.W. and Morton, A.C. 2007. Understanding basin sedimentary provenance: evidence from allied phytogeographic and heavy mineral analysis of the Palaeocene of the NE Atlantic. *Journal of Geological Society, London* 164: 553-563.

Kalsbeek, F. Ghisler, M. and Thomsen, B. 1974. Sand analysis as a method of estimating bedrock compositiions in Greenland, illustrated by fluvial sands from the Fiskenæsset region. *Grønlands Geologiske Undersøgelse Bulletin* 111, 32pp.

Kalsbeek, F., Thrane, K., Nutman, A.P. and Jepsen, H.F. 2000. Late Mesoproterozoic metasedimentary and granitic rocks in the King Oscar Fjord region, east Greenland Caledonides fold belt: evidence for Grenville orogenesis. *Journal of the Geological Society, London* 157: 1215-1225.

Karson, J.A. and Brooks, C.K. 1999. Structural and magmatic segmentation of the Tertiary East Greenland volcanic rifted margin. *In*: Mac Niocaill, C and Ryan, P.D. (eds.) *Continental Tectonics*. Geological Society, London, Special Publications 164: 313-338.

Keulen, N., Frei, D., Bernstein, S., Hutchison, M.T., Knudsen C., and Jensen L. 2008. Fully automated analysis of grain chemistry, size and morphology by CCSEM: examples from cement production and diamond exploration. *Reviews of the Survey's Activities 2007,* Geological Survey of Denmark and Greenland Bulletin 15: 93-96.

Keulen, N., Frei, D. Riisager, P. and Knudsen C. 2012. Analysis of heavy minerals in sediments by computer-controlled scanning electron microscopy (CCSEM): Principles and applications. *Mineralogical Association of Canada Short Course* 42: p167-184.

Keulen, N. and Heijboer, T. 2011. The provenance of garnet: semi-automatic plotting and classification of garnet compositions. *Geophysical Research Abstracts* 13: EGU2011-4716-1.

Knott, S.D., Burchell, M.T., Jolley, E.J. and Fraser, A.J. 1993. Mesozoic to Cenozoic plate reconstructions of the North Atlantic and hydrocarbon plays of the Atlantic margins. *In*: Parker, J.R.*: Petroleum Geology of Northwest Europe*: Proceedings of the 4th Conference. Petroleum Geology '86 Ltd. The Geological Society, London: 953-974.

Kolb, J., Thrane, K. and Bagas, L. (2013). Field relationship of high-grade Neo- to Mesoarchaean rocks of South-East Greenland: Tectonometamorphic and magmatic evolution. *Gondwana Research* 23: 471-492.

Kosler, J. and Sylvester, P.J. 2003. Present trends and the future of zircon in geochronology: Laser ablation ICP-MS. *In*: Hanchar, J.M, Hoskin, P.W.O. (eds.), Zircon. *Reviews in Mineralogy and Geochemistry* 53, Mineralogical Society of America, Washington, DC: 243-275.

Larsen, M. 1996. Sedimentology and Basin Evolution of the Cretaceous-Early Tertiary Kangerlussuaq Basin, southern East Greenland. *Danmarks og Grønlands Geologiske Undersøgelse Rapport* 1996/35.

Larsen, M., Nøhr-Hansen, H., Whitham, A.G. and Kelly, S.R.A. 2005. Stratigraphy of the pre-basaltic sedimentary succession of the Kangerlussuaq Basin. Volcanic basins of the North Atlantic. *Danmarks og Grønlands Geologiske Undersøgelse Rapport* 2005/62.

Ludwig, K.R., 1999. Isoplot/Ex version 2.00 – A geochronological toolkit for Microsoft Excel. *Berkeley Geochronology Center, Special Publication* No. 2

Morton, A., Ellis, D., Fanning, M., Jolley, D and Whitham, A., 2012. Heavy mineral constraints on Paleocene sand transport routes in the Faroe-Shetland Basin. *In*: Varming, T. and Ziska, H. (eds), *Faroe Islands Exploration Conference: Proceedings of the 3rd Conference*. Annales Societatis Scientiarum Faeroensis, **56**, 59-83.

Morton, A., Ellis, D., Fanning, M., Jolley, D and Whitham, A., 2012. The importance of an integrated approach to provenance studies: a case study from the Paleocene of the Faroe-Shetland Basin, NE Atlantic. *In*: Rasbury, E.T.,

Hemming, S.R. and Riggs, N.R. (eds), *Mineralogical and Geochemical Approaches to Provenance*. Geological Society of America, Special Paper, **487**, 1-12.

Morton A., Hallsworth, C. and Chalton, B. 2004. Garnet compositions in Scottish and Norwegian basement terrains: a framework for interpretation of North Sea sandstone provenance. *Marine and Petroleum Geology* 21: 393–410.

Morton, A.C., Hallsworth, C.R. and Whitham, A.G. 2005a. Heavy mineral provenance of Paleocene-Eocene sandstones in the Faroe-Shetland Basin – results from conventional petrographical and mineral-chemical techniques. *In*: Frei, D., Frei, M. and Knudsen, C. (eds.): Linking the Faroese area and Greenland: an innovative, integrated provenance study. *Danmarks og Grønlands Geologiske Undersøgelse Rapport* 2005/54: 17-49.

Morton, A.C., Whitham, A.G., Fanning, C.M. and Claoué-Long J. 2005b. The role of East Greenland as a source of sediment to the Vøring Basin during the Late Cretaceous. *Norwegian Petroleum Society Special Publications* 12: 83–110.

Morton, A.C., Whitham, A.G. and Fanning, C.M. 2005c. Provenance of Late Cretaceous to Paleocene submarine fan sandstones in the Norwegian Sea: Integration of heavy mineral chemical and zircon age data. *Sedimentary Geology* 182:, 3-28.

Myers, J.C., Dawes, P.R. and Nielsen, T.F.D. 1988. Geological map of Greenland, 1:500 000, Kangerdlugsuaq, Sheet 13. Copenhagen: Grønlands Geologiske Undersøgelse.

Nutman, A.P., Kalsbeek, F. and Friend, C.R.L. 2008. The Nagssugtoqidian Orogen in South-East Greenland: evidence for Paleoproterozoic collision and plate assembly. *American Journal of Science* 308: 529-572.

Nøhr-Hansen, H., Larsen, M., Kelly, S.R.A. and Whitham, A.G. 2006. Biostratigraphy zonation (palynology and macrofossil) for the Upper Cretaceous – Lower Palaeogene based on the sedimentary succession in the Kangerlussuaq, southern East Greenland. Phase 1 report for the Sindri Group, March 2006, *Danmarks og Grønlands Geologiske Undersøgelse Rapport* 2006/23.

Rehnström, E.F., Thrane, K., Kokfelt, T.F. and Frei, D. 2010. Age distribution of detrital zircon grains in sandstones and stream sediments from East Greenland north of 70°N. *Danmarks og Grønlands Geologiske Undersøgelse Rapport* 2010/130. Confidential until 31.12.2015.

Sircombe, K.N. 2004. AgeDisplay: an Excel workbook to evaluate and display univariant geochronological data using binned frequency histograms and probability density distributions. *Computer and Geosciences* 30: 21-31.

Strachan, R.A., Nutman, A.P and Friderichsen, J.D. 1995. SHRIMP U-Pb geochronology and metamorphic history of the Smallefjord sequence, NE Greenland Caledonides. *Journal of the Geological Society, London* 152: 779-784.

Watt, G.R. and Thrane, K. 2001. Early Neoproterozoic events in East Greenland. *Precambrian Research* 110: 165-184.

Weibel, R. and Knudsen, C. 2008. Provenance of sediments in the Faroe-Shetland Basin: constraints from whole-rock geochemistry. *In*: Frei, D., Weibel, R. and Knudsen, C. (eds.): Provenance of sediments in the Faroese-Shetland basin: Integration of wells in the Faroese sector. *Danmarks og Grønlands Geologiske Undersøgelse Rapport* 2008/21: 35-68.

Whitham, A.G., Morton, A.C. and Fanning, C.M., 2004. Insights into Paleocene sediment transport
paths and basin evolution in the North Atlantic from a heavy mineral study of sandstones from southern East Greenland. *Petroleum Geoscience* **10:** 61-72.

Appendix

Zircon data

The Kettla Member
An overview from the Faroe-Shetland Basin

ÓLUVA R. EIDESGAARD AND HERI ZISKA

Jarðfeingi (Faroese Earth and Energy Directorate), Brekkutún 1, PO Box 3059,
FO-110 Tórshavn, Faroe Islands. oei@jf.fo

*Corresponding author: oluva.eidesgaard@jardfeingi.fo

Abstract

The Kettla member is a geographically widespread partially volcaniclastic unit in the Faroe-Shetland Basin. The source of the volcaniclastic components is still unproven. This study aims to get a better idea of the distribution and sedimentary pathways of the Kettla member in order to establish its provenance.

The unit is thickest in and around the Judd- and Flett Sub-basins. Close to the Judd Sub-basin, in Well 6004/8a-1 the member is almost 150 m thick and consists primarily of coarse-grained volcaniclastics and tuffs. In a southwesterly direction from Well 6004/8a-1 the member thins out and the material changes from high-energy to low-energy facies.

Close to the Flett Sub-basin, in Well 205/9-1 the Kettla member is almost 200 m thick and consists largely of claystones and sandstones. The basal 50 m are mostly composed of tuff. In an easterly direction the member thins out and again the material changes into more low-energy facies. Variations in the lithology of the member suggests there may be different sources for the volcaniclastic component of the member in the Judd- and the Flett Sub-basins. The coarse and mostly poorly-sorted volcaniclastic material found in the wells close to the Judd Sub-basin indicate, together with the thickness variations seen in the correlation profiles, that the volcanic component in the member most likely comes from a source proximal to the Corona High. Similarly, the source for the Kettla member in the Flett Sub-basin is also likely to be found in the proximity of the Corona High, but on its eastern side, as the High might have acted as a barrier for the source which fed into the Judd Sub-basin on the western side.

The Kettla member thus provides evidence of extrusive volcanism in the Faroe-Shetland Basin (north to northeast of the Judd Sub-basin), in the earliest Thanetian, possibly earlier.

Faroe Islands Exploration Conference: Proceedings of 4th Conference.
Annales Societatis Scientiarum Færoensis Supplementum LXIV.

Introduction

Before sea floor spreading of the North Atlantic Ocean began, Greenland and the Faroe Area were adjacent to one another (Ellis et al., 2002). Today Cretaceous sedimentary units are exposed onshore on the eastern side of Greenland. They overlie an irregular erosion surface of Precambrian aged gneisses which slopes towards the east and south, indicating that there might be older and most likely sedimentary stratigraphic units present beneath the basalts of the adjoining Faroese Continental Shelf (FCS) (Larsen et al., 1999; Larsen and Withham, 2005).

The evolution of the North Atlantic Igneous Province (NAIP) was initiated in Paleocene time. The North Atlantic was affected during this period by extension and rifting causing widespread thermal doming and uplift. This culminated with plate separation along the NW European Atlantic margin in the early Eocene (Doré et al., 1999). Areas affected by major basaltic magmatism include Greenland, the Vøring margin and the Rockall-Hatton area (Coffin, 1992; White and McKenzie, 1989) (Figure 1). Today the NAIP covers large areas of the FCS and the Faroe-Shetland Basin.

Although the understanding of the Paleogene basalts is increasing, the early stages of the volcanic systems are only poorly understood. The Kettla member is a mixed volcaniclastic and siliciclastic unit (Knox et al., 1997), which can be found in certain areas of the Faroe-Shetland Basin. The volcanic component is one of the older volcanic units in the area.

The aim of this paper is to use well data to get a clearer picture of the volcanism associated with the deposition of the Kettla member in the Judd- and Flett Sub-basins (Figure 1).

Geological Setting

The Faroe-Shetland Basin (Figure 1) is a Mesozoic-Paleozoic rift basin along the NE Atlantic margin. It has a complex geological history (Doré et al., 1999) with the margin having been through several different phases of structural evolution. The process of opening the Northeast Atlantic Ocean in the Early Palaeogene was characterised by the eruption of vast volumes of basalt followed by renewed subsidence and sedimentary deposition during the Eocene (Doré et al., 1999; Saunders et al., 1997; (Ritchie et al., 1999).

The volcanic rocks, dominated by basalts that cover the Faroe Platform today, extend from onshore Faroe Islands into the Faroe-Shetland Basin and the Faroe Bank Channel (Figure 1). The lava dominated succession is named the Faroe Islands Basalt Group (FIBG) and is a part of the NAIP. It has a stratigraphic thickness up to 6500-7000 m of which 3000 m are exposed onshore (Ellis et al., 2002).

Ziska (2012) introduced the idea of a two rift

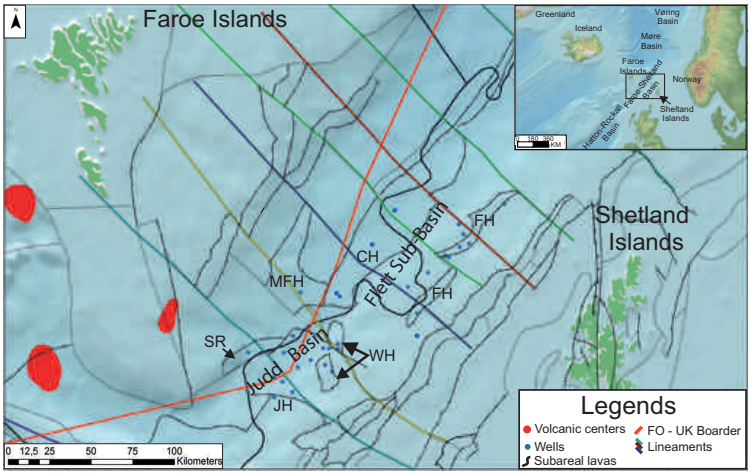

Figure 1
The study area including the wells used in this paper. SR = Sjúrður Ridge, MFH = Mid Faroe High, JH = Judd High, WH = Westray High, CH = Corona High, FH = Flett High. Right corner map: An overview map of the Northeast Atlantic.

system, with one NNW/SSE oriented rift to the west of the Faroes Islands, resulting in the older onshore volcanic units – the Lopra- and the Beinisvørð formations, and a second E/W-ENE/WSW oriented rift, the opening of the North Atlantic Ocean, resulting in a second phase of volcanism and the younger onshore basalt units – the Malinstindur- and Enni formations.

The Faroe and Moray groups

The stratigraphic framework of the part of the Faroe-Shetland Basin covered in this paper comprises the Faroe group and the Moray group of Paleocene to Eocene age, however the focus of this paper will be on the Faroe group (Figure 2). The Moray group consists of the Flett formation and the Balder formation. The Faroe group is Late Paleocene in age and comprises the Lamba and the Vaila formations (e.g. Knox et al., 1997; Stoker and Varming, 2011).

The FIBG which is partly exposed on the Faroe Islands correlates with the Moray and possible the Faroe groups in the Faroe-Shetland Basin. According to Ellis et al. (2002) and Jolley and Bell (2002) the FIBG correlates to the Flett formation in the Moray group, while according to Waagstein et al. (2002), they have been dated as older, correlating to the lower Balder formation, the Flett and Vaila formation and most of the underlying Danian aged Sullom formation (Figure 2).

The Lamba formation is Late Paleocene, Selandian to Thanetian, in age. In the central parts of the Faroe-Shetland Basin it was deposited in a deep marine environment (Lamers and Carmichael, 1999) and comprised of mudstones with sandstones in the thicker, basinal sections. It is found throughout the study area except at the margins where it is removed by erosion. The maximum thickness is > 700 m (Knox et al., 1997) in the Flett Sub-basin. The lowermost part of the Lamba formation consists in many areas of a widespread volcaniclastic unit, the Kettla member.

The highest Palaeocene sedimentation rates in

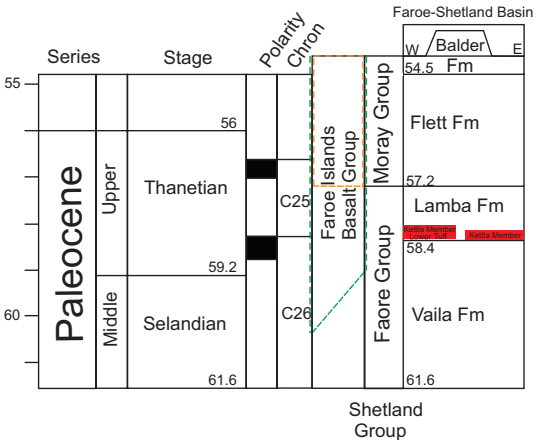

Figure 2

Simplified and modified chronostratigraphy showing the age of the Kettla member and the „Lower tuff“ (in red). Timescale: Gradstein (2012). UK lithostratigraphy: Modified from Knox et al. (1997); chronostratigraphic placement after Jolley et al. (2005), Passey and Jolley (2009), & Passey and Hitchen (2011). Faroe lithostratigraphy: Passey and Jolley (2009), Passey and Hitchen (2011) (orange dotted box), Waagstein et al. (2002), Storey et al. (2007), Mudge (2014) (green dotted box).

the basin were reached in the upper Vaila to lower Lamba interval, with input of a series of major turbiditic fans from the south and west (Ebdon et al., 1995; Jolley and Bell, 2002). The Kettla tuff member returns a prominent seismic reflection, and is sparsely offset by faults, indicating the termination of the Palaeocene rift episode (Smallwood and Gill, 2002).

The Kettla member and the „Lower tuff“

Knox et al. (1997) has described the Kettla member based on Well 214/27-2 as a type section and Well 206/2-1a as a reference section. It occurs at a similar stratigraphic level as the Andrew tuff/Glamis member or the Balmoral tuffite of the central North Sea.

The suggested age of the Kettla member is Late

Paleocene (Selandian) and it consists primarily of dark grey-green tuffaceous siltstone grading into silty tuffite. The siltstone units are often divided by a thin mudstone unit.

The member appears to have been deposited during a lowstand and rests directly on a depositional sequence boundary. It is also believed to pass northwards, eastwards and southwards into mudstone (Knox et al., 1997).

The Kettla member is one of the oldest known volcaniclastic units of the NAIP and is found in a number of wells from the Faroe-Shetland Basin. Based on three wells from the Faroe Sector (Well 6005/15-1, 6004/12-1/1z and 6004/16-1/1z) the Kettla member is a mixed volcaniclastic and siliciclastic unit in a ratio of 1:3 (Bell, 2003). The general interpretation is that the member has been deposited as debris flows and the westward thickening of the member suggests derivation from a volcanic terrain to the west of quadrants 205/206 and 214 (Knox et al., 1997). This is also supported by Jolley et al. (2005) who found a flora composition in the Kettla member referred to as the "Greenland Flora" which represents sediments from the west in a number of wells in the Faroe-Shetland Basin. This flora is associated with the volcaniclastic component of the Kettla member, but the source has yet to be identified (Jolley and Morton 2007). Heavy mineral studies of the member show low rutile:zircon (RuZi) ratios, while other Paleocene aged sandstones in the Danian Sullom, Vaila and Lamba formations derived from the Orkney-Shetland Platform to the east contain higher RuZi ratios. This indicates that there must be a different source for the Kettla member's heavy minerals, most likely from the west (Jolley and Morton 2007, Jolley et al., 2005; Morton et al., 2002).

Linnard and Nelson (2005) suggest based on in-house petrographic analysis that the Kettla "tuff" is not an air-fall deposit, as the name suggests, but that it instead might be the last major influx of basaltic washout material, prior to subsidence and the onset of fully marine conditions in the overlying Lamba formation.

According to Knox et al. (1997) the tuffaceous lithologies of the Kettla member have a characteristic low-gamma, high-velocity, high-density log signature and thus constitute a strong reflector. Additionally the unit has a high resistivity wireline log signature, and has been proposed to act as a regional pressure seal in the centres of the basin (Loizou et al., 2006 ; Knorz, M. et al. 2008).

The name of the volcaniclastic unit described below varies from the Kettla tuff to the Andrew tuff and the Kettla member in the original composite logs and reports.

In two of the Faroes Wells; Well 6004/12-1/1z and Well 6004/17-1 an additional tuffaceous sedimentary section described in the composite log and geological reports as the "Lower tuff" has been recognized below the Kettla member. In these two wells and additionally Well 6004/16-1/1z, Well 205/9-1 and Well 204/16-1 the Kettla member and the "Lower tuff"s volcaniclastic sedimentary section occur above the base of the Lamba formation, and do therefore not comprise the base of the Lamba formation as seen in other wells. The "Lower tuff's" lithology is described below together with the Kettla member.

Methodology and Data

The database consists mostly of literature, composite logs and reports from commercial drillings in the Judd- and the Flett Sub-basins. The majority of the published literature is based on research from the UK Continental Shelf (UKCS) (e.g. Jolley et al., 2005; Knox et al., 1997), while additional unpublished reports and composite logs from both Faroe and UK sector have been added to the research material.

Correlation profiles to highlight thickness and lithology were made across the Judd- and Flett-Sub basins (Figures 3 – 9). Finally a distribution- and an isopach map were produced based on well information to get an aerial overview of the member throughout the investigated basins (Figure 10).

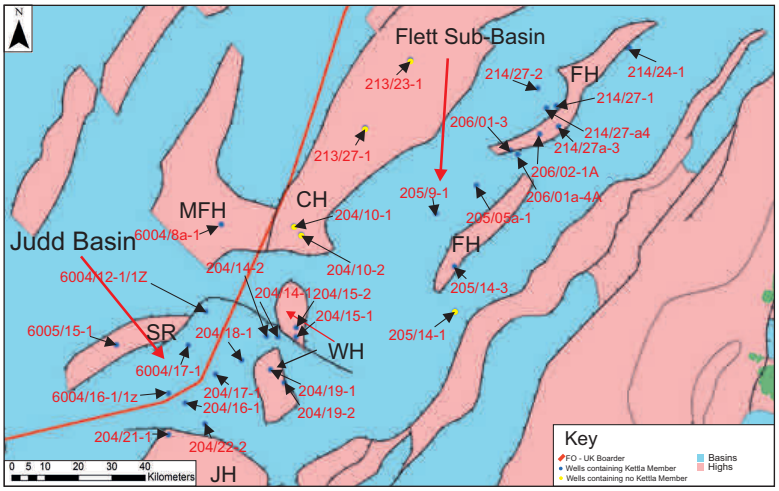

Figure 3
All included wells

Results

Well database

The Kettla member has been identified in five well from the Faroe Sector (Figure 3); 6005/15-1 (Longan), 6004/16-1/1z (Marjun), 6004/17-1 (Marimas), 6004/12-1/1z (Svínoy), and in 6004-8a-1 (Anne Marie), varying from 36 to 146.2 m in thickness. In two of the wells, Marimas and Svínoy, an additional „Lower tuff" unit similar to the Kettla member has also been identified. The thickness of the „Lower tuff" unit in Marimas and Svínoy is 52 and 67.2 m, respectively. Due to its similarities to the Kettla member it will be included for further discussion in this paper.

From the UK Sector 26 wells were picked from the Judd- and the Flett Sub-basin (Figure 3). Out of the 26 wells, 21 wells contain the Kettla member in varying thicknesses from 7 to 197 m (blue circles). The remaining 5 wells have been included in the study in order to demonstrate the limits of the unit (yellow circles). All 26 wells have been used in the distribution map (Figure 10).

All lithological description of the Kettla member are based on information from the composite logs, the geophysical logs and reports from the wells, no additional analysis have been done (Appendix 1).

For an overview of the thickness distribution and the lithology of the Kettla member in the Judd Sub-basin and the Flett Sub-basin, six correlation profiles based on composite logs and well reports were made. The profiles have been flattened at the top of the Kettla member. 18 wells from both the Faroe- and the UK sector were used when creating the profiles. Below is a detailed description of the thickness and lithology of the Kettla member based on the correlation profiles.

Thickness and distribution of the Kettla member, Faroe-Shetland Basin

Three profiles cover the Judd Sub-basin and adjacent areas; JSBCP1, JSBCP2 and JSBCP3, and three profiles cover the Flett Sub-basin and adjacent areas; FSBCP1, FSBCP2 and FSBCP3 (Figure 3).

Correlation profiles

On correlation profile JSBCP1 (Figure 4) it is clear that the Kettla member is absent at the crest of the Corona High, but thickens to almost 150 m on the Mid Faroe High. The succession on the Mid Faroe High is varied with both basalt and volcaniclastics interbedded with siliclastic components towards the base. Continuing southwestwards shows a consistently diminishing thickness, but

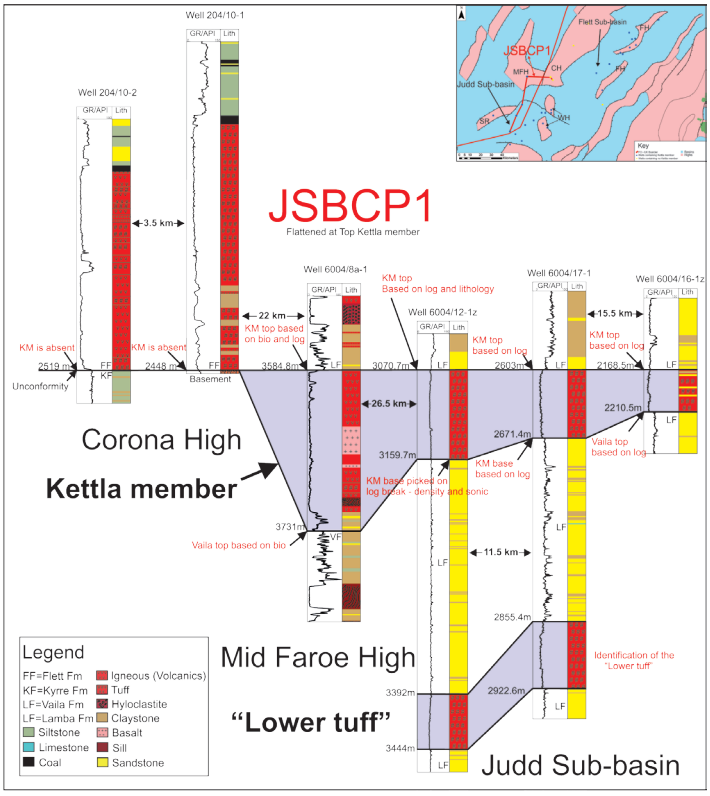

Figure 4
Detailed JSBCP1 showing the thickness and lithologies of the Kettla member in the six wells used in the profile.

also a much more uniform unit of volcaniclastic sediments. The exception is the southwesternmost well (6004/16-1/1z), where the volcaniclastic component is interbedded with siliclastic sediments. The "Lower tuff" is only found in two of the wells (6005/12-1z and 6005/17-1) and has a fairly consistent thickness (Figure 4). In both wells it is found above the base of the Lamba formation.

In correlation profile JSBCP2 (Figure 5) the Kettla member is found in all four wells. The profile crosses from the Sjúrður Ridge to the northwest of the Judd Sub-basin and continues southeastwards into the Judd Sub-basin. The lithology and thickness of the Kettla member successions in the three Judd Sub-basin wells are fairly consistent with only a slight decrease in thickness in Well 204/16-1z and some sand stringers in Well 6004/16-1/1z. On the Sjúrður Ridge the Kettla member is of a similar thickness as the three Judd Sub-basin wells, but it is more heterogeneous (Figures 3 and 5).

Correlation profile JSBCP3 (Figure 6) crosses from the Mid Faroe High southwards into the Judd Sub-basin before stopping towards the southeast on the Westray High (Figures 3 and 6). There is a clear thinning of the Kettla member throughout the profile from more than 150 m on the Mid Faroe High (Well 6008/8a-1) to 22 m on Westray High (204/19-2).

The lithology is heterogeneous on the Mid Faroe High but changes to being more homogenous in the Judd Sub-basin (6004/12-1/1z) before turning into a predominately siltstone unit interbedded with tuffs on the Westray High (204/19-2). The „Lower tuff" is only penetrated in one well.

Correlation profile FSBCP1 (Figure 7) crosses from the almost 150 m thick Kettla member on the Mid Faroe High, continues over the crest of the

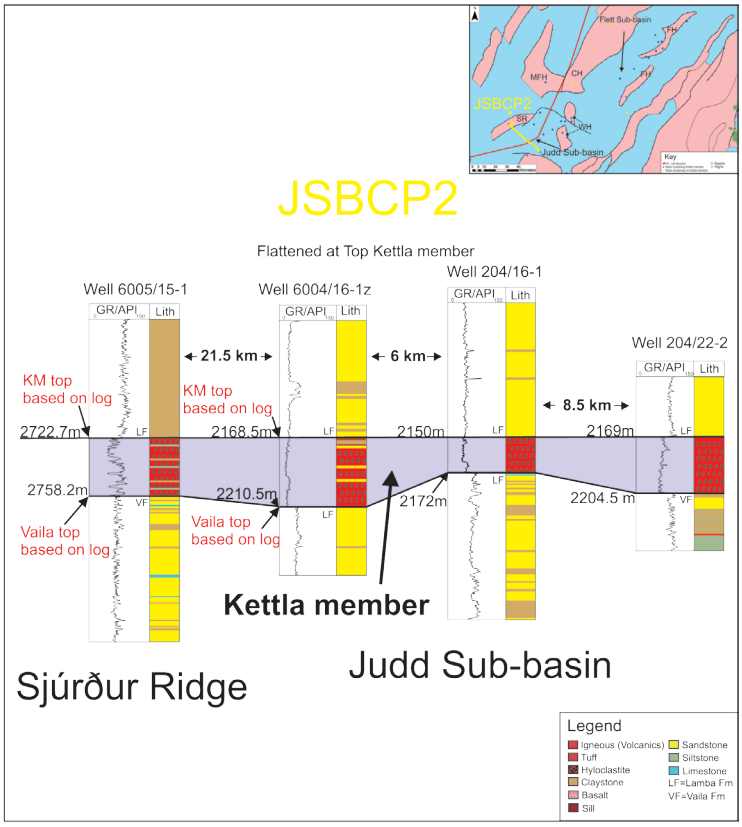

Figure 5
Detailed JSBCP2 showing the thickness and lithologies of the Kettla member in the four wells used in the profile.

Corona High where it is absent, before entering the Flett Sub-basin to the east where it is approximately 200 m thick in Well 205/09-1. The profile ends on the Flett High to the east of the Flett Sub-basin where it thins out (Figures 3 and 7).

The lithology of the Kettla member varies from being heterogeneous and dominated by volcanic material on the Mid-Faroe High to being heterogeneous but containing more siliciclastic material towards the east. No tuffs were found on the Flett High in Well 206/02-1A.

Correlation profile FSBCP2 (Figure 8) starts at the crest of the Corona High where the Kettla member is absent. Crossing eastwards into the Flett Sub-basin relatively thick units of the Kettla member appear in two wells in the centre of the basin. The lithology of the Kettla member is heterogeneous in both centre basin wells and comprised by a majority of siliciclastic material. FSBCP2's final well is on the crest of the Flett High and contains more than 50 m of the Kettla member. Again, the lithology is heterogeneous and consists largely of siliciclastic sandstones (Figures 3 and 8).

Correlation profile FSBCP3 (Figure 9) begins at the northern crest of the Flett High where the Kettla member is more than 20 m thick, the profile crosses in a southwesterly direction into the Flett Sub-basin where it increases into almost 200 m before thinning out into approximately 15 m on the Westray High (Figures 3 and 9).

The lithology of the member changes over the correlation profile from tuff dominated on the northern flank of the Flett high into silt- and claystone dominated in a southwesterly direction in the Flett Sub-basin before again being tuff dominated on Westray High (Figures 3 and 9).

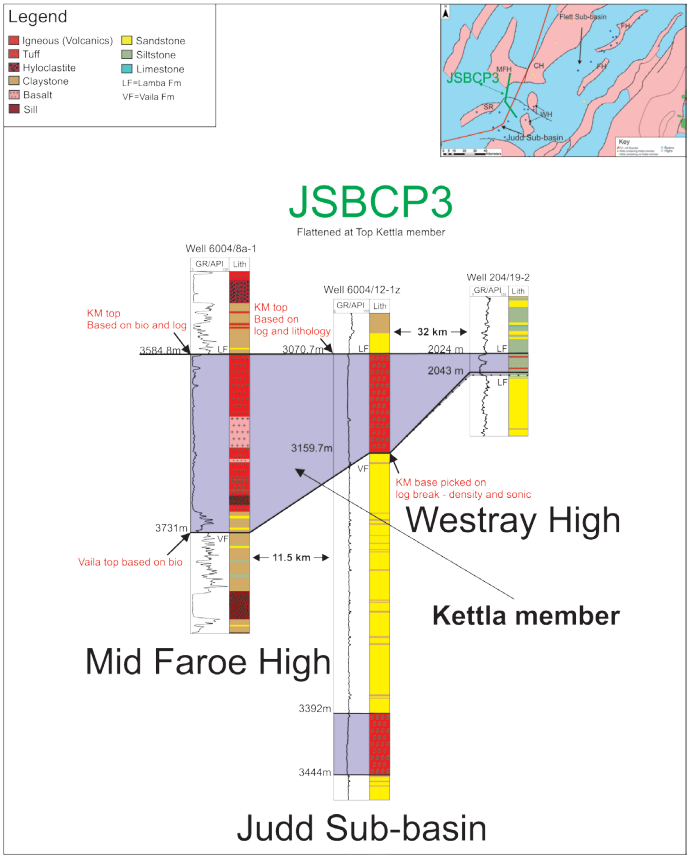

Figure 6
Detailed JSBCP3 showing the thickness and lithologies of the Kettla member in the three wells used in the profile.

Distibution and Isopach Maps

The distribution and the isopach maps (Figure 10) show the extent and the thickness of the Kettla member based on well data. On the distribution map it is clear that the Kettla member is concentrated in the Judd- and Flett Sub-basins while it is thin or absent on the Highs (Figure 10). Based on the isopach map, the Kettla member is thickest on the Mid Faroe High while it thins out towards the Judd Sub-basin towards the west. In the Flett Sub-basin the thickest units are found in the proximity of the Corona High before it thins out towards the west. The limitation of well data has to be kept in mind.

Discussion

Based on well log information from 13 wells from the UK sector and 5 wells from the Faroe Sector it is clear that the Kettla member is a heterogeneous unit which is not easy to correlate throughout the Judd- and Flett Sub-basins. The unit is often described as consisting of both volcaniclastic and siliciclastic material but sometimes as only a tuff. The GR log response reflects the same heterogeneity, but the low GR log signature divided by a peak related to a mudstone unit as seen by Knox et al. (1997), is not the most common GR signature of the Kettla member in the investigated wells, although it was recognized in four wells (Wells; 214/24-1, 206/02-1, 204/19-2 and 204/15-1 (Figures 6 and 9). In two wells a “Lower tuff” unit was found to correspond with a minor decrease in the GR log (Figure 4).

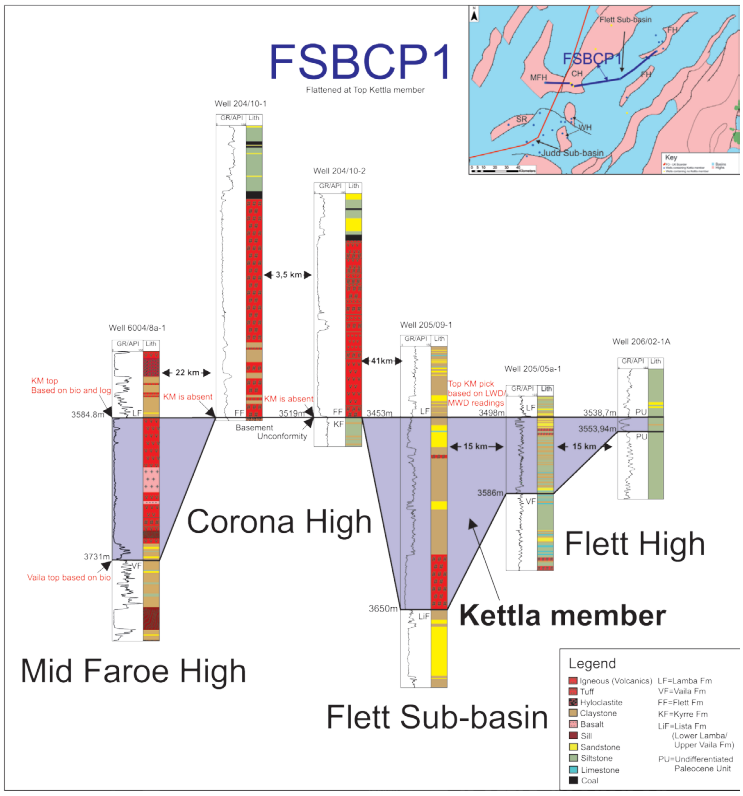

Figure 7
Detailed FSBCP1 showing the thickness and lithologies of the Kettla member in the six wells used in the profile.

In a well report based on three wells (6004/16-1/1z, 6004/12-1/1z and 6005/15-1, the first and second in the Judd Sub-basin and the third on the Sjúrður Rigde) all drilled in 2001 and south of the Mid Faroe High in the Faroes sector, the Kettla member has been described as a volcaniclastic section with a ratio of volcanic to non-volcanic as of 1:3 (Bell 2003).

Additional descriptions of the member in the well reports and the composite logs, indicate that the Kettla member often consists of volcaniclastic material which by definition has been transported by water or wind. According to Fisher and Schmincke's (1984) pyroclastic classification scheme a tuff contains 75-100 % of ash (< 2mm), up to 25 % of lapilli (2-64 mm) or up to 25 % of blocks and bombs (> 64 mm), indicating that a tuff is comprised by material ejected from an active volcano. Therefore it is possible to conclude that the Kettla section in the Faroe-Shetland Basin is not a tuff and that the Kettla member is a more accurate name.

Based on the correlation profiles presented above (Figures 4-9), it is clear that the thickest units of the Kettla member are found to the southwest and to the southeast of the Corona High, in Wells; 6004/8a-1 (< 150 m) and 205/9-1 (< 200 m), but due to large lithology differences in the member in the Judd Sub-basin verses the Flett Sub-basin, the units will be discussed separately. In the Flett Sub-basin the unit is predominately comprised by clay-, sand- and mudstones while in the Judd Sub-basin it is tuff dominated (Figures 4-9).

Judd Sub-basin

The isopach map (Figure 10b) in the Judd Sub-basin indicates that the Kettla member has

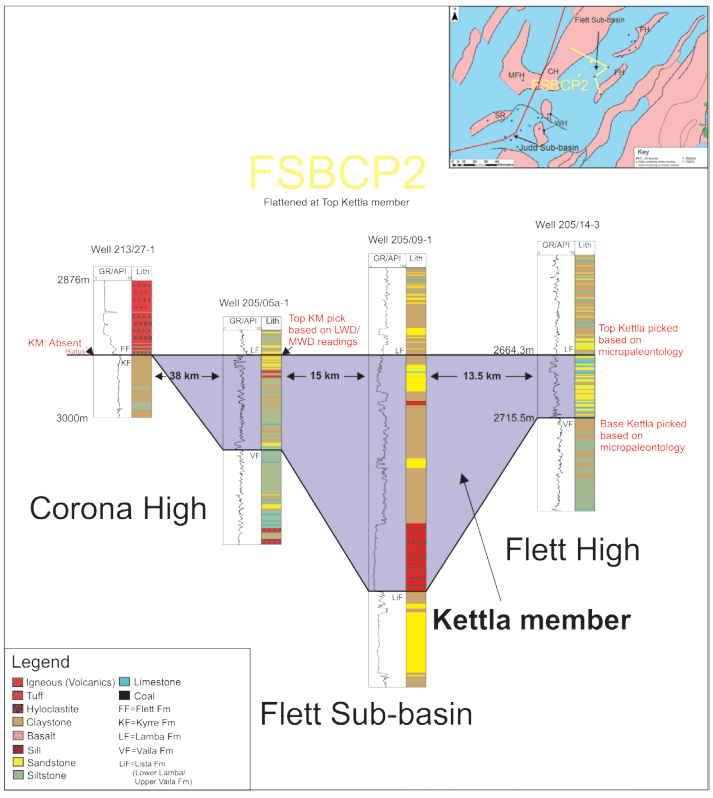

Figure 8
Detailed FSBCP2 showing the thickness and lithologies of the Kettla member in the four wells used in the profile.

been deposited as a mass flow originating from the northeast of the Judd Sub-basin. The thickness variations in the profiles, the changes from high energy facies material in Well 6004/8-1a to low energy facies in a southwesterly direction also indicate that a likely provenance area may be found to the northeast of the basin. This area could be found in the proximity of the Corona High. The source may be a volcanic centre located close to the Mid Faroe High, or possibly volcanic fissures close by. This interpretation is being supported by Jolley and Bell (2002) who state that the occurrence of mixed siliciclastic and volcaniclastic sediments in the Kettla member hints at a volcanic source more proximal to the Faroe-Shetland area than West Greenland.

The siliciclastic material found in Well 6004/8a-1 has been described as fine to medium grained, sub-angular to sub-rounded and moderately sorted, which indicates a longer travel time than the coarse grained, amorphous to sub-blocky volcaniclastic units of the member in the same well. This could indicate that the source for the siliciclastic material may be found further up the Corona High or possible from other interbasinal ridges (Ziska and Andersen, 2005). Very coarse siliciclastic material was described in Well 6004/17-1 to the southwest of Well 6004/8a-1 which could indicate several siliciclastic source areas, possible from an area to the south or southeast of the Judd Sub-basin.

In Well 6004/16-1/1z in the Judd Sub-basin, to the south/southwest of the Mid Faroe High, the combination of poor sorting but high degree of lithoclast roundings, suggests that we are in the distal part of a possible debris flow deposit, with volcaniclastic debris having been shed from the volcanic centre on or in the vicinity of the Corona

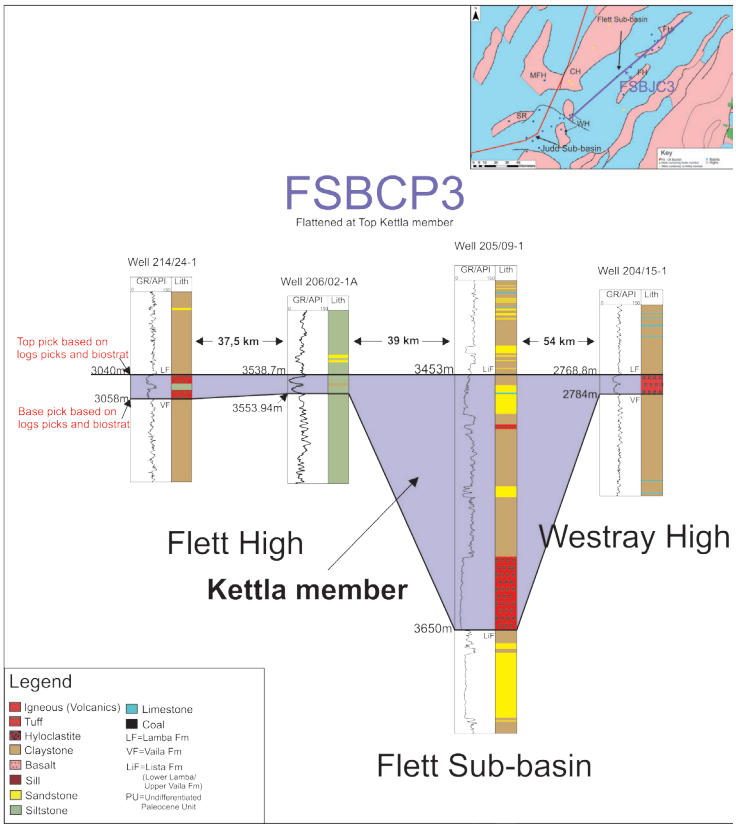

Figure 9
Detailed FSBCP3 showing the thickness and lithologies of the Kettla member in the four wells used in the profile.

High, resulting in linear aprons of debris flow type deposits, as previously noted by Knox et al. (1997) and in the Post evaluation report from Well 6004/16-1/1z (Harding, 2002).

That the Kettla member occurs as a thick unit on the Mid Faroe High raises the question about the nature of this structural high, which requires further investigation (Figure 10).

Flett Sub-basin

Overall the wells in or near the Flett Sub-basin do not contain as much tuff and other volcaniclastic material as the wells in or near the Judd Sub-basin.

The tuffaceous sandstones in Well 205/9-1 from the Flett Sub-basin are described as containing spherical lithics, which are heterogeneous and poorly-sorted, indicating the source for the tuff to be close to the well. A source west of the Corona High is unlikely because the high most likely acts as a barrier. A possible source area might instead be in or near to the Corona High. This is supported by the isopach map which indicates that the source area most likely can be found to the west of the Flett Sub-basin.

The siliciclastic mudstones found in Well 205/9-1 are described as homogeneous, silty and containing very fine quartz, which could also indicate a long transport time, possibly from the south. Jolly and Morton (2007) suggest derivation of the siliciclastic component from predominately gneissic basement.

In Well 205/05-1a the siliciclastic sandstones are described as fine- to medium-grained, moderate sorted, sub-rounded to sub-angular indicating transport, although possibly not as far as the silici-

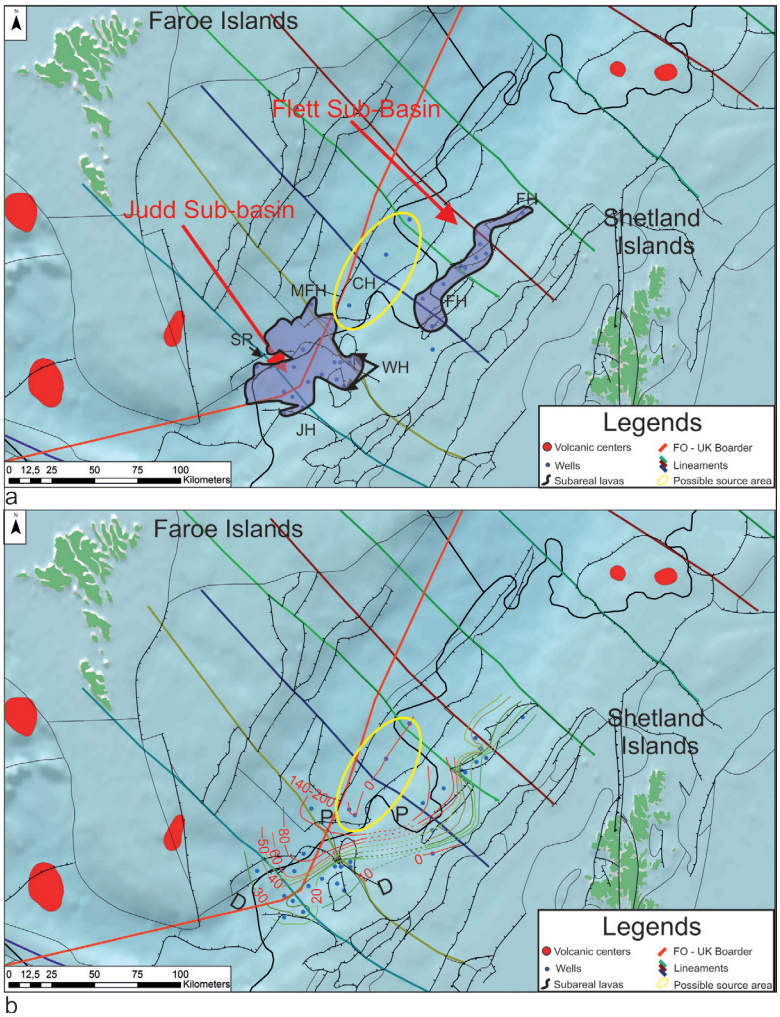

Figure 10
a) The upper map shows the horizontal distribution of the Kettla member based on well information. b) The lower isopach map shows the thickness distribution of the member. The yellow circle on both maps is the possible source area for the volcanic components of the Kettla member. P stands for proximal and D for distal based on thickness and the reworked nature of the material.

clastic sediments in Well 205/9/1. The tuffs are described as pale steel grey to blue grey, mottled, soft, crumbly with deformed shards with an ashy matrix containing abundant white clay, indicating it is an ash and not a debris flow deposit like the epi-volcaniclastic components. This also indicates volcanic eruption close by during time of deposit.

Paleogeography and Timing

If the Kettla member in the Judd Sub-basin is a mass deposit flow there may have been high relief of the source area, alternatively result of a delta front failure sourcing re-deposited material. The Sneis formation onshore the Faroe Islands is believed to be a mass deposit (Passey and Jolley 2009) and could be used as a litological analogue of the Kettla member.

The stratigraphic position of the Kettla member, at the base or the near-base of the Lamba formation, places it in upper Paleocene time. The volcanic material in the Kettla member does therefore indicate volcanic activity in the vicinity of the Corona High within the Faroe-Shetland Basin during earliest Thanetian and possibly Selandian times.

Conclusions

- The Kettla tuff/member, also referred to as the Andrew tuff/member or Balmoral tuffite, is not entirely a tuff. It is a partly volcaniclastic partly silisiclastis unit which contains tuffs.
- Differences in the lithology of the Kettla member between the Judd- and Flett Sub-basins, indicate that the Kettla member in the two basins may have different sources.
- Stratigraphic thickness, grain size and the reworked components of the volcaniclastic sediments in the Kettla member in the Judd Sub-basin indicate a proximal source to Well 6004/8a-1 and 6004/12-z most likely close to the Corona High.
- The Kettla member in the Judd Sub-basin has most likely been deposited as a debris flow (Harding, 2002) and (Knox et al., 1997).
- In the Flett Sub-basin the source is most likely close to Well 205/9-1, possible from near the Corona High, which may have acted as a barrier for the volcanic material from the Mid Faroe High area.
- The siliciclastic material in both the Judd- and the Flett Sub-basin may originate from the interbasinal ridges.
- The stratigraphic position and the different volcanic lithologies of the Kettla member indicate that there has been volcanic activity in the Faroe-Shetland Basin in the earliest Thanetian, possible earlier.

Further research

There are still many unsolved issues concerning the early stages of volcanism in the Faroe-Shetland Basin, and one way of getting more answers would be to systematically look closer at all well penetrations in the basin in order to establish the first traces of volcanism. Cores, side-wall cores and cuttings could be used for further analytic research in order to try and establish the possible origins and age of the volcanic material and if there is more than one source to the volcanic components of the Kettla member in the Judd- and Flett Sub-basins. This way it will be possible to map a paleogeographical environment of the early volcanism in the Faroe-Shetland Basin, a key issue in the hydrocarbon exploration in the area.

Acknowledgements

First of all I would like to thank Jarðfeingi for giving me access to the well data that form the base of this literature research. Additionally I would like to thank my co-author and colleagues at Jarðfeingi for always being there when needed.

Appendix 1

Thickness and lithology of the Kettla member, Faroe-Shetland Basin

Faroe Sector

Well 6004/8a-1

In Well 6004/8a-1 the Kettla member is named the Kettla member equivalent. It was identified as a 146.2 m thick tuffaceous and basaltic section. The unit is heterogeneous and the top and base of the unit were picked based on log response and biostratigraphic analysis. From the base it has been described to consist of approximately 18 m of claystones and sandstones with a thin string of limestone approximately 9 m from the base. These sandstones have in the composite log been described to contain loose quartz grains predominately very fine- to fine-grained, sub-rounded, sub-spherical and moderately sorted. The overlying 40 m consist of volcanic material, hyaloclastites and tuff, before an approximately 3 m thick basalt unit. Above the basalt unit more volcanic material makes up the next approximately 9 m followed by another 25 m of basalt. From the top of the second basalt unit to the top of the member the remaining approximately 50 m are described as volcanic material. The Gamma Ray (GR) log response shows a clear decrease in API units at the top of the unit and it becomes more variable shortly before increasing at the base of the unit (Figures 4, 6 and 7). The formation consists of coarse-grained volcaniclastics at the

top grading downwards to tuffaceous siltstone. The coarse-grained volcaniclastics have a light to dark grey colour; they are mainly homogeneous, sub-blocky and soft to firm. In parts they are grading into light grey, firm to moderately hard, brittle flaked tuff.

The tuffaceous claystones, which are found at the top of the section, and most likely only appear as claystones due to bit action (Composite log), are medium dark grey to dark grey, grey to black grey to greyish black, dark greenish black to greenish black, brownish grey to olive grey, soft to firm, amorphous to sub-blocky, slightly silty occasionally grading to siltstone, slightly sticky, calcareous with occasional traces of muscovite. The sandstone is clear to translucent, fine- to medium-grained, sub-angular to sub-rounded and moderately sorted. The identified limestone is very light grey to yellowish grey, milky white soft to firm, amorphous to sub-blocky, argillaceous, microcrystalline and the basalt is dark grey to black, hard, sub-blocky, fine crystalline, slightly glassy. Minor amounts of tuffaceous claystone and coal were also found within the unit in the well (Hutchings, S. and Eynon 2011).

Well 6004/12-1/1z

In Well 6004/12-1/1z the Kettla member is 89 m thick and has been described as extrusive igneous material containing e.g. tuff, pale green to medium green to grey green, soft, blocky, silty, slightly calcareous. The top and base were identified by log response, particularly the density and sonic logs, but also on lithology. In Bell (2003) the unit consists of various volcaniclastic lithologies. The GR log response does not show any clear indication of decrease in API (Figures 4 and 6).

The "Lower tuff" was also identified in Well 6004/12-1/1z with a thickness of 52 m. It is compositionally similar to the Kettla member's tuffaceous sandstone rock type, but differs in that calcite is also present. The GR response shows a minor decrease through the "Lower tuff" (Figures 4 and 6).

The "Lower tuff" is pale grey, has a moderate hardness, is heterogeneous with fine to medium igneous clasts and is also sandy.

In this well the "Lower tuff"does not occur at the base of the Lamba formation which continues for approximately 75 more m before entering the Vaila formation.

Well 6005/15-1

In Well 6005/15-1 the Kettla member was encountered as a 36 m thick unit described as a tuff interfingered with thin units of clay and siltstone. Top and base were picked based on log response. The GR shows a decrease at the top and a peak at the base, but is not consistently low throughout the section. The section is heterogeneous and does contain mud and siltstone stringers (Figures 4 and 5). The tuff is described to be dark grey to greenish black, fine to medium grained with dark green fragments in a grey matrix. It is firm, crumbly and sandy. The siltstone/claystone is medium dark grey, silty, firm, and blocky (Hovden et al.).

Well 6004/16-1/1z

In Well 6004/16-1/1z the Kettla member is 42 m thick and consists of volcaniclastic sandstone with vesicular shards of palagonitised basaltic glass and degraded crystalline basalt in clay/zeolite cement. The basal 12 m are described as a tuff while the remaining 30 m are described as tuff interfingered with sandstones and claystones. Top and base of the Kettla member were picked on log response, where the GR shows a minor decrease at the top of the unit and a major increase at the base (Figures 4 and 5).

The coarser, poorly sorted volcaniclastic siltstones and sandstones comprise a high proportion of well-rounded lithoclasts of basaltic material (Harding et al.).

Well 6004/17-1

In Well 6004/17-1 the Kettla member is 68.4 m thick and consists of a green black to dark green grey, mottled, poorly indurated, crumbly, sandy tuff, with coarse well-rounded volcanic sands. Again the top and base of the unit were picked on log response where the GR is low through the unit compared to the under- and overlaying units. In the composite log the whole section is described

as a tuff, but in the Final well report the Kettla member has been described as a tuff containing intra tuff-sand and claystones. The sandstones are described to be medium grey to pale to red brown, very fine to very coarse, sub-spherical, loose, arkosic and slightly micaceous, while the claystones have been described as medium to dark grey, brownish grey, blocky, poorly to moderately indurated, slightly silty and occasionally tuffaceous.

The „Lower tuff" was identified in this well as a 67.2 m thick dark green grey to green black, mottled, crumbly, poorly indurated and sandy tuff, similar to the Kettla member. The GR log response shows a decrease through the „Lower tuff" (Figure 4) (Well 6004/17-1 – Final Well Geological Report). Below the „Lower tuff" the Lamba formation continues for another approximately 30 m before entering the Vaila formation (Figure 4) (ENI UK Limited 2003 and Composite log).

UK Sector

Well 204/10-1 and 2

Well 204/10-1 and 2 have been taken into account in this article due to the absence of the Kettla member in the wells. Both wells are located on the Corona High (Composite logs) (Figures 4 and 7). Well 204-10-1 penetrates tuffs identified as the Flett formation which rest unconformably on the Cretaceous Kyrre formation and in Well 204/10-2 the tuffs interfinger a basalt unit of most likely Late Paleocene age.

Well 204/15-1

In Well 204/15-1 the Kettla member (in the composite log referred to as the Kettla tuff) was encountered as a 21 m thick unit and has been described as a green black, earthy, firm, blocky, silty and very fine tuff. The GR log response shows a distinctive decrease at the top with a slight increase in the middle of the unit (Composite log) (Figure 9).

Well 204/16-1

The Kettla member (in the composite log referred to as the Kettla tuff) is identified in Well 204/16-1 as a 22 m thick unit and has been described as a dark greenish grey to greenish black tuff. It is speckled with mottled dark brown to pale grey feldspar fragments, firm to moderately hard, subblocky to blocky, commonly friable with traces of mica and glauconite and occasionally very hard with traces of pyrite. It is described as a non-calcareous but in places slightly calcareous tuff (Composite log). The GR log response is low throughout the unit (Figure 5).

Well 204/19-2

In Well 204/19-2 the Kettla member (in the report referred to as the Andrew member) was identified as a 19 m thick section consisting of tuffaceous siltstone and sandstone divided by a mudstone which has a low gamma ray signature in the tuffaceous sections and a higher gamma ray signature in the mudstone. The gamma ray response does not change dramatically until approximately 2 m below the log pick of the base of the unit (Figure 6).

Well 204/22-2

The lithology description is based on side wall cores with moderate recovery. The mudstone is medium to dark grey, crumbly, silty, fine to medium quartz, non-calcareous and non-swelling. The sandstone contains quartz, it is argillaceaus, friable, fine, well-sorted and grading into siltstones in parts. The siltstone also contains quartz. It is medium to dark grey, crumbly, fine, argillaceaus, non-calcareous and non-swelling. The GR log response shows a clear decrease at the top and base of the unit, with an increasing peak approximately in the middle of the unit corresponding with the claystone unit (Composite log) (Figure 6).

In Well 204/22-2 the Kettla member (in the Composite log referred to as the Andrew tuff) was identified with a thickness of 35.5 m. It has a distinctively low gamma gay response compared

to the surrounding units. The Kettla member is described in the composite log as a light grey, pale bluish grey tuff. It is also described as very firm, blocky, homogeneous but with a silty texture and a common brown silty lamination, which locally contains very fine sand grains. It is non-calcareous but very fine crystalline inclusions are common. The GR log response shows a clear decrease through the whole unit (Composite log) (Figure 5).

Well 205/05a-1

In Well 205/05a-1 the Kettla member has a thickness of 88 m. In the composite log the unit is divided into two parts with the top 81 m referred to as the Kettla Superior and the baseal 7 m as the Kettla Inferior. The main lithology of the member is predominately siliciclastic silt- and claystones, but silty sandstones were also encountered. From the base of the unit the sandstones are interfingering with the silt- and claystones, and towards the top 2 m thin tuff units are described in the composite log. Throughout the unit four approximately 1 m thick limestone stringers appear. The unit is heterogeneous. The GR log does show a decrease at the top of the unit as well as an increase at the baset, but is otherwise heterogeneous throughout. The siltstone and the sandy siltstone is described as medium grey occasionally brownish grey, soft to occasionally firm, crumbly, predominantly calcareous, disseminated pyrite, carbonaceous/coal flecks, feldspathic grains, sandy with rare to locally occasional ashy/tuffaceous texture. The sandstones are described to be fine to medium, moderately sorted, sub-rounded to sub-angular while the tuff has been described as pale steel grey-blue grey, mottled, soft, crumbly, ashy, containing abundant white clay (Composite log) (Figures 7 and 8).

Well 205/9-1

In Well 205/9-1 the Kettla member (in the composite log referred to as the Andrew tuff) is identified as a 197 m thick unit consisting of mudstone interfingered with thin tuff units grading into tuffaceaos sandstone. The mudstone has been described in the composite log as a light grey, occasionally medium grey, soft occasionally firm, crumbly to blocky. It is homogeneous, silty and contains very fine quartz. The GR log response shows a minor decrease at the top of the unit, but is generally heterogeneous (Composite log) (Figures 7 – 9).

The basal 56 m of the unit is described as a tuff on the composite log. The tuff is overlain by a 90 m thick unit of claystone, which is divided by at sandstone unit. The claystone unit is overlain by a 6-7 m thick tuff, which again is overlain by a 9 – 10 m thick claystone. On top of the claystone unit a sandstone of about 14-15 m appears which again is overlain by an approximatly 1 m thin unit of limestone, which again is overlain by a 5 m thick sandstone. At the top of the unit there is an approximate 7 m thick unit of claystone (Figures 7 – 9).

The tuffaceous sandstones are described to contain rounded spherical lithics, medium to dark in colour, speckled, moderately hard, blocky, heterogeneous, vesicular poorly sorted, well cemented with poor to moderate visible porosity (Composite log).

Well 205/14-1

Well 205/14-1 also demonstrates the absent of the Kettla member as described by Loizou et al. (2005).

Well 205/14-3

In Well 205/14-3 the Kettla member (in the composite log referred to as the Kettla tuff) is 51.2 m thick and predominantly comprised of sandstones. Minor silty claystones and rare thin limestone stringers were found. The sandstone has been described as medium to light grey, brownish grey, colourless to white with quartz grains, silty to very fine, sub-angular, soft to firm, moderately to poorly sorted, friable. It contains very calcareous cement, with common muscovite and biotite micas. It is locally argillaceous and grades to grey silty claystone but no tuffs are described

in this unit. The light grey limestone was soft to firm, cryptocrystalline and argillaceous. The GR response shows a minor decrease at the top and a minor increase at the base of the unit, but is otherwise not different from the surrounding units (Composite log) (Figure 8).

Well 206/2-1A

Well 206/2-1A penetrated a 15.24 m thick unit of the Kettla member which in the composite log is referred to as the Kettla tuff. Based on the lithology description in the composite log, the unit is a siltstone divided by a thin claystone, which is also reflected in the gamma ray log response, where the log shows a clear decrease in the top and base units of the member, divided by a peak when penetrating the claystone (Composite log) (Figures 7 and 9).

Well 213/27-1z

In Well 213/27-1z the Kettla member is absent. Like 204/10-1 and 2, the well has been included to show the limit of the Kettla member's distribution where this is possible. The well is also situated on the Corona High and TD's in Carboniferous sediments. At the stratigraphic level where the Kettla member would be expected there is a hiatus in the well (Composite log) (Figure 8).

Well 214/24-1

In Well 214/24-1 the Kettla member (in the composite log also referred to as the Erlend/Andrew tuff) is 18 m thick. The unit consists of two tuff units divided by a siltstone, which is also reflected in the gamma ray response (Figure 9). In the Well Report, the unit is described as the Andrew tuff and is described as a claystone, which is white-light grey, occasionally light brown, containing loose angular coarse quartz grains, is moderately hard, miceceous, argillaceous, carboneceous, glauconitic, grading into sandstone. The sandstone is described as very fine to fine grained, sub-rounded, sub-sperhical, moderately well sorted, calcitic and dolomitic cement with no visible porosity. The top and base Kettla were picked by logs, and there is a clear decrease on the GR log at the top and base of the unit. Approximately in the middle of the unit there is a siltstone unit which correlates with an increase on the GR log (Composite log, Garden et al. 1998) (Figure 9).

References

Bell, B. R., 2003, Report: Lithostratigraphic Correlation between Wells 6005/15-1 (Longan), 6004/16-1/1z/1Z (Marjun) & 6004/12-1/1Z (Svinoy), Faroe-Shetland Basin.

Coffin, M. F. E., O., 1992, Volcanism and continental break-up: a global compilation of large igneous provinces, Geological Society Special Publications, 17-30 p.:

Doré, A. G., Lundin, E. R., Jensen, L. N., Birkeland, Ø., Eliassen, P. E., and Fichler, C., 1999, Principal tectonic events in the evolution of the northwest European Atlantic margin, *in* Fleet, A. J., and Boldy, S. A. R., eds., Petroleum Geology of Northwest Europe: Proceedings of the 5th Conference: London, Geological Society, p. 41-61.

Ebdon, C. C., Granger, P. J., Johnson, H. D., and Evans, A. D., 1995, Early Tertiary evolution and sequence stratigraphy of the Faeroe-Shetland Basin: implications for hydrocarbon prospectivity, *in* Scrutton, R. A., Stoker, M. S., Shimmield, G. B., and Tudhope, A. W., eds., The Tectonics, Sedimentation and Palaeoceanography of the North Atlantic Region, Volume 90: London, Geological Society, p. 51-69.

Ellis, D., Bell, B. R., Jolley, D. W., and O'Callaghan, M., 2002, The stratigraphy, environment of eruption and age of the Faroes Lava Group, NE Atlantic Ocean, *in* Jolley, D. W., and Bell, B. R., eds., The North Atlantic Igneous Province: Stratigraphy, Tectonic, Volcanic and Magmatic Processes, Volume 197: London, Geologial Society, p. 253-269.

ENI UK Limited, 2003, Final Well Geological Report, Marimas Prospect.

Fisher, R. V., and Schmincke, H.-U., 1984, Pyroclastic Rocks, Berlin, Springer-Verlag.

Garden, A.S. and Waller, M., 1998, 214/24-1 – End of Well Report.

Harding, A., Smallwood, J, Sorensen, M, 2002, Well 6004/16-1/1z & 1Z Marjun Faroes License 001 Post Well Evaluation Report, Amerada Hess, p. 232.

Harding, A., Smallwood, J. and Sorensen, M., 2002, Well 6004/16-1/1z – Marjun – Faroes Licence 001 – Post Well Evaluation Report.

Hovden, Ø., Joma, I. and Holm, I, 2002, Final Well Report Well 6005/15-1, Longan.

Hutchings, S. and Eynon, M., 2011, Geological Final Well Report – Well 6004/8a-1 – Anne-Marie Prospect.

Jolley, D. W., and Bell, B. R., 2002, The evolution of the North Atlantic Igneous Province and the opening of the NE Atlantic rift, *in* Jolley, D. W., and Bell, B. R., eds., The North Atlantic Igneous Province: Stratigraphy, Tectonic, Volcanic and Magmatic Processes, Volume 197, Geological Society, London, Special Publications, p. 1-13.

Jolley, D. W., Morton, A., and Prince, I., 2005, Volcanogenic impact on phytogeography and sediment dispersal patterns in the NE Atlantic, *in* Doré, A. G., and Vining, B. A., eds., Petroleum Geology: North-West Europe and Global Perspectives—Proceedings of the 6th Petroleum Geology conference, Volume 1: London, Geological Society, p. 969-975.

Jolley, D.W. and Morton, A. 2007, Understanding basin sedimentary provenance: evidence from allied phytogeographic and heavy mineral analysis of the Palaeocene of the NE Atlantic: Journal of the Geological Society, London, Vol. 164, 2007, pp. 553–563.

Knorz, M., Bernigolle, B., Manfredini, D., Holm, G. and Chevallier, B., 2008, Tormore – 205/5A1 – Final Well Report WOS Exploration Well.

Knox, R. W. O. B., Holloway, S., Kirby, G. A., and Bailey, H. E., 1997, Stratigraphic Nomenclature of the UK North West Margin. 2. Early Paleogene Lithostratigraphy and Sequence Stratigraphy, Nottingham, British Geological Survey.

Lamers, E., and Carmichael, S. M. M., 1999, The Paleocene deepwater sandstone play West of Shetland, *in* Fleet, A. J., and Boldy, S. A. R., eds., Petroleum Geology of Northwest Europe: Proceedings of the 5th Conference, Volume 1: London, Geological Society, p. 645-659.

Larsen, M., Hamberg, L., Olaussen, S., Norgaard-Pedersen, N., and Stemmerik, L., 1999, Basin evolution in southern East Greenland: An outcrop analog for Cretaceous-Paleogene basins on the North Atlantic volcanic margins: Aapg Bulletin-American Association of Petroleum Geologists, v. 83, no. 8, p. 1236-1261.

Larsen, M., and Withham, A. G., 2005, At the edge of a new ocean: post-volcanic evolution of the Palaeogene Kap Dalton Group, East Greenland, *in* Doré, A. G., and Vining, B. A., eds., Petroleum Geology: North-West Europe and Global Perspectives—Proceedings of the 6th Petroleum Geology Conference, Volume 1: London, Geologica Society, p. 923-932.

Linnard, S., and Nelson, R., 2005, Effects of Tertiary Volcanism and later Events upon the Faroes Hydrocarbon system, *in* Ziska, H., Varming, T., and D., B., eds., Faroe Islands Exploration Conference Proceedings of the 1st Conference: Tórshavn, Føroya Fróðskaparsetur, p. 44-53.

Loizou, N., Andrews, I. J., Stoker, S. J., and Cameron, D., 2006, West of Shetland revisited: the search for stratigraphic traps: Deliberate Search for the Stratigraphic Trap, v. 254, p. 225-245.

Morton, A. C., Boyd, J. D., and Ewen, D. F., 2002, Evolution of Paleocene sediment dispersal systems in the Foinaven Sub-basin, west of Shetland., *in* Jolley, D. W., and Bell, B. R., eds., The North Atlantic Igneous Province, Tectonic, Volocanic and Magmatic Processes., Volume 197: London, Geological Society, p. 69-93.

Passey, S. R., and Jolley, D. W., 2009, A revised lithostratigraphic nomenclature for the palaeogene Faroe Islands basalt Group, North

Atlantic: Eart and Environmental Science Transaction of the Royal Society of Edinburg, v. 99, p. 127-158.

Ritchie, J. D., Gatliff, R. W., and Richards, P. C., 1999, Early Tertiary magmatism in the offshore NW UK margin and surrounds, *in* Fleet, A. J., and Boldy, S. A. R., eds., Petroleum Geology of Northwest Europe: Proceedings of the 5th Conference: London, Geological Society, p. 573-584.

Saunders, A. D., Fitton, J. G., Kerr, A. C., Norry, M. J., and Kent, R. W., 1997, The North Atlantic Igneous Province, *in* Mahoney, J. J., and Coffin, M. L., eds., Large Igneous Provinces: Continental, Oceanic, and Planetary Flood Volcanism, Volume 100, American Geophysical Union, Geophysical Monographs, p. 45-93.

Smallwood, J. R., and Gill, C. E., 2002, The rise and fall of the Faroe-Shetland Basin: evidence from seismic mapping of the Balder Formation: Journal of the Geological Society, London, v. 159, p. 627-630.

Stoker, M. S., and Varming, T., 2011, Cenozoic (sedimentary), *in* Ritchie, J. D., Ziska, H., Johnson, H., and Evans, D., eds., Geology of the Faroe-Shetland Basin and adjacent areas: Keyworth, Nottingham, UK: British Geological Survey and Tórshavn, Faroe Islands: Jarðfeingi, p. 151-208.

Waagstein, R., Guise, P., and Rex, D., 2002, K/Ar and $^{39}Ar/^{40}Ar$ whole-rock dating of zeolite facies metamorphosed flood basalts: the upper Paleocene basalts of the Faroe Islands, NE Atlantic, *in* Jolley, D. W., and Bell, B. R., eds., The North Atlantic Igneous province: Stratigraphy, tectonic, Volcanic and Magmatic Processes, Geological Society of London, p. 219-251.

White, R. S., and McKenzie, D., 1989, Magmatism at rift zones: the generation of volcanic continental margins and flood basalts: Journal of Geophysical Research, v. 94, no. B6, p. 7685-7729.

Ziska, H., 2012, Fracture orientations onshore Faroe Islands (North Atlantic); evidence for dual rifting episodes in the Palaeogene, *in* Varming, T., Ziska, H., ed., Faroe Islands Exploration Conference Proceedings of the 3rd Conference, Volume 3: Tórshavn, Fróðskapur, p. 40-58.

Ziska, H., and Andersen, C., 2005, Exploration Opportunities in the Faroe Islands, *in* Ziska, H., Varming, T., and Block, D., eds., Faroe Islands Exploration Conference Proceedings of the 1st Conference: Tórshavn, Føroya Fróðskaparsetur, p. 146-162.

Plagioclase mineral chemistry in the Faroe Islands Basalt Group

B. DAHREN[1], V.R. TROLL[1], A.K. BARKER [1], F.C. MEADE[1], C. FREDA[2], P.M. HOLM[3], N. SØAGER[4]

1: CEMPEG, Department of Earth Sciences, Uppsala University. Villavägen 16, Uppsala 752 36, Sweden
2: Istituto Nazionale de Geofisica e Vulcanologia, Via di Vigna Murata 605, 00143 Rome, Italy
3: Geological Institute, University of Copenhagen, Geocenter Copenhagen, DK-1350, Copenhagen, Denmark
4: GEOMAR Helmholtz Centre for Ocean Research Kiel, 24148 Kiel, Germany

*Corresponding author: borje.dahren@geo.uu.se, +46 18 471 2557

Abstract

The published literature on the Faroe Islands Basalt Group (FIBG) contains a large number of of whole rock (bulk) chemical analyses, but there is an obvious dearth of mineral chemical data. Plagioclase is the dominant phenocryst phase in the FIBG lavas, and is widely used to help constrain magmatic processes and magma storage conditions. The present study aims to rectify the paucity of plagioclase compositional information for the FIBG by systematically examining compositions of plagioclase feldspar from a series of representative basaltic rock samples. We present analysis of 92 individual plagioclase crystals from 18 stratigraphically constrained rock samples, and provide 663 new mineral spot analyses. The range of anorthite contents of plagioclase from the FIBG have a notably bimodal distribution and can be separated into two dominant populations, one with ~An_{60-80} and another with ~An_{80-90}. Remarkably, each of the analysed rock samples contains plagioclase of one population only. The two compositional plagioclase groups in the FIBG likely represent two distinct magma storage regions, where the higher anorthite plagioclase group corresponds to a deep and likely hotter zone of crystallisation, while the lower anorthite plagioclase formed under a shallower and probably cooler regime in the mid- to upper crust beneath the current Faroe Islands.

Faroe Islands Exploration Conference: Proceedings of 4th Conference.
Annales Societatis Scientiarum Færoensis Supplementum LXIV.

Introduction

The opening of the North Atlantic Ocean in the early Paleogene resulted in extensive volcanism as recorded in the thick basalt piles and extinct volcanic centres in e.g. the Faroe Islands, Greenland, Scotland and Ireland. The Faroe Islands Basalt Group (FIBG) is associated with the early Icelandic hot spot (55 Ma) and with decompressional melting that followed the breakup of the North Atlantic (White and McKenzie, 1989; Holm *et al.*, 1992). Geophysical surveys show that the FIBG is up to 6 km thick (Richardson *et al.*, 1998), of which a large portion can be observed onshore and through the LOPRA drill holes (Ellis *et al.*, 2002). This extrusive sequence is underlain by ~30 km of Archean continental crust, the base of which appears to be underplated by several kilometres of mafic intrusives (Richardson *et al.*, 1998). The Archean crust is likely overlain by a sedimentary succession deposited prior to the onset of the Paleogene volcanism, though there is no direct evidence for these sedimentary rocks in outcrop. The influence of this crustal setting on the development of the Paleogene basalt groups has, as of yet, not been thoroughly explored from a mineral perspective. Here, we present a first systematic characterisation of plagioclase mineral compositions from the FIBG, the dominant mineral phase within these basalts, and provide a first order assessment of the pre-eruptive magmatic processes and magma storage conditions.

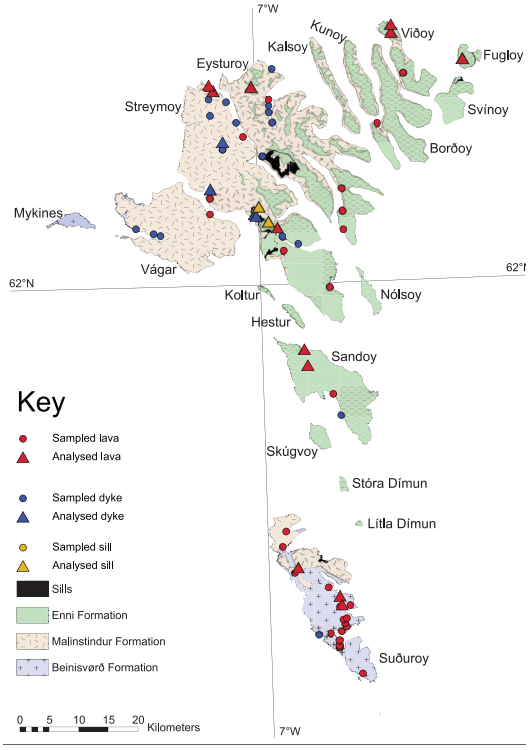

Figure 1
Geological map of the Faroe Islands (modified after Passey and Bell, 2009) with sample locations from our 2011 field campaign marked. Seven samples collected by Søager and Holm (2009, 2011) have been integrated into our dataset, and also shown on the map. The samples analysed for this study are indicated by triangles.

Methods

Lavas, dykes and sills of the FIBG were sampled in June 2011, targeting particularly fresh and porphyritic rocks with abundant plagioclase. The focus was on rocks with a low degree of alteration and low secondary mineralisation (e.g. no zeolites) to ensure investigation of primary magmatic mineral compositions. The three major stratigraphical units of the FIBG, the Beinisvørð, the Malinstindur and the Enni formations as defined in Passey and Jolley (2009), were sampled to provide a chronological record through the exposed volcanics. The lava samples were complemented by a selection of cross-cutting dykes and sills, and by a set of lava samples provided by the University of Copenhagen, which largely belong to the suite studied in Søager and Holm (2009). A total of 12 lavas, 4 dykes and 2 sills were analysed for this study. All sample localities are displayed in Figure 1 and the samples used belong to both the Low-Ti and the High-Ti groups (cf. Søager and Holm, 2009, 2011).

Plagioclase mineral compositions from lavas, dykes and sills within the FIBG were analysed by the Field Emission Gun Electron Probe Micro-

analyser (FEG-EPMA) facility at the Centre for Experimental Mineralogy, Petrology and Geochemistry (CEMPEG), Uppsala University, Sweden, using a JEOL JXA 8530F Hyperprobe. The FEG-EPMA analyses were run by WDS using an accelerating voltage of 15 keV and a current of 10 nA. Elemental mapping was performed by Wavelength Dispersive X-ray Spectroscopy (WDS) using a 4 µm beam and an accelerating voltage of 15 keV.

The following mineral standards and pure element oxides were used for calibration: Si, Ca – wollastonite, Na – albite, K – orthoclase, Al – Al_2O_3, Mg – MgO, Fe – Fe_2O_3. All elements were analysed by Kα spectral lines. Counting times of 10 seconds for peak positions and 5 seconds for upper and lower background were applied. The analysed WDS data set is based on 92 individual plagioclase crystals and a total of 663 spot analyses.

„For further detail, see Barker et al. (in press)."

Plagioclase petrography and composition

An overview of the plagioclase crystals in our samples was achieved using qualitative and visual techniques (petrographic microscope, BSE imaging, EDS analyses and WDS elemental mapping). Plagioclase occurs frequently as large phenocrysts in the Faroe island basaltic rocks and is usually present as smaller microcrysts in the groundmass (Fig. 2). The phenocrysts selected for investigation in this study are subhedral to euhedral and can be up to 20 mm in size, but are most commonly between 2 and 5 mm. There are no clear textural groupings amongst the studied plagioclase phenocrysts, and individual crystals may display any combination of the textures described below. Most crystals are isolated, but the occasional glomerocryst has been observed (e.g. Fig. 2f). Twinning is frequent, and some crystals show internal textural domains that likely represent partially resorbed cores (Fig. 2e). The groundmass microcrysts are typically 100 to 200 µm in size and occur as acicular needles and/or subhedral laths (Fig. 2a-b).

Representative plagioclase compositions are

Figure 2

a-c) Subhedral plagioclase crystals, between 1 and 4 mm long. d-e) Subhedral plagioclase crystals exhibiting concentric textural zoning. This textural zoning is not, however, coupled with major compositional zoning (see text for details). f) A glomerocryst (crystal clot), that consist of 1 to 3 mm plagioclase crystals together with 100 to 200 µm pyroxene crystals. The clot is a micro-gabbro. Note also the zeolite-lined vesicles in the center and right part of the image.

presented in Table 1. Limited compositional zoning is apparent in the plagioclase crystals investigated, although some crystals have ~10-150 µm rims of more sodium rich (albitic) composition (Fig. 3). These rims tend to become increasingly albitic towards the outer edge of the crystal, while in the interior of these crystals, µm-scale, oscillatory zoning can be discerned in the elemental maps (Fig. 3). The resorbed cores identified in some crystals (e.g. Fig. 2e), usually fail to show distinct compositional differences to the surrounding material.

To follow up on the qualitative analyses of the plagioclase phenocrysts, quantitave analyses

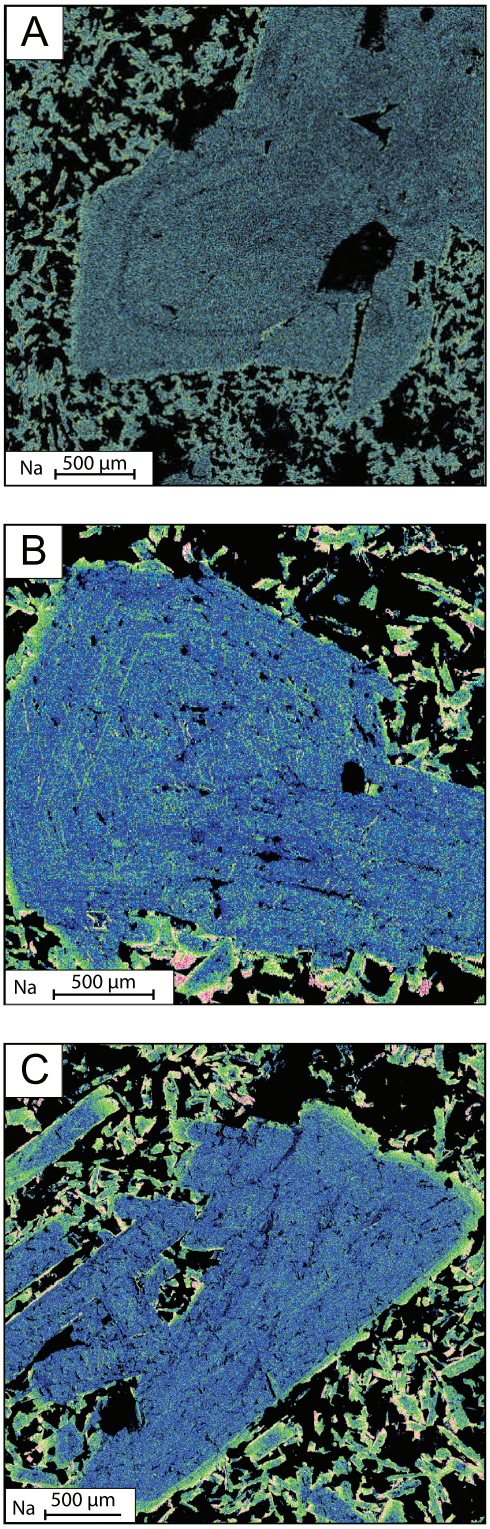

were performed by WDS. Despite the overall compositional simplicity of many crystals (Fig. 3), WDS analyses record a significant variation in plagioclase composition among different samples (Fig. 4). The total plagioclase compositional range of our data set is An_{42-91}, and if the Na-rich rims are discounted, the range is An_{61-91}. This latter range represents the bulk volume of the crystals analysed, as the rims only comprise a minute fraction of the total plagioclase crystal volume. When excluding the narrow albitic rims, the within crystal compositional variation in a single plagioclase usually spans only a few anorthite mol %, averaging about 4.8 mol % (range = 0.11 to 13.7 mol %) (Fig. 5). Most compositional variation in the plagioclase, excluding the narrow albitic rims, can be ascribed to small-scale oscillatory zoning or to rare patchy domains (cf. Vance, 1965). These intra-crystal variations are, however, relatively minor in terms of the overall compositional range of the plagioclase crystals studied. Pearce and Kolisnik (1990) argued that oscillatory anorthite variations of An ≤10 mol % generally correspond to small-scale pressure and temperature fluctuations within a relatively stable and presumably long-lived magma reservoir.

The within rock anorthite variation is usually also small (Fig. 5), with an average of 10.5 mol % (range = 5.8 to 17.6 mol %, excluding plagioclase rims) and in our dataset there are two dominant compositional groups or populations. These two groups are low anorthite plagioclase (~An_{60-80}) and high anorthite plagioclase (~An_{80-91}), respectively

Figure 3
Elemental maps of representative FIBG plagioclase crystals. The three WDS maps plot the relative abundance of Na in the crystals, reflecting overall rather homogenous interiors. Many crystals also show a thin albitic (Na-rich) rim. Light green colours indicate higher Na abundances while dark blue indicate lower Na abundances. The maps also reveal small amplitude oscillatory zoning in the interiors of these plagioclase crystals.

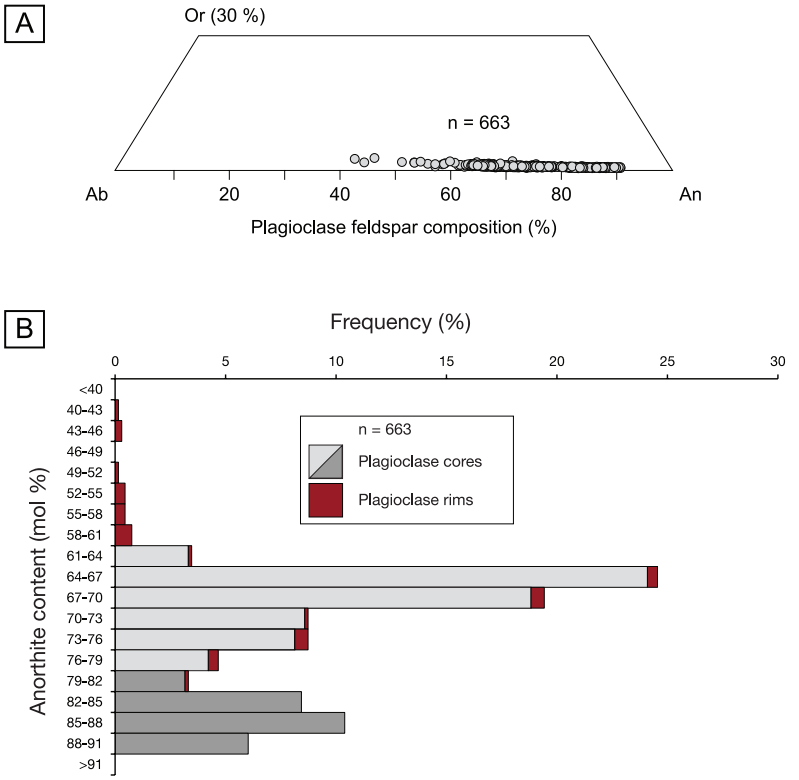

Figure 4
a) Ternary feldspar diagram (An, Ab, Or) of all analysed plagioclase compositions from this study. The total range of analysed plagioclase is $An_{42\text{-}91}$. b) Frequency distribution plot of anorthite contents in the analysed plagioclase crystals (n = 663). Note the bimodal distribution. The majority of the datapoints plot in either the $An_{60\text{-}80}$ or the $An_{80\text{-}91}$ range.

(Fig. 4 and 5). Interestingly, these populations are representative of the analysed rocks as a whole, in the sense that each rock sample studied appears to contain plagioclase of mainly one compositional group. Notably, the available samples from the LOPRA-1 drilling project also show a limited compositional range of plagioclase phenocrysts within each rock sample (Hald and Waagstein, 1984). About 70 % of our analysed rocks contain plagioclase with compositions between ~$An_{60\text{-}80}$, while 30% of the rocks show $An_{80\text{-}91}$. Interestingly, all dyke samples display plagioclase of the low anorthite group, while all sill samples show high anorthite plagioclase. Plagioclase from the lava samples, in turn, can plot in either of the two compositional groups.

Discussion

On the basis of the data presented, four main points will be discussed: a) plagioclase compositional homogeneity, b) plagioclase compositional groups, c) the thin albitic rims surrounding many of the plagioclase crystals, and d) the petrological-implications of the two plagioclase populations.

Plagioclase compositional homogeneity

The limited 'within crystal' and 'within rock' plagioclase compositional variation is a striking feature in this study (Fig. 5). In the literature, compositional zoning or the presence of multiple plagioclase populations is generally interpreted as indicators of processes such as polybaric fractionation, magma mixing, or assimilation, i.e. due to significant changes in thermodynamic conditions (e.g. Stamatelopoulou-Seymour *et al.*, 1990; Tepley *et al.*, 1999, 2000; Troll and Schmincke, 2002; Gerbe and Thouret, 2004; Troll *et al.*, 2004; Chadwick *et al.*, 2007; Meade *et al.*, 2014). The lack of intense zoning patterns in the studied crystals, except for the narrow outer rims, thus implies

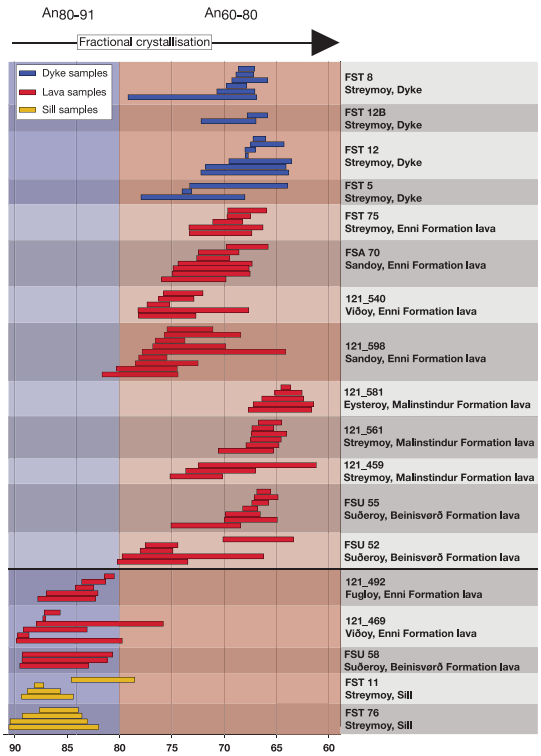

Figure 5
The range of anorthite plotted for each crystal in our samples suite, but excluding data from the narrow albitic rims (each bar represents the range of anorthite for a single analysed crystal). Red bars represent lava samples, while blue and yellow are from sills and dykes, respectively. The relative 'within crystal' plagioclase homogeneity is a feature observed throughout the analysed FIBG rocks. In addition, all rocks analysed show a relatively narrow range of plagioclase compositions, which implies that most plagioclase crystals formed under semi-stable physical conditions and over considerable periods of time.

relatively stable magma storage conditions for most of these crystals growth, and probably until final ascent commenced (cf. Pearce and Kolisnik, 1990). This realisation points to long-lived and stable magma reservoirs where physical conditions did not fluctuate dramatically on short timescales (e.g. Marsh, 1995).

Plagioclase compositional groups

The presence of a high- and a low anorthite group within the FIBG is noteworthy (Fig. 4 and 5). Plagioclase in the dyke samples consistently plots in the low anorthite range, while plagioclase in the sill samples plots consistently in the high anorthite range. The lavas of the Beinisvørð and Enni formations contain plagioclase of both anorthite groups, yet individual lava samples show dominantly one type of plagioclase only. As of yet, only low anorthite plagioclase has been identified in the lavas of the Malinstindur Formation, which we attribute to the low sample density (n = 3) and the overall lower abundance of the high anorthite plagioclase relative to the low anorthite group (Fig. 5). We presume that further study will show both anorthite groups to be present also within the Malinstindur Formation. These results are consistent with plagioclase analyses on samples from the LOPRA-1 drill hole (Hald and Waagstein, 1984) that show both of the identified plagioclase populations are present there too. This realisation means that both high- and low anorthite plagioclase have been recorded in two out of the three exposed main lava formations of the FIBG.

Thin albitic rims

The thin albitic rims that surround many of the plagioclase crystals (commonly between 10 and 150 µm in thickness) record a drastic change in plagioclase composition from the relatively homogenous crystal interiors. The albitic rims are present in both plagioclase compositional groups. Thin rims indicate late stage magmatic processes and more specifically, they are expected to form during the very last stages of magma evolution, i.e. during the final ascent towards the surface (Tepley *et al.*, 1999, 2000; Zellmer *et al.*, 2003; Longpré *et al.*, 2008; van der Zwan *et al.*, 2013). This reasoning is supported by the fact that, as shown by the elemental mapping, the rims tend to grade outwards toward progressively more albitic compositions, a feature associated with decompression and cooling (Bowen, 1928). We therefore propose that the plagioclase rims crystallised in a magmatic system in rapid transition, possibly

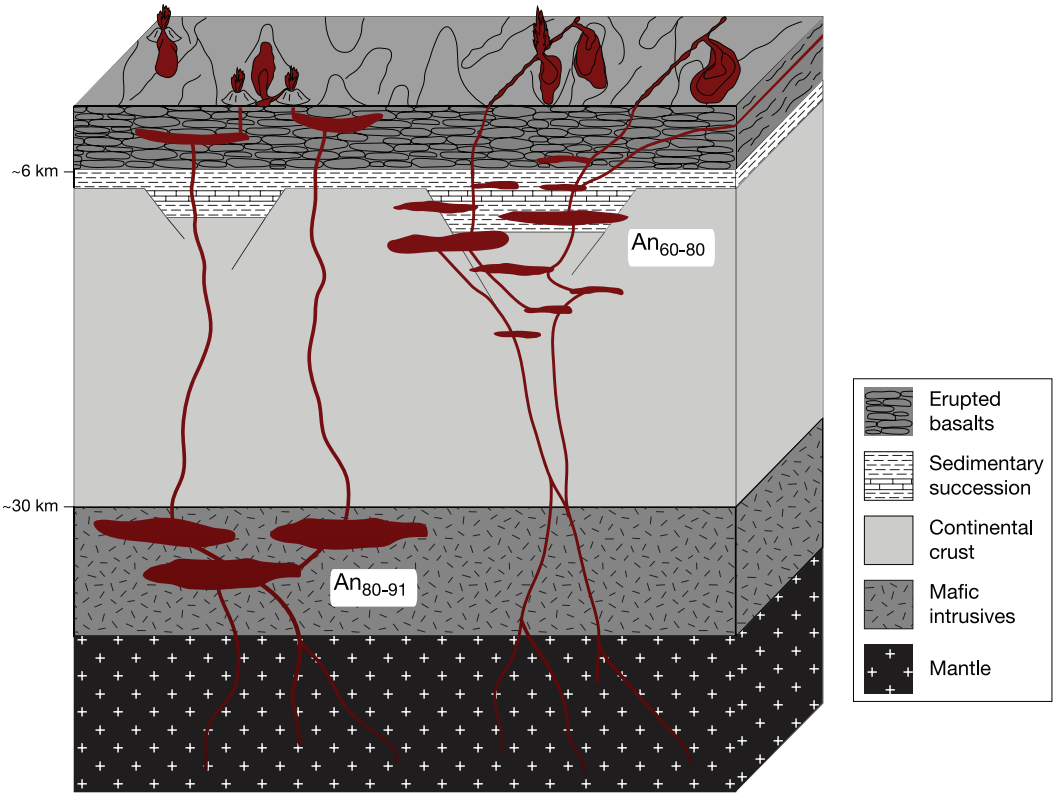

in an ascending magma subject to progressive decompression (Fig. 3), and reflect the conditions just prior to eruption or final emplacement.

Petrological implications

The homogeneity of the plagioclase interiors implies crystallisation conditions that require consistent and presumably prolonged magma storage, where the magma and associated crystal cargo resided for sufficient time to homogenise and equilibrate. The anorthite content of plagioclase has been shown to be dependent on both temperature and lithostatic pressure (Bowen, 1928; Lofgren, 1974; Fuhrman and Lindsley, 1988; Housh and Luhr, 1991; Panjasawatwong *et al.*, 1995; Danyushevsky *et al.*, 1997; Danyushevsky, 2001; Sugawara, 2001; Ghiorso, 2002; Putirka, 2005, 2008), and therefore the two anorthite populations might be explained by crystallisation at different temperatures and depths. We hence suggest that a common, long-

Figure 6

Schematic illustration of the proposed magma plumbing system that could have fed the Faroe Islands Basalt Group. All analysed sill samples plot within the high anorthite group, whereas the dyke samples contain low anorthite plagioclase exclusively (Fig. 5). The two proposed storage regions or regimes were likely situated at distinct depth levels in the crust beneath the FIBG. The high anorthite plagioclase would likely have formed in magmas at deeper levels, while the low anorthite plagioclase crystallised at a shallower depth. The inferred mafic intrusives at the base of the Archean crust (Richardson *et al.*, 1998) likely represent the solidified remnants of the magma reservoirs that fed the high anorthite lavas and the sills of our study.

lived plumbing system was active throughout the emplacement history of the FIBG, sampling two broad and temporally stable magma storage regions beneath the Faroe Islands. In the case of a highly complex and polybaric magma plumbing system, one would expect less homogenous plagioclase phenocryst compositions, as well as systematic changes in plagioclase composition over time. This would result in marked zonation (e.g. Chadwick *et al.*, 2007), which is not observed in our data. In our scenario, the magmas hosting the high anorthite plagioclase likely stalled in a deep and hot region of the crust. Conversely, the magmas containing the low anorthite plagioclase would have formed from a cooler and thus more evolved and bouyant magma, residing at shallower levels. The two plagioclase populations thereby define two major storage regions (Fig. 6, cf. Yoder *et al.*, 1957; Lofgren, 1974; Huppert and Sparks, 1985; Housh and Luhr, 1991; Panjasawatwong *et al.*, 1995; Manley and Bacon, 2000; Putirka, 2005; Dahren *et al.*, 2012).

In this context, it is conceivable, even likely, that the mafic intrusives inferred to make up the base of the crust beneath the Faroes (Richardson *et al.*, 1998) represent the solidified remnants of a deep Paleogene magma storage system, which probably coincide with the former magma reservoir for the high-An plagioclase population. The low-An magma storage region, in turn, would then have to be located at mid- to upper crustal depths, or maybe even within the lower parts of the then progressively growing lava pile (Fig. 6). These results of a two-tiered plumbing system are analogous to the general model for plumbing systems in continental flood basalt provinces elsewhere (Cox, 1980), based on observations in the Karoo, the Deccan Traps, and West Greenland.

The residence time for plagioclase in the FIBG can be approximated using established plagioclase growth rates for deep and large (steady state) magma chambers (e.g. 10^{-11} cm/s; Higgins, 1996). Plagioclase in the FIBG are commonly between 2 and 5 mm across, with extreme crystals of up to 20 mm. The typical crystal sizes (2 to 5 mm) correspond to growth durations, and so to magma chamber residence times of ~600 to 1600 years, whereas the large crystals equate to residence times in excess of 6000 years. The calculated residence times have to be treated as minimum estimates, as individual crystals could theoretically grow discontinuously (e.g. when isolated in a mush zone for some time), thus prolonging the time span represented by simple crystal size and continuous growth models. The internal resorption surfaces observed in several crystals (Fig. 2e), likely indicate such stalls in growth, and imply a resorption event before crystal growth resumed in these examples. Assuming that the magmas beneath the FIBG indeed stalled at two main storage levels corresponding with the two anorthite populations of our study, then these probably represent the main supply routes for magmas to the surface. It is hence conceivable that the calculated residence times broadly relate to repose times between eruptive periods for the lavas, which would mean that volcanic activity was suspended for hundreds or even thousands of years in between the emplacement of individual lava flows. Such repose intervals would provide ample time for the formation of advanced ecosystems and extensive soil horizons, evident in the noteable paleosols within the FIBG. These former soils contain palynological evidence for widespread forestation on the Faroe Islands during the Paleogene (Ellis *et al.*, 2002; Passey and Jolley, 2009) and imply considerable time breaks inbetween many of the FIBG eruptions.

Long-term, large volume storage of magma and associated crystals in the deep and shallow reservoirs would then be interrupted by rapid ascent, during which the growth of albitic rims took place. Using the average rate of plagioclase crystal growth for ascent and/or degassing (10^{-10} cm/s; Higgins, 1996), we find that rims with a thickness of between 10 and 150 μm would require between 0.25 and 5 years to grow, respectively. Assuming that the thin outer rims formed exclusively during final magma ascent, this range of time estimates can be used to constrain the rate of

magma ascent. Such a model requires an estimate of magma storage depth, i.e. the distance travelled by the magma, for which we assume a range of possible magma storage levels of between 5 to 30 km. Based on these estimated growth times and storage depths, ascent rates of $3x10^{-5}$ to $3x10^{-3}$ m/s are derived. Such ascent rates are similar to those recorded for mafic to intermediate effusive eruptions elsewhere (e.g. Nakada *et al.*, 1995; Rutherford and Gardner, 1999; Armienti *et al.*, 2012), and are considerably below explosive rates that are thought to commence at values of about 0.2 m/s (Rutherford and Gardner, 1999).

Conclusions

This study has shown that plagioclase phenocrysts in the FIBG can be divided into two main compositional groupings of An_{60-80} and An_{80-91}. Notably, each analysed rock sample contains dominantly plagioclase from one of these populations. The two plagioclase populations found throughout the FIBG indicate that neither magma mixing nor multi-level magma storage were major processes during the evolution of the Faroe Island Basalt Group. Instead, the two plagioclase compositional groups imply that long-term magma storage likely took place in two dominant storage regions. The high anorthite plagioclase likely formed from a high temperature magma residing at lower crustal levels or at the base of the crust, possibly in a fashion analogous to large underplating zones in ocean islands and other areas of the North Atlantic Igneous Province (Rohrman and Van Der Beek, 1996; Japsen and Chalmers, 2000; Klügel *et al.*, 2005; Persano *et al.*, 2007; Longpré *et al.*, 2008; Anell *et al.*, 2009). The shallow storage level, in turn, was likely located at mid- to upper crustal levels, possibly even within the extrusive lava pile, similar to what is seen in many volcanic regions in different tectonic regimes, such as e.g. Gran Canaria, Tenerife, La Palma, Anak Krakatau, Mt St. Helens and Gunung Kelud (Hansteen *et al.*, 1998; Cashman and McConnell, 2005; Klügel *et al.*, 2005; Peccerillo *et al.*, 2006; Longpré *et al.*, 2008; Dahren *et al.*, 2012; Jeffery *et al.*, 2013). The presence of the two dominant crystal populations, independent of stratigraphy, suggests that this magma plumbing architecture was long-lived and relatively stable, and must have fed the Faroese volcanism throughout most of its active history (Fig. 6).

Long term magma storage on the order of several hundreds to thousands of years was then interrupted by relatively rapid ascent and eruption or shallow level emplacement, reflected in the widespread occurrence of narrow albitic rims (Fig. 3). The magma ascent rates, from various potential magma storage depths fall between $3x10^{-5}$ and $3x10^{-3}$m/s and are similar to magma ascent rates established for mafic to intermediate effusive eruptions elsewhere.

Acknowledgements

Valuable advice and assistance was provided by the Faroese Earth and Energy Directorate (Jarðfeingi) during our field work. The final version of this paper was very much improved by the constructive reviews by C.H. Emeleus and an anonymous referee. This project would not have been possible without the funding provided by SINDRI, Uppsala University, Jänes Stipendiefond, the Royal Swedish Academy of Sciences (KVA), the Swedish Research Council (VR) and Otterborgska Donationsrådet.

Table 1: Representative plagioclase compositions

Sample	FST 76 plag 1			FSU 58 plag 2			FST 12 plag1			FST 11 plag 1			121_581_plag A			121_598_plag A			121_492_plag C	
position	rim	mid	core	rim	core	rim	mid	core	rim	mid	core	rim	core	rim	mid	core	rim	mid
SiO_2	49.74	45.57	46.07	49.13	46.41	46.44	52.36	52.36	55.58	47.55	46.45	52.22	53.75	50.22	49.91	50.37	52.05	48.47
TiO_2	0.06	0.00	0.02	0.04	0.06	0.03	0.05	0.08	0.10	0.08	0.03	0.07	0.00	0.08	0.05	0.00	0.15	0.03
Al_2O_3	30.00	33.45	32.80	30.95	33.50	33.50	29.01	29.23	27.02	32.58	32.51	29.05	28.19	30.86	30.44	30.59	28.07	31.76
FeOtot	0.73	0.63	0.62	0.62	0.53	0.51	0.93	0.62	0.74	0.54	0.69	0.59	0.54	0.68	0.51	0.54	1.28	0.78
MgO	0.19	0.15	0.21	0.20	0.15	0.10	0.29	0.19	0.14	0.27	0.11	0.17	0.19	0.21	0.16	0.15	0.11	0.09
CaO	15.05	18.28	17.79	15.64	17.57	17.92	13.22	13.37	10.73	17.29	17.52	13.09	12.64	15.48	15.62	14.42	13.24	16.24
Na_2O	3.11	1.07	1.37	2.57	1.33	1.17	3.84	3.76	4.64	1.32	1.39	3.99	4.27	2.67	2.32	2.98	3.25	2.13
K_2O	0.06	0.02	0.02	0.06	0.00	0.02	0.09	0.11	0.16	0.03	0.03	0.12	0.11	0.07	0.08	0.07	0.17	0.06
Total	98.94	99.17	98.90	99.20	99.54	99.69	99.78	99.72	99.11	99.65	98.73	99.31	99.70	100.27	99.08	99.13	98.32	99.56
Anorthite	73	90	88	77	88	89	65	66	56	88	87	64	62	76	78	72	69	81
Albite	27	10	12	23	12	11	34	34	43	12	13	35	38	24	21	27	30	19
Orthoclase	0.32	0.12	0.14	0.34	0.02	0.10	0.50	0.65	0.97	0.16	0.20	0.67	0.67	0.43	0.45	0.40	1.07	0.37

References

1. White, R. & McKenzie, D. (1989). Magmatism at Rift Zones : The Generation of Volcanic Continental Margins. *J. Geophys.* **94**, 7685–7729
2. Holm, P. M., Hald, N. & Nielsen, Troels, F. D. (1992). Contrasts in composition and evolution of Tertiary CFBs between West and East Greenland and their relations to the establishment of the Icelandic mantle plume. *Magmat. Causes Cont. Break.* 349–362
3. Richardson, K. R., Small wood, J. R., White, R. S., Snyder, D. B. & Maguire, P. K. . (1998). Crustal structure beneath the Faroe Islands and the Faroe–Iceland Ridge. *Tectonophysics* **300**, 159–180
4. Ellis, D., Bell, B. R., Jolley, D. W. & O'Callaghan, M. (2002). The stratigraphy, environment of eruption and age of the Faroes Lava Group, NE Atlantic Ocean. *Geol. Soc. London, Spec. Publ.* **197**, 253–269
5. Passey, S. R. & Jolley, D. W. (2009). A revised lithostratigraphic nomenclature for the Palaeogene Faroe Islands Basalt Group, NE Atlantic Ocean. *Earth Environ. Sci. Trans. R. Soc. Edinburgh* **99**, 127
6. Søager, N. & Holm, P. M. (2009). Extended correlation of the Paleogene Faroe Islands and East Greenland plateau basalts. *Lithos* **107**, 205–215
7. Søager, N. & Holm, P. M. (2011). Changing compositions in the Iceland plume; Isotopic and elemental constraints from the Paleogene Faroe flood basalts. *Chem. Geol.* **280**, 297–313
8. Vance, J. A. (1965). Zoning in Igneous Plagioclase : Patchy Zoning. *J. Geol.* **73**, 636–651
9. Pearce, T. & Kolisnik, a (1990). Observations of plagioclase zoning using interference imaging. *Earth-Science Rev.* **29**, 9–26
10. Hald, N. & Waagstein, R. (1984). Lithology and chemistry of a 2-km sequence of Lower Tertiary tholeiitic lavas drilled on Suduroy, Faeroe Islands (Lopra-1). *Deep Drill. Proj. 1980–1981 Faeroe Islands* 15–38
11. Stamatelopoulou-Seymour, K., Vlassopoulos, D., Pearce, T. H. & Rice, C. (1990). The

record of magma chamber processes in plagioclase phenocrysts at Thera Volcano, Aegean Volcanic Arc, Greece. *Contrib. to Mineral. Petrol.* **104**, 73–84

12. Tepley III, F. J., Davidson, J. P. & Clynne, M. . (1999). Magmatic Interactions as Recorded in Plagioclase Phenocrysts of Chaos Crags, Lassen Volcanic Center, California. *J. Petrol.* **40**, 787–806
13. Tepley III, F. J., Davidson, J. P., Tilling, R. I. & Arth, J. G. (2000). Magma Mixing , Recharge and Eruption Histories Recorded in Plagioclase Phenocrysts from El Chichón Volcano, Mexico. *J. Petrol.* **41**, 1397–141114. Troll, V. R. & Schmincke, H.-U. (2002). Magma Mixing and Crustal Recycling Recorded in Ternary Feldspar from Compositionally Zoned Peralkaline Ignimbrite A', Gran Canaria, Canary Islands. *J. Petrol.* **43**, 243–270
15. Gerbe, M.-C. C. & Thouret, J.-C. C. (2004). Role of magma mixing in the petrogenesis of tephra erupted during the 1990-98 explosive activity of Nevado Sabancaya, southern Peru. *Bull. Volcanol.* **66**, 541–561
16. Troll, V. R., Donaldson, C. H. & Emeleus, C. H. (2004). Pre-eruptive magma mixing in ash-flow deposits of the Tertiary Rum Igneous Centre, Scotland. *Contrib. to Mineral. Petrol.* **147**, 722–739
17. Chadwick, J. P. *et al.* (2007). Carbonate Assimilation at Merapi Volcano, Java, Indonesia: Insights from Crystal Isotope Stratigraphy. *J. Petrol.* **48**, 1793–1812
18. Meade, F. C. *et al.* (2014). Bimodal magmatism produced by progressively inhibited crustal assimilation. *Nat. Commun.* **5**, 4199
19. Marsh, B. D. (1995). Solidification fronts and magmatic evolution. **60**, 5–40
20. Zellmer, G. F., Sparks, R. S. J., Hawkesworth, C. J. & Wiedenbeck, M. (2003). Magma Emplacement and Remobilization Timescales Beneath Montserrat : Insights from Sr and Ba Zonation in Plagioclase Phenocrysts. *J. Petrol.* **44**, 1413–1431
21. Longpré, M.-A., Troll, V. R. & Hansteen, T. H. (2008). Upper mantle magma storage and transport under a Canarian shield-volcano, Teno, Tenerife (Spain). *J. Geophys. Res.* **113**, 1–11
22. Van der Zwan, F. M., Chadwick, J. P. & Troll, V. R. (2013). Textural history of recent basaltic-andesites and plutonic inclusions from Merapi volcano. *Contrib. to Mineral. Petrol.* **166**, 43–63
23. Bowen, N. L. (1928). *The Evolution of the Igneous Rocks*. 132pp
24. Lofgren, G. (1974). An Experimental Study of Plagioclase Crystal Morphology: Isothermal crystallization. *Am. J. Sci.* **274**, 243–273
25. Fuhrman, M. L. & Lindsley, D. H. (1988). Ternary-feldspar modeling and thermometry. *Am. Mineral.* **73**, 201–215
26. Housh, T. B. & Luhr, J. F. (1991). Plagioclase-melt equilibria in hydrous systems. *Am. Mineral.* **76**, 477–492
27. Panjasawatwong, Y., Danyushevsky, L. V, Crawford, A. J. & Harris, K. L. (1995). An experimental study of the effects of melt composition on plagioclase – melt equilibria at 5 and 10 kbar : implications for the origin of magmatic high-An plagioclase. *Contrib. to Mineral. Petrol.* **118**, 420–432
28. Danyushevsky, L. V, Carroll, M. R. & Falloon, T. J. (1997). Origin of high-An plagioclase in Tongan high-Ca boninites; implications for plagioclase-melt equilibria at low P(H_2O). *Can. Mineral.* **35**, 313–326
29. Danyushevsky, L. (2001). The effect of small amounts of H_2O on crystallisation of mid-ocean ridge and backarc basin magmas. *J. Volcanol. Geotherm. Res.* **110**, 265–280
30. Sugawara, T. (2001). Ferric iron partitioning between plagioclase and silicate liquid: thermodynamics and petrological applications. *Contrib. to Mineral. Petrol.* **141**, 659–686
31. Ghiorso, M. S. (2002). The pMELTS: A revision of MELTS for improved calculation of phase relations and major element partitioning related to partial melting of the mantle to 3 GPa. *Geochemistry Geophys. Geosystems* **3**

32. Putirka, K. D. (2005). Igneous thermometers and barometers based on plagioclase + liquid equilibria: Tests of some existing models and new calibrations. *Am. Mineral.* **90**, 336–346
33. Putirka, K. D. (2008). Thermometers and Barometers for Volcanic Systems. *Rev. Mineral. Geochemistry* **69**, 61–120
34. Yoder, H. S., Stewart, D. B. & Smith, J. R. (1957). Feldspars. *Carnegie Inst. Washingt. Year B. 56* 206–214
35. Huppert, H. E. & Sparks, R. S. J. (1985). Cooling and contamination of mafic and ultramafic magmas during ascent through continental crust. *Earth Planet. Sci. Lett.* **74**, 371–386
36. Manley, C. R. & Bacon, C. R. (2000). Rhyolite Thermobarometry and the Shallowing of the Magma Reservoir , Coso Volcanic Field , California. *J. Petrol.* **41**, 149–174
37. Dahren, B. *et al.* (2012). Magma plumbing beneath Anak Krakatau volcano, Indonesia: evidence for multiple magma storage regions. *Contrib. to Mineral. Petrol.* **163**, 631–651
38. Cox, K. G. (1980). A Model for Flood Basalt Vulcanism. *J. Petrol.* **21**, 629–650
39. Higgins, M. D. (1996). Crystal size distributions and other quantitative textural measurements in lavas and tuff from Egmont volcano (Mt. Taranaki), New Zealand. *Bull. Volcanol.* **58**, 194–204
40. Nakada, S., Motomura, Y. & Shimizu, H. (1995). Manner of magma ascent at Unzen Volcano (Japan). *Geophys. Res. Lett.* **22**, 567
41. Rutherford, M. J. & Gardner, J. E. (1999). Rates of Magma Ascent. *Encycl. Volcanoes* 207–218
42. Armienti, P., Perinelli, C. & Putirka, K. D. (2013). A new model to estimate deep-level magma ascent rates, with applications to Mt. Etna (Sicily, Italy). *J. Petrol.* **54**, 795–813
43. Rohrman, M. & Van Der Beek, P. (1996). Cenozoic postrift domal uplift of North Atlantic margins: An asthenospheric diapirism model. *Geology* **24**, 901–904
44. Japsen, P. & Chalmers, J. A. (2000). Neogene uplift and tectonics around the North Atlantic : overview. *Glob. Planet. Change* **24**, 165–173
45. Klügel, A., Hansteen, T. H. & Galipp, K. (2005). Magma storage and underplating beneath Cumbre Vieja volcano, La Palma (Canary Islands). *Earth Planet. Sci. Lett.* **236**, 211–226
46. Persano, C., Barfod, D. N., Stuart, F. M. & Bishop, P. (2007). Constraints on early Cenozoic underplating-driven uplift and denudation of western Scotland from low temperature thermochronometry. *Earth Planet. Sci. Lett.* **263**, 404–419
47. Anell, I., Thybo, H. & Artemieva, I. M. (2009). Cenozoic uplift and subsidence in the North Atlantic region: Geological evidence revisited. *Tectonophysics* **474**, 78–105
48. Hansteen, T. H., Klügel, A. & Schmincke, H.-U. (1998). Multi-stage magma ascent beneath the Canary Islands: evidence from fluid inclusions. *Contrib. to Mineral. Petrol.* **132**, 48–64
49. Cashman, K. V. & McConnell, S. M. (2005). Multiple levels of magma storage during the 1980 summer eruptions of Mount St. Helens, WA. *Bull. Volcanol.* **68**, 57–75
50. Peccerillo, A., Frezzotti, M. L., De Astis, G. & Ventura, G. (2006). Modeling the magma plumbing system of Vulcano (Aeolian Islands, Italy) by integrated fluid-inclusion geobarometry, petrology, and geophysics. *Geology* 34, 17–20
51. Jeffery, A. J. *et al.* (2013). The pre-eruptive magma plumbing system of the 2007–2008 dome-forming eruption of Kelut volcano, East Java, Indonesia. *Contrib. to Mineral. Petrol.* 166, 275–308
52. Manley, C. R. & Bacon, C. R. (2000). Rhyolite Thermobarometry and the Shallowing of the Magma Reservoir, Coso Volcanic Field, California. *J. Petrol.* **41**, 149–174
53. Barker AK, Troll VR, Carracedo J-C, Nicholls PA (in press) The magma plumbing system for the 1971 Tenguía eruption, La Palma, Canary Islands. Contrib Mineral Petrol doi: 10.1007/s00410-015-1207-7

3D Mapping of an Intrusive Complex in the Faroe-Shetland Basin

JIM Á HORNI[1], LARS OLE BOLDREEL[2] AND MICHAEL LARSEN[3]

1: Faroese Earth and Energy Directorate, Brekkutún 1, P.O. Box 3059, FO-110 Tórshavn, Faroe Islands
2: University of Copenhagen, Department of Geology & Geography, Østervold Gade 10, DK-1350, Denmark
3: DONG Energy, Exploration and Production, Nesa Alle 1, DK-2820 Gentofte, Denmark

*Corresponding author: Jim á Horni: jim.a.horni@jardfeingi.fo

Abstract

The sedimentary section in the Faroe-Shetland Basin is strongly influenced by the magmatic events of the Palaeogene North Atlantic Igneous Province. The western part of the basin is covered by basaltic lavas and hyaloclastite deposits whereas numerous magmatic sills, known as the Faroe-Shetland Sill Complex (FSSC), are prominent in the central and eastern part. The FSSC has primarily been intruded into the Upper Cretaceous and Palaeogene sedimentary section of the basin.

Based on interpretation of high quality 3D reflection seismic, acquired in 2008 and 2009, a large number of sill morphologies is found and grouped into four depth levels. The morphology and flow patterns of a connected complex covering 6,3 x 5,0 km has been analysed and the spatial connections between individual intrusions are determined from 2D map views, 2D section and 3D figures. It is concluded that the intrusions in the complex are connected in a larger intrusive system, and hence possibly emplaced from the same intrusive event.

The distribution of the sills in the Faroe-Shetland Basin is compared to the distribution of exposed sills onshore on the Faroe Islands and it is shown that the sills are emplaced below and within the basaltic lava succession on the Faroe Islands.

Faroe Islands Exploration Conference: Proceedings of 4th Conference.
Annales Societatis Scientiarum Færoensis Supplementum LXIV.

Introduction

Magmatic intrusions in rift basins along continental margins occur as a consequence of continental breakup, and the sills may cover huge areas up to 100 km^2 (Karoo Basin, South Africa) (Planke *et al*., 2005; Polteau *et al*., 2008). Flood basalts associated with the break-up between the Faroe Islands and East Greenland extend over 250.000 km^2 and at least 40.000 km^2 lie in the Faroe-Shetland Channel area (Smallwood and Maresh, 2002).

Due to the hydrocarbon exploration in the NE Atlantic area, 2D and 3D seismic surveys have been acquired and in addition exploration wells have been drilled, providing samples and wireline log data. Based on interpretation on seismic and well data, studies have been published on sill complexes on the north European continental margin (Bell and Butcher, 2002; Cartwright and Hansen, 2006; Planke *et al*., 2005; Smallwood and Harding, 2009; Smallwood and Maresh, 2002) likewise studies of modelling of intrusive bodies have been published (Galland *et al*., 2006; Galland *et al*., 2009; Malthe-Sørenssen *et al*., 2004; Mathieu *et al*., 2008).

An extensive number of igneous sills, known as the Faroe-Shetland sill complex (FSSC), have been imaged by 3D reflection seismic surveys and some of the sills have been penetrated by exploration wells and samples of sills have been acquired and wireline logs retrieved (Bell and Butcher, 2002; Smallwood and Harding, 2009) (Fig. 1).

The mapping and interpretation of the FSSC show that sills, presumed to be of the same intrusion age as in the centre of the Faroe-Shetland Basin, are typically emplaced into Upper Cretaceous strata (Smallwood and Maresh, 2002) (Fig. 2), whereas they in the eastern part of the Faroe-Shetland Basin (on the margin of the Shetland platform) were emplaced in Lower Paleocene strata (Bell and Butcher, 2002). It is known that upward migrating magma has to overcome a certain lithostatic pressure, before the intrusions can start to develop sills at a level of hydrostatic equilibrium with neutral buoyancy (Bradly, 1965; Francis, 1982; Malthe-Sørenssen *et al*., 2004). Therefore it is argued that the lithostatic pressure in a sedimentary basin is controlled by the depth of the basement (Bell and Butcher, 2002; Francis, 1982; Polteau *et al*., 2008), and hence the intrusions are emplaced into the older strata (Upper Cretaceous) in the deeper central part of the Faroe-Shetland Basin and in younger strata (Lower Paleocene) at less depth on the margin close to North Shetland Platform.

Intrusions have been mapped onshore in outcrops on the Faroe Islands and estimates of their lateral extension, up to 50.5 km^2 have been published (Hansen *et al*., 2011). In various explorations wells: 6005/15-1(Varming, 2009), Lopra-1(Boldreel, 2006; Passey and Jolley, 2009) and in exploration wells in the UK area of the Faroe-Shetland Basin (Andersen *et al*., 2009) intrusions have been identified on wireline logs.

The aim of this paper is to present a detailed description and interpretation of magmatic intrusions emplaced into the sedimentary succession of the Faroe-Shetland Basin, based on recently acquired 3D reflection seismic data of high quality. Based on these data the morphology of the intrusions, their emplacement mechanisms and furthermore the internal flow patterns of a sill complex is determined, and thus it is shown that there is a spatial connections between the intrusions inferring that they originate from the same intrusive event.

Geological Setting

The Faroe-Shetland Basin is located in the central and eastern part of the Faroe-Shetland Channel, between the Faroe Islands and the Shetland Islands on the north-west European continental margin (Fig. 1) (Earle *et al*., 1989).

The continental break-up caused large scale volcanism from the Paleocene to the Early Eocene (e.g. (Cartwright and Hansen, 2006)) that created the North Atlantic Igneous Province. The flood basalts associated with the break-up between the Faroe Islands and East Greenland, extend over

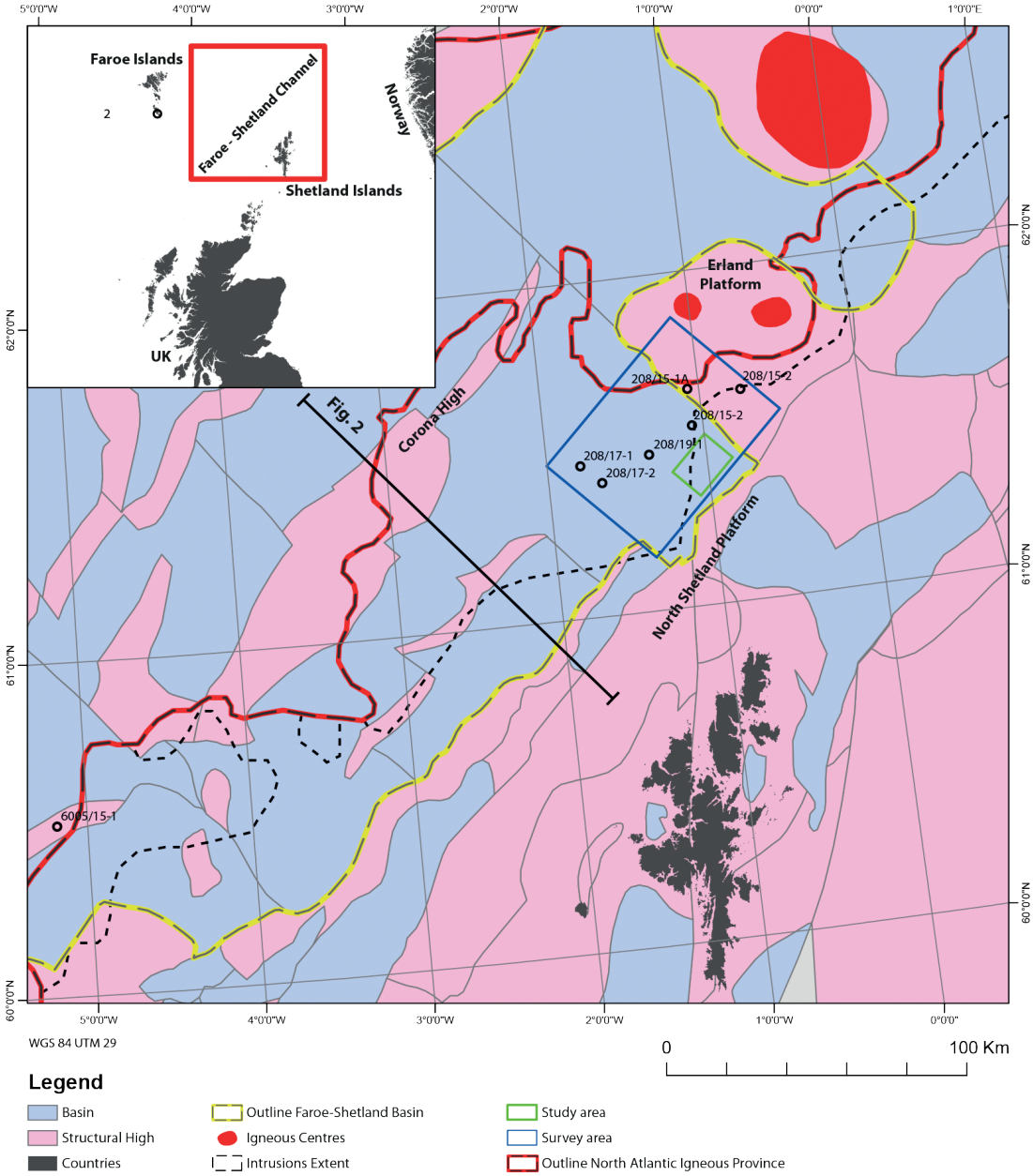

Figure 1

Overview map over the North Atlantic showing the location of the Faroe-Shetland Channel. Map of the Faroe-Shetland Basin, showing the survey area and location of the wells used in this study and the general geological setting in the area. The Lopra-1 well is displeyd on the overview map.

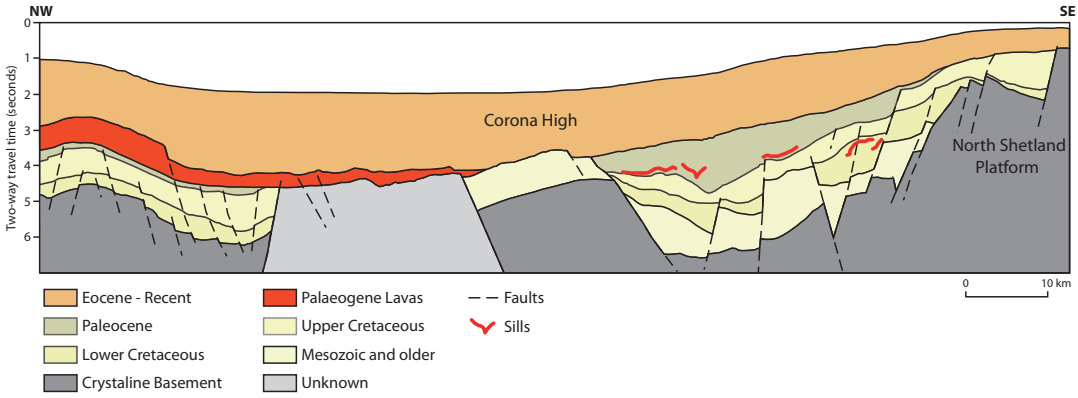

Figure 2
Cross section from the eastern part of the Faroe-Shetland Basin based on 2D seismic section. Location indicated on Fig. 1. (Modified from: (Ritchie et al., 2011).

250.000 km^2 and at least 40.000 km^2 lie in the Faroe-Shetland Channel area (Smallwood and Maresh, 2002).

The Faroe-Shetland Basin is bounded to the south-east by the North Shetland Platform, to the west by the Corona High, to the north-east by the Erlend Platform (Dean *et al*., 1999) and to the north-west by the northern part of the Faroe-Rockall Plateau (e.g. (Boldreel and Andersen, 1993; Smallwood and Maresh, 2002)) (Fig. 1).

The Faroe-Shetland Basin is a major Jurassic – Cretaceous rift basin subsequently modified by Paleocene tectonism and subsidence (Mudge and Rashid, 1987). The basin has a north-east to south-west trend and is an asymmetric half-graben filled by a wedge of Upper Cretaceous sediments, which thickens toward its north-western part where a series of low-angle normal faults mark the margin of the basin (Mudge and Rashid, 1987) (Fig. 2).

In the Faroe-Shetland Basin rifting is demonstrated in the Cretaceous and Paleocene, whereas Jurassic rifting is likely but has not been proved. The area has been affected over a prolonged period with at least five shifting phases from the Permo-Triassic to Paleocene (Dean *et al*., 1999). Late Cretaceous rifting coincided with high sea-level and the rift fill is predominantly fine clastics of marine origin (Dean *et al*., 1999). The Paleocene rifting was coincident with the development of the Icelandic mantle plume which caused uplift of the UK mainland followed by erosion and renewed influx of coarser clastic material in the Faroe-Shetland Basin (Dean *et al*., 1999).

The sedimentary section of the basin is highly influenced by the magmatic events of the North Atlantic Igneous Province. Areas covered by extrusive basaltic lavas have proven difficult to image seismically, although non-covered areas, such as parts of the Faroe-Shetland Basin, provide good possibilities for deep 3D seismic imagining.

Methods and Data

Seismic data

The 3D seismic dataset used for this project consists of three surveys, acquired in 2008 – 2009, and has been made available for this study by

DONG. The dataset covers approximately 2000 km^2 some 95 km north of the Shetland Islands (Survey area) (Fig. 1).

The source for the acquisition of the data was two air-guns, with a separation of 25 m meters and with a depth of 7.5 m below sea level. The recording equipment consists of 16 x 4800 m long streamers with hydrophones with 12.5 m interval kept at a depth of 9 m below sea level. This creates a 3D grid with 12.5 m between the lines and a recording length of 7168 ms.

Using a sedimentary velocity interval of 2000 – 3000 m/s, with the highest frequency of 206 Hz and an average frequency that approximately lies a little lower, the vertical resolution is around 10 – 15 m.

The data used underwent state of the art processing, including final migration. The data was loaded on workstations and seismic interpretation was carried out by the use of the Petrel software. Data standard used is zero phase European polarity and amplitudes are shown in a multicolored scale.

Wells

Six explorations wells have been drilled in the survey area (Fig. 1) and among these 208/17-1 penetrates an interval that from wire line logs are characterized with a relative high velocity comparing with the surrounding host rock, low neutron porosity (ΦN<10-20 LUP), high density ($\rho_B \approx 2.7\text{-}3.0$ g/cm^3) and where velocities, resistivities and gamma radiation is in the same range as for other basaltic rocks ($V_p \approx 5\text{-}6$ km/s, $R \approx 10\text{-}1000\Omega$m and generally below 30 GAPI) and thus interpreted as magmatic intrusions (Fig. 3) using the principles by e.g. Andersen & Boldreel (2009).

Biostratigraphic markers found in two wells (208/15-2 and 208/19-1) (Fig. 1) are used as well ties for stratigraphic dating of a hydrothermal vent found in this study (Fig. 4).

Criteria for identification of intrusions on reflection seismic profiles

The following criteria have been used in this study for interpreting a seismic event as a sill: (1) hard (positive) high amplitude, (2) locally the high amplitude transgress the sedimentary stratification, commonly at very oblique angles, (3) abrupt termination of the high amplitude event and (4) specific geometries or shapes, (described in the section *„Classifications and terminology of intrusions"* below). Furthermore, a seismic event may be interpreted as a sill when correlated with interpreted sills on a crossing section or if it shows a circular appearance on a time slice section (Fig. 5).

The reliability of the interpretation of sills depends on how well the four criteria are fulfilled. Only reflection events with high degree of fulfilment of the four criteria have been interpreted as sills. When interpreting intrusive bodies, difficulties occur, especially in areas below intrusions at shallow depth, as multiples, are produced that hampers the interpretation of events at deeper levels thus making structures and events difficult to image (Fig 11 and 12). These difficulties occur because of the significant acoustic impedance contrast produced of the high velocity intrusions, and when the intrusion produces such significant high amplitude the seismic wave loses most of its energy and/or the signal gets disrupted. The loss of energy, disrupted signal and the multiples associated with the intrusions makes the quality of the seismic very poor below magmatic intrusions, and hence the interpretation difficult.

Classification and terminology of intrusions

Igneous intrusions emplaced in sedimentary basins are typically sheet-like bodies several tens of metres thick (less commonly over 100m thick) and extend for tens of kilometres along strike (Golden valley sill) (Planke *et al*., 2005; Polteau *et al*., 2008).

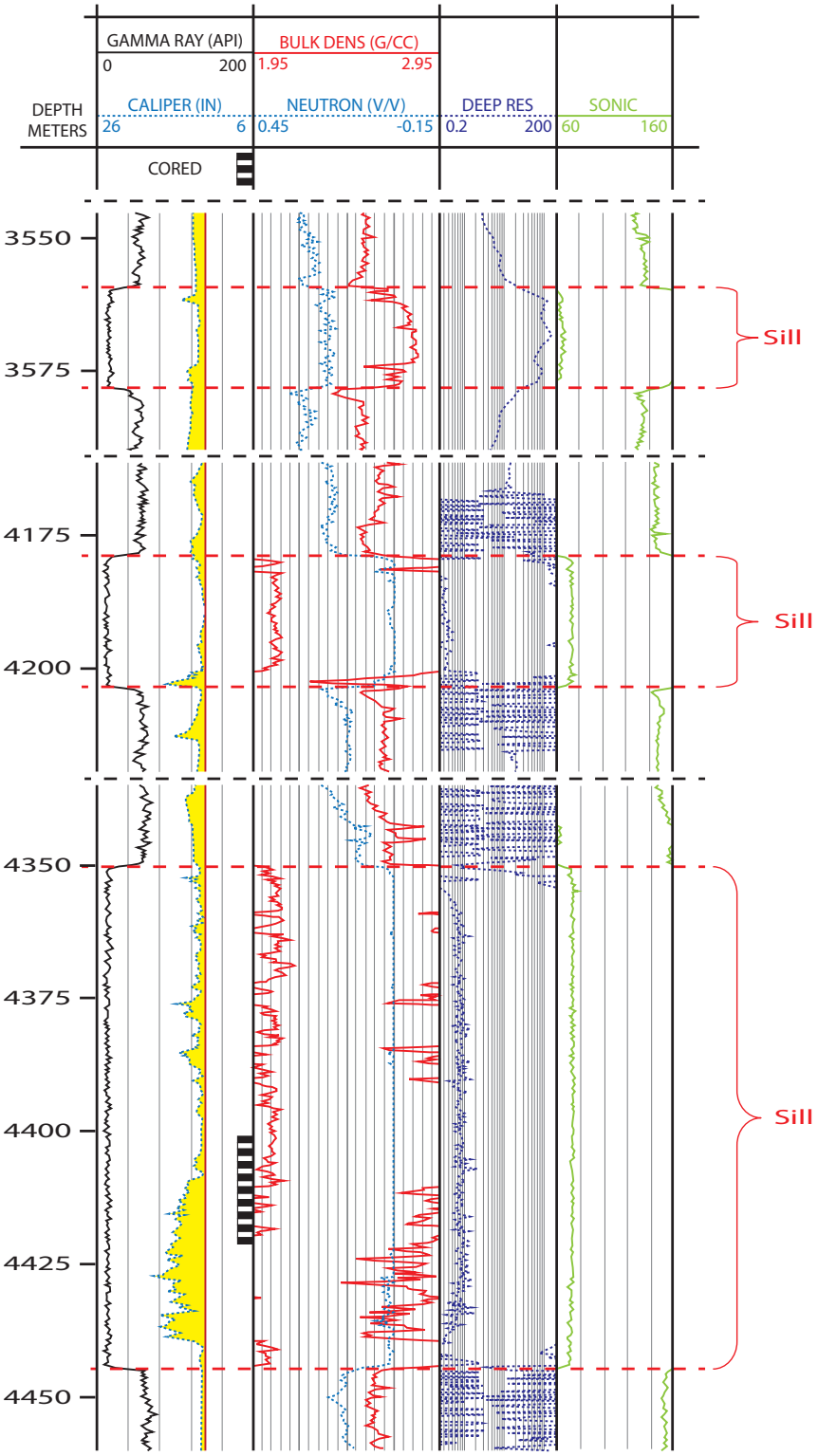

Figure 3
A simplified version of the Wireline logs from well 208/17-1 penetrating through three high amplitude structures that are interpreted as sills.

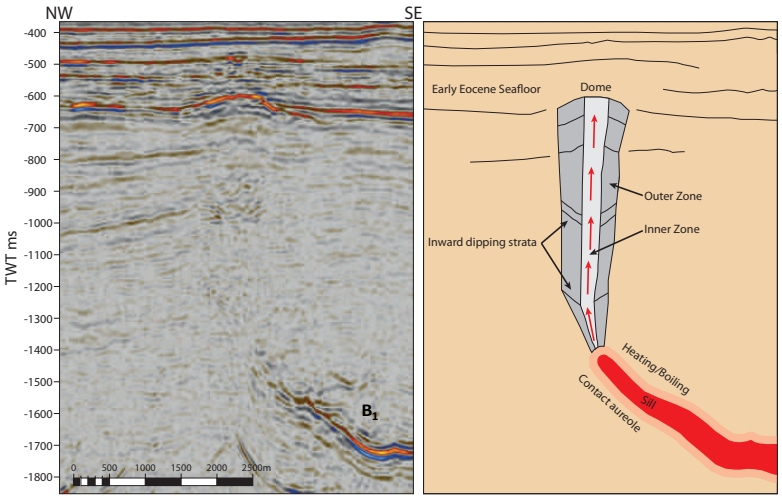

Figure 4
On left the seismic section of the hydrothermal vent located above B1 intrusion. On the right a drawing of the interpretations of the seismic section of the hydrothermal vent, showing the characterized dome and the inward dipping reflectors in the outer zone.

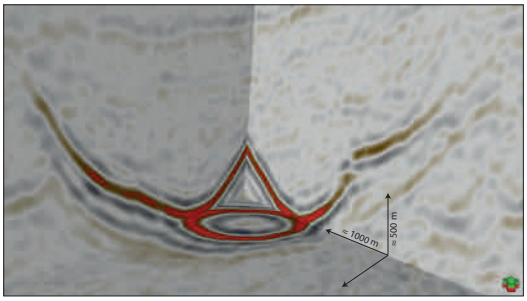

Figure 5
An example of an imaged cup-shaped intrusion on the 3D seismic data, where the cup-shape is clearly imaged on the XLine and InLine, and the circular form is clearly imaged on the time-slice. Red corresponds to an increase in the acoustic impedance created by the interface between sediments and the top of the magmatic body. It is seen that the intrusion transgresses the sedimentary bedding and has abrupt termination.

The variation of shapes described and the different possible genetic relations between the individual units, makes classification of intrusions based on their shapes difficult (Mathieu *et al*., 2008; Planke *et al*., 2005). Magmatic intrusions are classified in accordance with their morphological characteristic and in this study the focus is on the five most common intrusion types observed in the study area: *angled-*, *cone-shaped*, *cup-shaped-* and *saucer-shaped-*, and *connected-*complexes (Fig. 6 a to e).

The *angled intrusions* have been identified on seismic sections as high amplitude steep angle events that cut through the host strata in which the high amplitude event is truncating (Fig. 6.a). The distribution of the *angled-intrusions* varies, although typically they are planar and can be traced over large areas from tens to hundreds of square kilometres. They are interpreted as intrusions that tend to follow fault planes and stratigraphically weak zones, such as faults and bedded strata, or they are emplaced perpendicular to the axis of least principal stress (Planke *et al*., 2005; Smallwood and Maresh, 2002). It can be difficult to distinguish between intrusions and fault planes so the identification of *angled intrusions* can be difficult.

Cone-shaped intrusions are typically circular and with steep high angle sidewalls that dip inward toward a focal point (Fig. 6.b). They are identified on seismic sections as high amplitude V-shaped reflection events and a circular shape on a time-slice (Fig. 5).

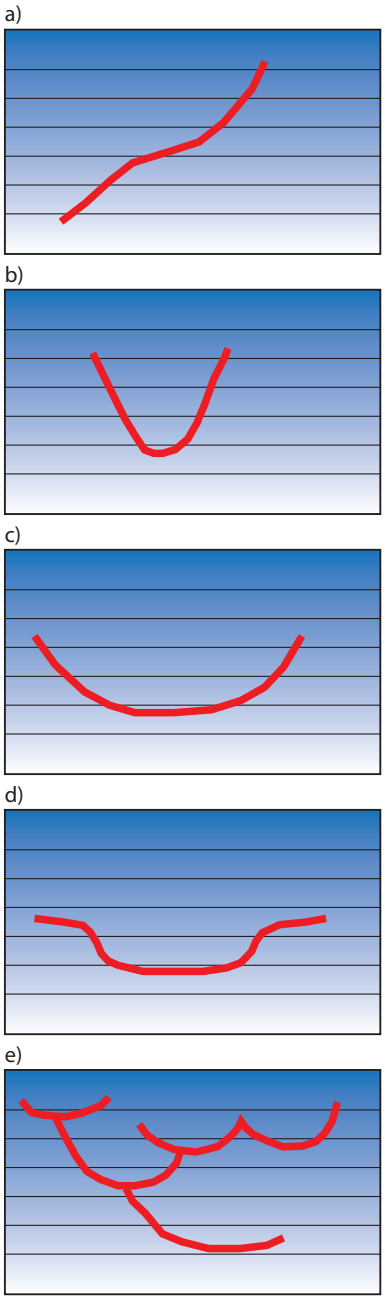

Figure 6
Classifications of intrusions. a) Angled-intrusion. b) Cone-shaped intrusion. c) Cup-shaped intrusion. d) Saucer-shaped intrusion. e) Connected-complex.

Cup-shaped intrusions are circular, varying from a lower low-angle part to a higher angle at the upper part on the sides (Fig. 6.c). On seismic sections they are identified by their high amplitude *cup-shaped* event (Mathieu *et al*., 2008).

Saucer-shaped intrusions are circular features with a flat inner rim, transgressing dipping sides that build upward and outward and their sides can range from high angle to low angle dips (Fig. 6.d). On seismic sections they appear as a high amplitude *saucer-shape* event with the remarkable flat inner rim and transgressing sides (Planke *et al*., 2005).

Connected complexes are intrusions that are connected in a larger complex and the intrusions can have almost all geometric forms (Fig. 6.e). These complexes vary in size but are typically up to tens of kilometres across, comprising several intrusions within each complex. Connected complexes in this study represent the amalgamation of two or more sills which may have been be fed from one or several feeders.

Results

3D screening of the Survey Area

To obtain an overview of the intrusions and the structural trend of the basin within the 3D survey area, two screening methods were used: volume rendering and 3D auto-tracking.

The high amplitude intrusions are well imaged with the *volume rendering* method due to the large acoustic impedance contrast between the host rock and the intrusion and typically the intrusions turned out to be *cup-* or *saucer-shaped*. The volume rendered survey shows that the high amplitude intrusions are predominantly located at a shallow level in the south-east and at a deeper level towards the north-west (Fig. 7).

Using the *3D auto-tacking* method the interpreter decides which high amplitude structure is to be mapped. When the tool is used for screening, the interpretation is undertaken every 100 lines, corresponding to a spacing of 1250 m. With this interval between interpreted seismic lines, minor errors occur where the tool may traces structures that are not intrusions, but it is considered satisfactory for this study to use every 100 lines for screening to get a better overview. Based on this screening of the survey area, smaller areas

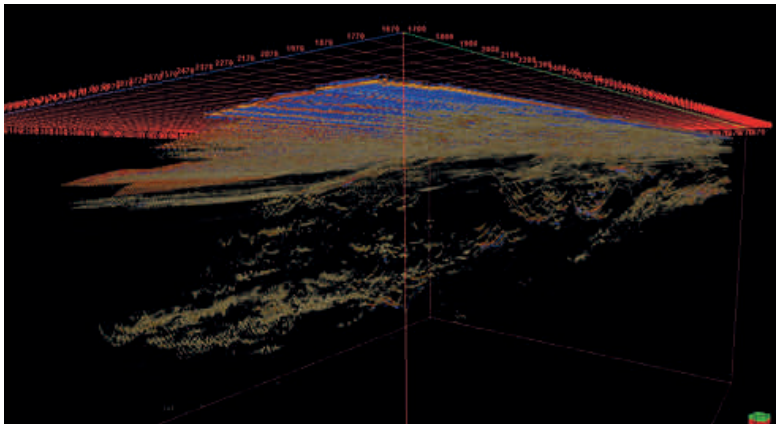

Figure 7
3D seismic window showing the volume rendered survey where high amplitude structures are made opaque and the rest is made transparent.

were subsequently chosen to illustrate the intrusions in more details.

Intrusions

The intrusions in the study area were divided into four dept levels, A to D (A being the deepest level and D the shallowest, (Fig. 8 and 9)). Intrusions at each level are further distinguished by numbers, according to stratigraphic depth, e.g. B_1 is located at a deeper level than B_2 (Fig. 8 and 9).

Intrusions at level A tend to be *angled intrusions*; intrusions at level B are larger, mostly single, *cup-shaped*. At level C the intrusions form a large *connected-complex*, of interconnected sills of all different shapes including some single outstanding *cone-shaped* and *cup-shaped* intrusions. Level D intrusions are *cone-, cup-* and *saucer-shaped*.

The maps in this paper are based on manual interpretation of the selected horizons chosen from volume rendering and auto tracking on seismic sections. These horizons have been converted into surfaces displayed as 2D and 3D figures (Fig. 8 and 9). The surfaces are created from the interpreted upper boundary of the intrusion, and hence do not show the thickness of the intrusions.

A relatively large local intrusive complex, named C_3 and located towards the north to north-east part of the study area (Fig. 1) has been subjected to further detailed study. C_3 is the largest intrusion/complex mapped in the survey area, and it has a maximum areal extent of 6.3 km by 5.0 km. The complex lies in a depth interval between 600 to 1100 ms. C_3 is subdivided into six smaller units $C_{3,1}$ to $C_{3,6}$. (Fig. 10).

$C_{3,1}$ is located in the south-western part of the C_3 intrusion, in the depth interval between 750 to 1100 ms, and is the deepest located intrusion. The south-eastern part of $C_{3,1}$ is circular and *cone-shaped* with the deepest point located in the centre of the cone (Fig. 11 and 12). Towards the west, the upper part of $C_{3,1}$ becomes rather flat, with a reduced dip angle when compared to its deeper parts (Fig. 11 and 12).

$C_{3,2}$ is located in the eastern part of the C_3 intrusion and lies in the depth interval of 750 to 1050 ms (Fig. 10). $C_{3,2}$ is circular with a diameter of 1.5 km, and is *cone-shaped* with a upward concave form at the bottom of the intrusion. The deepest point is located in the centre of $C_{3,2}$.

$C_{3,3}$ is found towards the north of the C_3 intrusion and is situated at a depth from 850 to 1100 ms (Fig. 10 and 12). $C_{3,3}$ is circular and has a *cone-shape,* with the deepest point located close to the centre, slightly on the eastern side of the complex.

$C_{3,4}$ is located in the south-eastern part of the C_3 intrusion and is found in the depth interval between 650 to 850 ms (Fig. 10). The south-eastern part of $C_{3,4}$ consists of an ellipsoidal V-shaped

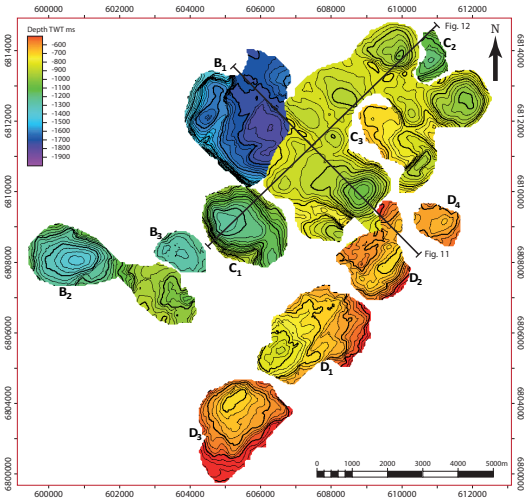

Figure 8

Mapped intrusions, from B to D, in the study area, where the interpreted horizons are converted in to surfaces. The surfaces are contour coloured, showing the depth in TWT in ms. Outline of the survey area is marked on figure (1) and Xline and inline location are shown.

structure, with its the long axis orientated in a north-east to south-west direction, which is the deepest point of $C_{3,4}$. The north-western part of $C_{3,4}$ is flatter, when compared to the general outline of $C_{3,4}$, but with some local depressions.

$C_{3,5}$ is a large flat structure located toward the north-west of the study area and is found at a depth interval of 750 to 950 ms (Fig. 10 and 12). $C_{3,5}$ constitutes two large interconnected forms, one *cup-shaped* towards the south-west, and one more *saucer-shaped* towards the north-east. The two forms are also connected with $C_{3,3}$ to the north-east and $C_{3,1}$ to the south-west.

$C_{3,6}$ is located in the southern part of the C_3 intrusion and lies at a depth of 800 to 850 ms (Fig. 10). $C_{3,6}$ is an ellipsoidal *cup-shape* with the long axis oriented north-east to south-west. One arm north of $C_{3,6}$ is connected to $C_{3,1}$. The mapping of $C_{3,6}$ hampered by imaging problems due to the fact that it lies beneath the shallower intrusion at the D-level.

C_3 has been interpreted to be fed from at least four points, i.e. the deepest part of $C_{3,1}$, $C_{3,2}$ and $C_{3,3}$ and the eastern part of $C_{3,4}$. Not all parts of the C_3 complex have been interpreted to be fed from its deepest point, but fed by the connected deeper part, where the magma is transgressing downward. Minor continuous amplitude „wings“ on the edges of some of the *cup-* and *saucer-shaped* structures can be followed within C_3 (Fig. 11 and 12) and are used to estimate the internal flow direction within the intrusive complex .

A hydrothermal vent is located above the south-western tip of intrusion B_1 (Fig. 4), and is located at an old seafloor of Early Eocene age. The Early Eocene seafloor horizon is mapped over a limited area and tied to two exploration wells 208/15-2 & 208/19-1 (Fig. 1) located fairly close (10-15 km) to the hydrothermal vent. With biostratigraphic available for these two exploration wells it is possible to estimate the time of emplacement of intrusion B_1, which is estimated to be the same age for both wells, Early Eocene (48.6 -55.8 Ma).

Interpretation of Complex C

The volume rendered survey shows that the high amplitude intrusions are dominantly situated at a shallow level toward the south-east and at a deeper level toward the north-west. This indicates that the intrusions follow the depth of the basement, which is shallower toward the south-east close to the margin of Shetland Platform and deeper towards the north-west in the centre of the basin. This suggests that the depth of emplacement was controlled by the depth of the basement (Smallwood and Maresh, 2002).

C_3 is interpreted to consist of several connected intrusions that form a large connected complex. C_3 is divided in six smaller complexes, from $C_{3,1}$ to $C_{3,6}$ (Fig. 10). The grouping is defined on the basis of which intrusion has the deepest point, i.e. $C_{3,1}$ is the deepest and $C_{3,6}$ the shallowest. C_3 has been interpreted to be fed from at least four points, the deepest part of $C_{3,1}$, $C_{3,2}$, $C_{3,3}$ and the eastern part of $C_{3,4}$.

Most parts of the C_3 complex are interpreted

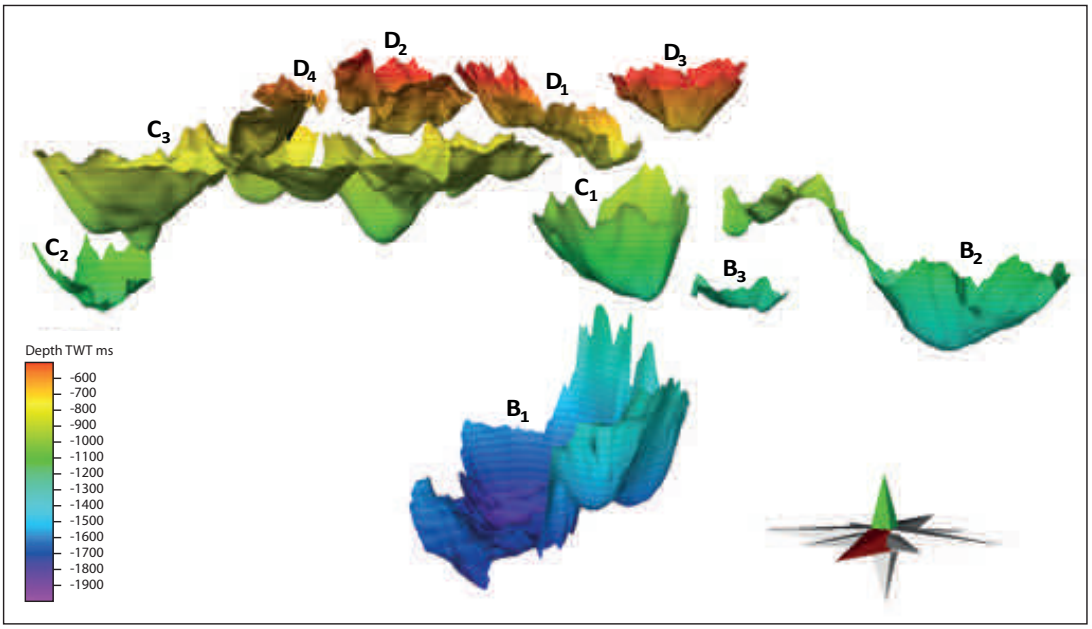

Figure 9

3D view of the mapped intrusions, from B to D, to illustrate the morphology/shape which is used to describe the intrusions. Also give an insight to the spatial (3D) relationship between sills. The surfaces are contour coloured, showing the depth in TWT in ms. Notice that the figure does not show the thickness of the intrusions, but only the top reflector.

to have been fed from its deepest point, but some parts are fed by the connected deeper part, where the intrusion is transgressive.

The plan view area of the C_3 intrusion can be relatively precisely estimated to be 11.66 km^2 using *geobody interpretations* facility in Petrel. On the other hand, the volume calculations, using the velocity of the intrusion is imprecise, because the *geobody interpretations* facility tends to automatically include the underlying multiples to the 'geobody'. Using the aspect ratio (length parameter : thickness) of sills, which is suggested to be 2000 : 1 (Bell and Butcher, 2002), the thickness of the intrusion can be estimated. Using this method the intrusion is estimated to have a thickness of only < 2 m, which is highly unlikely when it is so significantly imaged on the seismic data, with an estimated vertical resolution of 10 – 15 m. Therefore, to determine the volume of intrusion C_3 an estimated thickness of ≈ 45 m, corresponding to determined values for sills penetrated in the exploration well 208/17-1 is used to calculate the volume. Thus, using a thickness of ≈ 45 m the C_3 intrusion has a volume of ≈ 0.5 km^3.

Discussion

The two screening methods, *volume rendering* and *3D auto-tracking*, were used to get an overview of sill distribution and at what stratigraphic depth the sills were emplaced in the survey area. On the overview map of 3D auto-tracked intrusions it is seen that the intrusions found at the deepest level are located toward the north-west, in the deeper part of sedimentary basin and the intrusions found at the shallowest level are located toward the south-east, on the margin of the North Shetland Platform. This may support a model

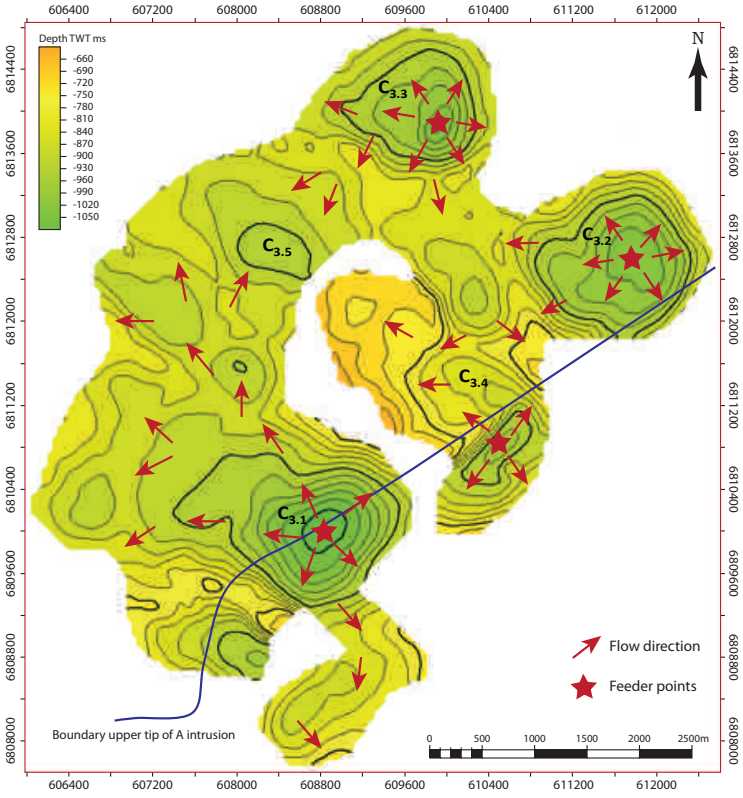

Figure 10
Map over intrusion C3 with suggested flow directions and feeder points. The blue line indicates an extrapolated line of the upper boundary of an A intrusion (angled-intrusion).

that the emplacement depth of intrusions is controlled by the depth of the crystalline basement in the Faroe-Shetland Basin, as suggested by (Bell and Butcher, 2002) and (Smallwood and Maresh, 2002).

The intrusions at the deepest level have a larger inner flatter rim (>5 km) of the *saucer-shape* before they start to transgress as compared to the smaller (<2.5 km) intrusions found at a shallower level towards the south-east. The intrusions toward the north-west cover 80-90 % of the area whereas the intrusions located towards the south-east cover 60-70 % of the area. This matches the observations of Bell and Butcher (2002), who noted that there are more sills at a shallower level on the margin of the basin than in the deeper central part of the basin, even though in the centre, where the crystalline basement is thinned to its largest extent, more numerous sills should be expected. Bell and Butcher (2002) argue that the reason for the lower number of sills in the centre of the basin is that the magma has climbed up through the crystalline basement fault blocks at the margin of the basin.

Vertical to sub-vertical structures are difficult to identify on seismic sections; therefore it is often not possible to identify what kind of feeder system have fed the sills. Furthermore, the feeder system generally is located beneath the sills and therefore poorly imaged because of disrupted seismic signal and noise e.g. multiples. However, it has been possible to identify potential feeders of individual sills in the area where a detailed interpretation is carried out, where the sills are feeding sills. Dike feeders do not possible to image on seismic data as they are vertical. Connections between sills that have been emplaced at different levels are recognized (Fig. 13). At locations where the highest tip of an underlying intrusion is located beneath, or close to, the deepest point of the overlying intru-

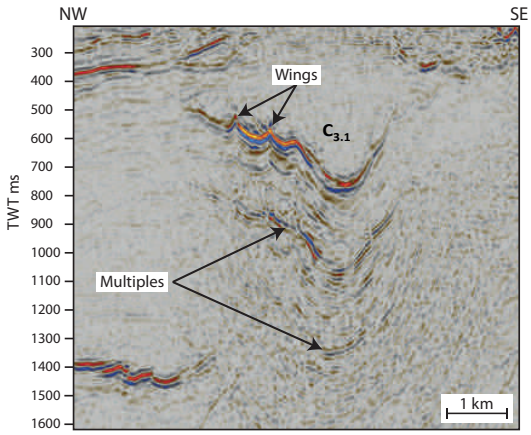

Figure 11

Seismic section showing the en-echelon structure in intrusion B1, intrusion C3.1 where the cup-shape is to the right and the more flat transgressing part to the left and intrusion D2 and how difficult it can be to interpret the shallow D intrusions because of other shallow disrupting structures. The continuous amplitudes „wings" are marked in the figure. Location indicated on Fig 8.

sion, it is suggested that the overlying intrusion was fed by the underlying intrusion during the same magmatic event. (Fig. 13) Illustrate one example of such interconnected intrusions. The intrusion, A, located at the deepest level, is *fault-controlled* and it is suggested that it is a feeder to the overlying intrusion, B_1. B_1 then builds further up and feeds the overlying intrusion, C_3, towards the west to south-west. The intrusion C_3 is building toward the south-east and feeds the intrusion, D_2. All these feeder systems are interpreted as point feeders, where the sill is fed by one point e.g. that the sills fed from one point, not necessarily from the centre of the sill but typically from the deepest point of the sill.

The mapped upper boundary of the A intrusion toward the south-east is indicated on (Fig. 10), close to three of the four interpreted feeder points of the C_3 intrusion, and hence intrusion A could be a potential feeder source to C_3. This feeder system is interpreted to be a *fault-controlled* dyke, although the specific feeders are still suggested to be represented by individual point sources.

This interpretation is supported by similar observations of feeders located at the deepest points on the two *saucer-shaped* parts of the Solsikke Sill Complex in the Møre Basin (Cartwright and Hansen, 2006). Smallwood and Harding (2009) argued that the inner Trýkleyvari Sill Complex in the Faroe-Shetland Basin appears to have been fed from below at one or more points at the periphery of underlying discordant intrusions. Cartwright and Hansen (2006) concluded that *saucer-shaped* sills are fed at their deepest, but not necessarily central, point and subsequently propagate outwards and upwards.

Studies of the Golden Valley sill in the Karoo basin in South Africa show that even if sills are interfingering, they may not have identical geochemical composition, and may, consequently, be interpreted to derive from two different magma sources which were emplaced during different intrusive events (Galerne *et al*., 2011; Galerne *et al*., 2008).

However, a connection between the intrusions in the survey area is suggested, as it looks as if the deepest part, which is interpreted as the feeder point, is located above the outer higher rim of the underlying intrusion.

The estimated dimensions of the onshore sills in the Faroe Islands (Hansen *et al*., 2011) have been used to calculate the approximately distribution of the sills intruded into the lava sequence of the Faroe Islands. Thus, the coverage of the lavas has been set to the size of the islands 1399 km^2 and the coverage of sills is calculated as 50.5 km^2 from the six largest sills (Hansen *et al*., 2011). From these numbers it is calculated that the coverage distribution of sills in the Faroese area is approximately 3.6 %.

The lateral coverage of sills in the survey area is estimated to be up to 90 % in some areas, which is significantly higher than the sill coverage onshore the Faroe Islands.

These numbers are however based on outcrop mapping of the sills onshore the Faroe Islands,

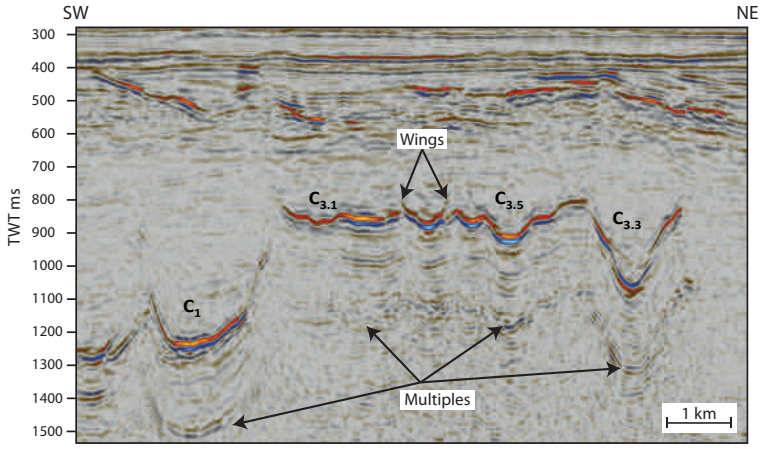

Figure 12
Seismic section showing the intrusion C1 with its flat inner rim, the north-western part of C3.1, the connected complex of C3.5 and the cone-shaped intrusion C3.3. The continuous amplitudes „wings" are marked in the figure. Location indicated on Fig. 8.

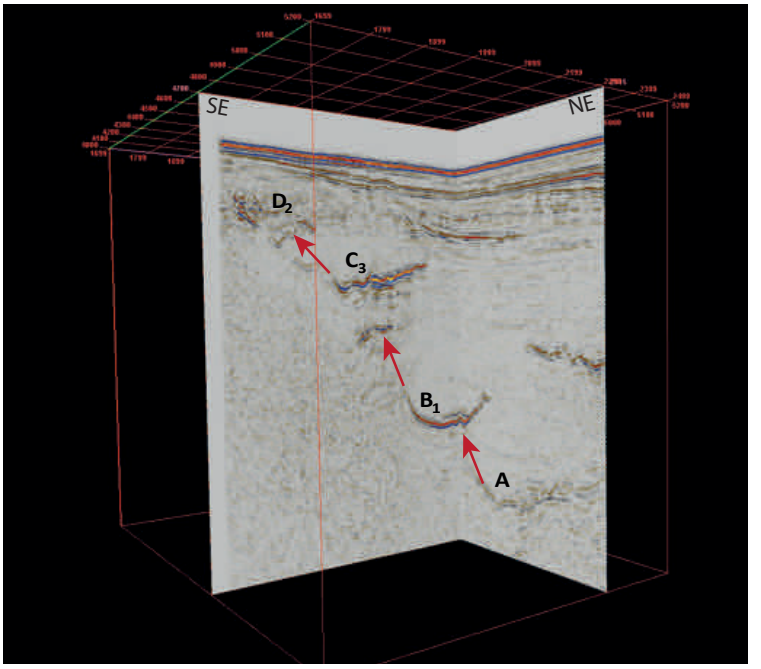

Figure 13
3D view of the study area with two seismic sections. The red arrows indicate the suggested connection between the different intrusions. A is suggested to build upward to feed B1. B1 is suggested to build upward to feed intrusion C3, which again is building upward to feed the shallow intrusion D2. The green line on the top is approximately 15 km.

without taking into consideration potential additional sills which may have been removed by erosion. This is in contrast to the estimated numbers from the surveyed area which are based on the seismic data allowing the mapping to include sills at various levels. This obviously gives a much better coverage as compared to the Faroe Islands as the number here is mostly based on plan level outcrop mapping. It could, consequently, be anticipated that more intrusions are present in the overall onshore succession, which also concur with the findings in the onshore Lopra-1 well in addition to the offshore Longan well (Fig. 1), where a stack of sills were encountered within the pile of otherwise extrusive basalt lavas.

Conclusion

Two seismic screening methods, *volume rendering* and *3D auto-tracking,* were successfully tested to get an overview of the survey area. They provided a fast and very good quality overview of the north-east to south-westerly trend of the Faroe-Shetland Basin, identified the location of high amplitude structures e.g. intrusions, and determined the distribution of deep sills in the north-westerly part and shallow sills towards the south-east.

It is suggested that the depth of sill emplacement is related to the depth of the crystalline basement, although this is not fully confirmed due to multiples and noise caused by the high amplitude intrusions, which hamper the mapping of the basement.

Detailed manual interpretation has been carried out that has led to the identification of a large number of various types of sills in the study area and intrusions are located at four levels, A-D, where A is the deepest intrusions and D the shallowest intrusions.

A large (11.66 km^2) connected sill complex is identified, which consists of at least four connected intrusions with their own local feeder, where three of these feeder points are suggested to be fed from the uppermost tip of the deepest underlying intrusion, A.

A sill complex, C_3, is identified and can be subdivided into six minor complexes.

A new method for estimating the flow direction, by looking at internal structures of continuous sills 'wings', is introduced and based on this it is possible to estimate the flow direction for intrusion C_3.

In the study area it is observed that the intrusions are connected to a larger complex and thereby interpreted to be caused by the same intrusive event, and hence be of the same age.

The age of the intrusions have been estimated to be of an Early Eocene age using well ties of a hydrothermal vent located within the survey area.

Acknowledgements

First of all I would like to thank DONG Energy for providing data and for permission to show examples of the data, models and interpretation. Thereafter I would like to thank Jarðfeingi for letting me finish this paper, and finally I would also like to thank Brian Bell and Kim Senger for the reviews resulting in a much better paper.

References

Andersen, M. S., Boldreel, L. O., and Group, a. T. S., 2009, Log responses in basalt sucessions in 8 wells from the Faroe-Shetland Channel – a classification scheme for interpretation of geophysical logs and case studies: Faroe Islands Exploration Conference: Proceedings of the 2nd Conference., p. 364-391.

Bell, B. R., and Butcher, H., 2002, On the emplacement of sill complexes: evidence from the Faroe-Shetland Basin, *in* Jolley, D. W., and Bell, B. R., eds., The North Atlantic Igneous Province: Stratigraphy, Tectonic, Volcanic and Magmatic Processes, Volume 197, Geological Society, London, Special Publications, p. 307-329.

Boldreel, L. O., 2006, Wire-line log-based stratigraphy of flood basalts from the Lopra-1/1A well, Faroe Islands, *in* Chalmers, J. A., and Waagstein, R., eds., Scientific Results from the Deepened Lopra-1 Borehole, Faroe Islands, Volume 9, Geological Survey of Denmark and Greenland Bulletin, p. 7-22.

Boldreel, L. O., and Andersen, M. S., 1993, Late Paleocene to Miocene compression in the Faeroe-Rockall area, *in* Parker, J. R., ed., Petroleum Geology of Northwest Europe: Proceedings of the 4th Conference: London, Geological Society, p. 1025-1034.

Bradly, J., 1965, Intrusion of major dolerite sills: Transactions of the Royal Society of New Zealand. Geology, v. 3 (4), p. 27-55.

Cartwright, J., and Hansen, D. M., 2006, Magma transport through the crust via interconnected sill complexes: Geology, v. 34, p. 929-932.

Dean, K., McLachlan, K., and Chambers, A.,

1999, Rifting and the development of the Faroe-Shetland Basin, *in* Fleet, A. J., and Boldy, S. A. R., eds., Petroleum Geology of Northwest Europe: Proceedings of the 5th Conference, Volume 1: London, The Geological Society, p. 533-544.

Earle, M. M., Jankowski, E. J., and Vann, I. R., 1989, Structural and Stratigraphic Evolution of the Faeroe-Shetland Channel and Northern Rockall Trough, *in* Tankard, A. J., and Balkwill, H. R., eds., Extensional Tectonics and Stratigraphy of the North Atlantic Margins, AAPG, p. 461-469.

Francis, E. H., 1982, Magma and sediment-I Emplacement mechanism of late Carboniferous tholeiite sills in northern Britain: Journal of the Geological Society, v. 139, no. 1, p. 1-20.

Galerne, C. Y., Galland, O., Neumann, E.-R., and Planke, S., 2011, 3D relationships between sills and their feeders: evidence from the Golden Valley Sill Complex (Karoo Basin) and experimental modelling: Journal of Volcanology and Geothermal Research, v. 202, no. 3-4, p. 189-199.

Galerne, C. Y., Neumann, E.-R., and Planke, S., 2008, Emplacement mechanisms of sill complexes: Information from the geochemical architecture of the Golden Valley Sill Complex, South Africa: Journal of Volcanology and Geothermal Research, v. 177, no. 2, p. 425-440.

Galland, O., Cobbold, P. R., Hallot, E., de Bremond d'Ars, J., and Delavaud, G., 2006, Use of vegetable oil and silica powder for scale modelling of magmatic intrusion in a deforming brittle crust: Earth and Planetary Science Letters, v. 243, no. 3-4, p. 786-804.

Galland, O., Planke, S., Neumann, E.-R., and Malthe-Sørenssen, A., 2009, Experimental modelling of shallow magma emplacement: Application to saucer-shaped intrusions: Earth and Planetary Science Letters, v. 277, no. 3-4, p. 373-383.

Hansen, J., Jerram, D. A., McCaffrey, K., and Passey, S. R., 2011, Early Cenozoic saucer-shaped sills of the Faroe Islands: an example of intrusive styles in basaltic lava piles: Journal of the Geological Society, v. 168, no. 1, p. 159-178.

Malthe-Sørenssen, A., Planke, S., Svensen, H., and Jamtveit, B., 2004, Formation of saucer-shaped sills, *in* Breitkreuz, C., and Petford, N., eds., Physical Geology of High-Level Magmatic Systems, Volume 234, Geological Society, London, Special Publications, p. 215-227.

Mathieu, L., van Wyk de Vries, B., Holohan, E. P., and Troll, V. R., 2008, Dykes, cups, saucers and sills: Analogue experiments on magma intrusion into brittle rocks: Earth and Planetary Science Letters, v. 271, no. 1-4, p. 1-13.

Mudge, D. C., and Rashid, B., 1987, The geology of the Faeroe Basin area, *in* Brooks, J., and Glennie, K. W., eds., Petroleum Geology of North West Europe: Proceedings of the 3rd Conference: London, Graham & Trotman, p. 751-763.

Passey, S. R., and Jolley, D. W., 2009, A revised lithostratigraphic nomenclature for the Palaeogen Faroe Island Baslat Group, NE Atlantic Ocean: Earth and Environmental Science Transactions of the Royal Society of Edinburgh, v. 99, p. 127-158.

Planke, S., Rasmussen, T., Rey, S. S., and Myklebust, R., 2005, Seismic characteristics and distribution of volcanic intrusions and hydrothermal vent complexes in the Vøring and Møre basins, *in* Doré, A. G., and Vining, B. A., eds., Petroleum Geology: North-West Europe and Global Perspectives – Proceedings of the 6th Petroleum Geology Conference: London, The Geological Society, p. 833-844.

Polteau, S., Mazzini, A., Galland, O., Planke, S., and Malthe-Sørenssen, A., 2008, Saucer-shaped intrusions: Occurrences, emplacement and implications: Earth and Planetary Science Letters, v. 266, no. 1-2, p. 195-204.

Ritchie, D. K., Ziska, H., Johnson, H., and Evans, D., 2011, Geology of the Faroe-Shetland Basin and adjacent areas, British Geological Survey, Edinburgh and Jarðfeingi, Tórshavn, 317 p.:

Smallwood, J. R., and Harding, A., 2009, New seismic imaging methods, dating, intrusion

style and effects of sills: A drilled example from the Faroe-Shetland Basin, *in* Varming, T., and Ziska, H., eds., Faroe Islands Exploration Conference Proceedings of the 2nd Conference: Tórshavn, Føroya Fróðskaparsetur, p. 104-123.

Smallwood, J. R., and Maresh, J., 2002, The properties, morphology and distribution of igneous sills: modelling, borehole data and 3D seismic from the Faroe-Shetland area, *in* Jolley, D. W., and Bell, B. R., eds., The North Atlantic Igneous Province: Stratigraphy, Tectonic, Volcanic and Magmatic Processes, Volume 197, Geological Society, London, Special Publications, p. 271-306.

Varming, T., 2009, Results from the drilling of the 1st license round wells in the Faroese part of the Judd Basin, *in* Varming, T., and Ziska, H., eds., Faroe Islands Exploration Conference Proceedings of the 2nd Conference: Tórshavn, Føroya Fróðskaparsetur, p. 346-363.

Geophysical aspects of basalt geology and identification of intrabasaltic horizons

UNI K. PETERSEN[1], R. JAMES BROWN[2], MORTEN S. ANDERSEN[3]

1: Jarðfeingi. Brekkutún 1, Hoyvík
2: Professor of Geophysics, Department of Petroleum Engineering,University of Stavanger
3: Senior research geophysicist, Geological Survey of Denmark and Greenland, Øster Voldgade 10

*Corresponding author: Uni Kárason Petersen: uni.petersen@jardfeingi.fo

Abstract

This work addresses geophysical aspects of Faroes basalt geology and aims to extend geological information onto conventional seismic data in the Faroes area. The work is based on VSP and surface seismic data acquired at Glyvursnes in 2003 (SeiFaBa project), recently reprocessed OF94/95 seismic data, and well logs from the Lopra, Vestmanna and Glyvursnes wells. Further, this work is intended as an aid to model-driven processing of data.

Differences in composition among the three major basalt formations lead to quite different seismic properties. The reflection series for the Malinstindur Fm has low amplitudes and appears transparent for seismic signals, with little scattering of seismic energy, while the overlying Enni and underlying Beinisvørð Fms have high amplitudes with much more apparent energy scattering. As a result, the division between the Beinisvørð and the Malinstindur Fms, the A-horizon, shows as a well-defined horizon on seismic data and it is expected that, with proper processing, it will be identifiable on a large part of the Faroese continental shelf and form a key seismic marker in deducing Cenozoic evolution.

Faroe Islands Exploration Conference: Proceedings of 4th Conference.
Annales Societatis Scientiarum Færoensis Supplementum LXIV.

Introduction

Obtaining good sub-basalt seismic images is known to be problematic. Loss of transmitted seismic energy due to low transmission coefficients at top- and base-basalt (e.g. Fruehn et al., 2001) and attenuation and scattering during propagation through basalts (e.g. Maresh et al., 2006) are often referred to as the main obstacles in sub-basalt imaging (e.g. White et al., 2003; Ziolkowski et al., 2003).

However, some seismic energy is indeed transmitted through basalt complexes, so the problem amounts to separating primary energy from noise (Planke et al., 1999). Gallagher and Dromgoole (2008) have demonstrated this by reprocessing a series of profiles with the main focus on filtering out high frequencies, removing multiples, and using velocity models that take into account geological models for the areas.

The need for using geological models as constraints on the velocity models applied during processing is due to a large and abrupt velocity contrast between basalts and sediments. Velocity models picked from conventional velocity analyses of seismic surface data do not typically catch the step-like increases of instantaneous velocity that occur on crossing sediment-basalt boundaries, but rather tend to exhibit more or less steep velocity gradients across such boundaries. Interval velocities at the top-basalt that are too low will result in interval velocities deeper down that are too high and will not yield the optimal stacking velocities for NMO corrections at depth.

Identification of basalt sections on preliminary stacks allows one to assign the high velocities expected for the top-basalt. This will result in a more appropriate velocity model and will affect all aspects of the processing, whether it be stacking, various 2D filtering methods or migration of the data—be it prestack or poststack.

Note that the term *basalt*, in connection with sub-basalt imaging, includes all basaltic rocks. During this paper the term *basalt* will be used for all rocks of basaltic origin, be they lava flows, volcaniclastics, hyaloclastics or intrusives.

Identification of base-basalt is usually much more complex than identifying top-basalt. The problem of proper interpretation of base-basalt is due to the seismic variability of basalt (Petersen et al., 2006) and to the fact that base-basalt is probably in many cases not a simple reflector. Formations consisting of subaerial lava flows could grade downward into hyaloclastites, as is the case in the Lopra-1A well (Christie et al., 2006). At the transition from subaerial flows to hyaloclastites the seismic response changes significantly towards lower amplitude. Better understanding of seismic facies of volcanic rocks gives the means for better estimates of total basalt thickness and thus better constraints on velocity models.

During the last decade or so interpretation of seismic data has been used to identify properties of volcanic sections as an aid in describing the development of the areas and emplacement of lavas. E.g., Spitzer et al. (2008) interpret seaward-dipping reflectors, hyaloclastites and flow-foot breccia sequences. Planke et al. (2000) present a rather extensive study of seismic volcanostratigraphy, identifying various facies such as: landward flows, lava delta, inner flows, inner seaward dipping reflectors (inner SDR), outer high, and outer SDR. While the previous studies have focused on identifying facies related to the emplacement type of the lava, we focus on intrabasalt reflections and compare subaerially emplaced lava formations.

The present paper continues an earlier investigation (Petersen et al., 2006) of the seismic response of volcanics around the Glyvursnes-1 well, which established a difference in the gross seismic response of the different lava formations based on modelling. We now present a continuing analysis of the well logs and the upgoing VSP arrivals, with the main focus on tying to the seismic data. Further, processing parameters derived from the Glyvursnes experiment are used to reprocess a conventional seismic profile in the vicinity of Glyvursnes with the aim of reproducing a seismic response similar to that observed at Glyvursnes. This work addresses geophysical aspects of the basalt geology. The aim is to extrapolate the geological information from well

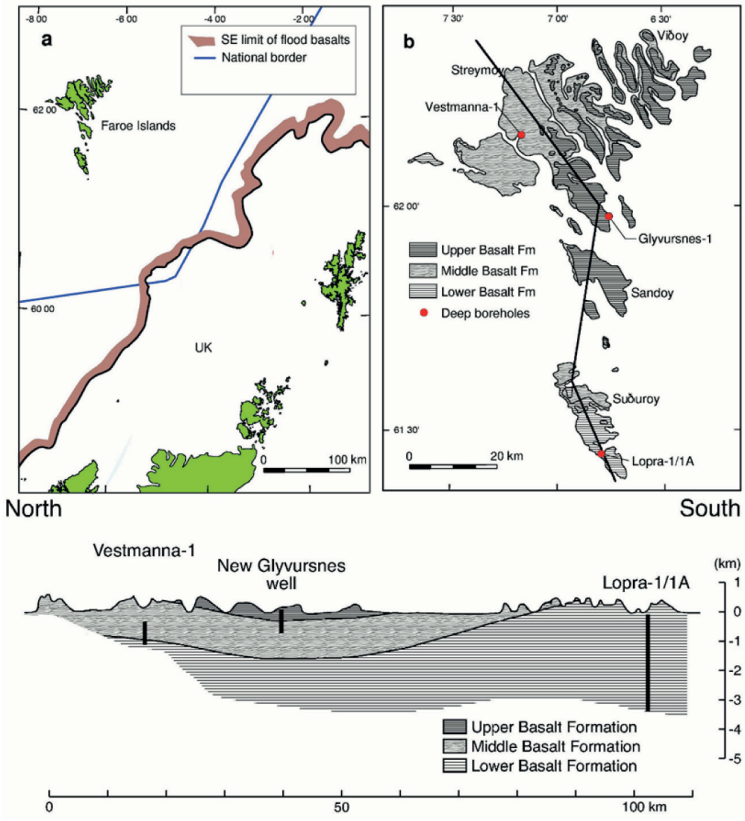

Figure 1
Upper a: Location of the Faroe Islands relative to the extent of flood basalts. The international border of the Faroes territory is shown as a blue line (modified from Sørensen, 2003). Upper b: Geological map of the Faroe Islands showing the locations of deep boreholes (Vestmanna-1, Glyvursnes-1 and Lopra-1/1A) and the distribution of the three Paleogene basalt formations (modified from Rasmussen and Noe-Nygaard, 1970). Lower: Geological section through the Faroe Islands with the three wells (modified from Waagstein, 1988). Location of profile is shown on upper b.

logs to the offshore area, thus providing better means for the interpretation and mapping of basalt formations in the Faroes area.

Geology

A lava pile, about 3 km thick, of the Faroe Islands Basalt Group (FIBG), is exposed on the Faroe Islands (Figure 1) (Rasmussen and Noe-Nygaard, 1970). The Lopra-1/1A well penetrated approximately a further 3 km of volcanic rocks below the exposed succession without reaching the base of the volcanic succession (Ellis et al., 2002). Andersen et al. (2002) suggested, that about 1 km of basalt may have been eroded from the top of the volcanic pile. The gross stratigraphic thickness of the Faroe basalt complex would thus be about 7 km, possibly more. Deep seismic results from wide-angle experiments support this estimate (e.g. Richardson et al., 1999).

The exposed basalts were divided into three formations: the lower, middle, and the upper basalt formations, representing the three eruptive sequences (Figure 1, upper b & lower) (Rasmussen and Noe-Nygaard, 1970; Waagstein, 1988). The stratigraphy of the Faroes has since been formalised following international guidelines (Passey and Jolley, 2009) (Figure 2). In this paper we will use the new stratigraphy; however, we will retain the old names for the separation between the Malinstindur and Beinisvørð Fms, i.e. the A-horizon, and the separation between the Enni and Malinstindur Fms, i.e. the C-horizon. The A- and C-horizons are chronostratigraphic horizons, but, though the A-horizon marks a lithological shift, the C-horizon does not do so everywhere (Rasmussen and Noe-Nygaard, 1969; Waagstein, 1988)

General properties of the lava formations are

Well name	Lopra-1/1A	Vestmanna-1	Glyvursnes-1
Section of stratigraphic sequence covered by well	Beinisvørð Fm below 900 m and top 1000 m of Lopra Fm	Lowest 560 m of Malinstindur Fm and uppermost 100 m of Beinisvørð Fm	top 350 m of Malinstindur Fm and bottom 350 m of Enni Fm
V_P (velocity)	High-frequency variations mainly between about 4 and 6 km/s relating to flows and beds while the average velocity from VSP is 5.25 km/s.[2]	Variation mainly between 5 and 6 km/s while the average velocity from VSP is 5.29 km/s.[1,3]	The Enni Fm shows similar variations to those from the Lopra-1/1A log, between 4 and 6 km/s; the Malinstindur Fm shows variations similar to those from the Vestmanna-1 well but here mainly between 4 and 5 km/s. The average velocity from VSP is 4.13 km/s.[1,3]
V_P/V_S ratio from log	1.84[2]	1.8[1]	1.8[1]
V_P/V_S ratio from VSP	1.81[2]	1.9[4]	2.0[4]
Quality factor, Q	35 on average[2]	25 on average[4]	25 on average, 15 for the Enni Fm and 30 for the Malinstindur Fm[4]

Table 1.
(From Petersen et al., 2013) Overview of velocity and attenuation information from three wells in the Faroes (Superscripts refer to: 1: Waagstein and Andersen, 2003; 2: Christie et al., 2006; 3: Shaw, 2006; 4: Shaw et al., 2008).

shown in Table 1 and are taken from the three deep wells located at Lopra, Vestmanna and Glyvursnes covering ~4.8 km of the Faroese volcanic succession.

The surface seismic data from Glyvursnes (Petersen et al., 2006) established that the seismic facies of the overlying Malinstindur Fm differs from those of the overlying and underlying Enni and Beinisvørð Fms, the Malinstindur Fm having much lower amplitude—being apparently more transparent to seismic signals. There is a significant reflection at ~0.6 s separating the Enni and Malinstindur Fms. Based on this, and on comparison of seismic facies of synthetic data versus field seismic data, an estimated thickness of the Malinstindur Fm of ~1050 m and depth of the Prestfjall Fm of ~1390 m at Glyvursnes were established.

Data base

The analysis is based on a seismic experiment at Glyvursnes combining land seismic data acquisition with combined land-marine seismic data acquisition in conjunction with well logs and zero-offset VSP. The Glyvursnes experiment was designed to facilitate model-driven analysis of the seismic facies of surface seismic profiles in an area with relatively well known geology. The thickness of the basalt succession at Glyvursnes is estimated to be several km. The modelling is based on well logs, synthetic seismograms (primaries-only) and full-waveform modelling. Ties have been made between well-logs and vertical seismic profiles (VSP). The work is based on data acquired as part of the SeiFaBa project (Japsen et al., 2006; Petersen, 2014). Subsequently, conven-

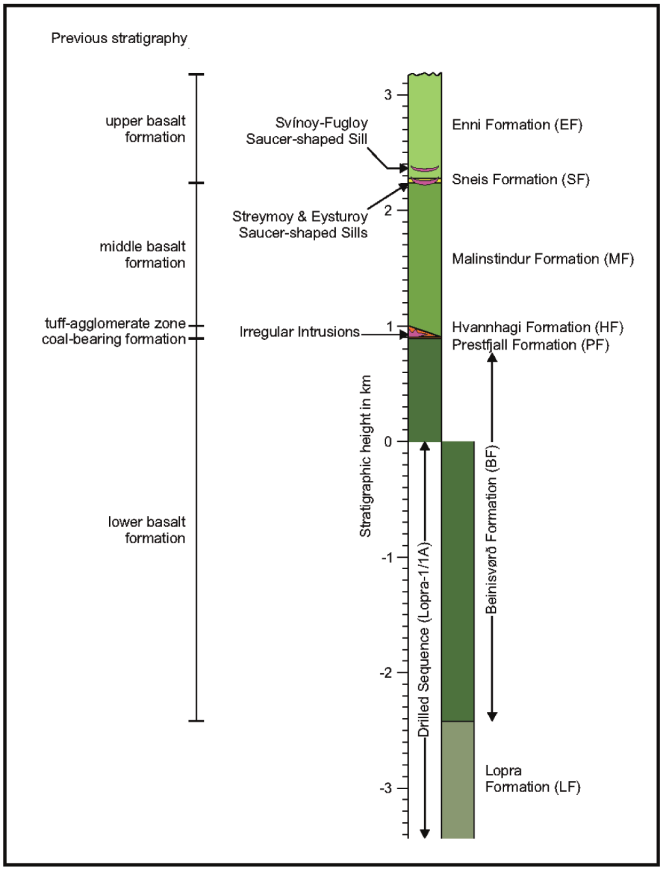

Figure 2
Stratigraphic column for the onshore FIBG. The previous stratigraphy is given to the left of the column for comparison (adapted from Passey and Bell, 2007).

tional seismic data from the Western Geophysical OF94 survey were included in the analysis.

Surface seismic data

The land seismic data consist of two 600-m long geophone layouts oriented perpendicular to each other. The total number of stations for each profile is 120 and station interval is 5 m. Shotpoint interval was ~10 m. Due to logistics some shotpoints were skipped and some shotpoints are missing due to misfires.

The combined data acquisition comprised two 400-m long geophone layouts and a 600-m long streamer deployed in conjunction with one of the geophone layouts. The recording profiles were oriented perpendicular to each other. The 400-m geophone layouts consisted of 80 elements placed at 5-m intervals. The streamer had 96 channels, with a 6.25-m group interval. The streamer was moored at 3 m depth between a jack-up rig at the shoreline and a tugboat at the other end. The source was towed at a depth of 4 m. The distance between shots was <20 m.

The two land seismic profiles and the single marine seismic profile are processed to stack with standard 2D processing while the combined air-gun-geophone recorded data are processed to stack with 3D processing. Figure 3 shows navigation for stacked data. The stacked data have previously been presented by Petersen et al. (2006) and a full description of the acquisition and processing parameters is given by Petersen (2014). Further,

refraction seismic modelling based on a subset of the data has been presented by Petersen et al. (2013).

Logs

In addition to the Glyvursnes-1 well, logs from the Lopra-1/1A and the Vestmanna-1 well drilled in 1980 and 1981 (Hald and Waagstein, 1984; Nielsen et al., 1984; Waagstein and Hald, 1984) have been analysed. These wells are located about 28 and 60 km, respectively, from Glyvursnes (Figure 1b). The Lopra-1/1A well was deepened and logged again in 1996 (Chalmers and Waagstein, 2006) making P-wave sonic and bulk-density logs available from the depth interval 200 – 3600 m. The Glyvursnes-1 well was drilled in 2003 and at the same time the Vestmanna-1 well was reamed. Full-waveform sonic and bulk-density logs in the Vestmanna-1 and Glyvursnes-1 boreholes were acquired as part of the SeiFaBa project (Waagstein and Andersen, 2003; Japsen et al., 2005).

Based on these wells, and based on the mapping of the boundaries of various stages of volcanism (Rasmussen and Noe-Nygaard, 1970; Waagstein, 1988), a model, i.e. a composite log, of seismic properties was constructed for the three major basalt formations. The model has previously been presented by Petersen et al. (2006).

VSP upgoing wavefield and tie to well logs

Zero-offset VSPs were acquired in both the 700-m-deep Glyvursnes well and the 660-m-deep Vestmanna well as part of the SeiFaBa project. The VSP at Glyvursnes was sampled at 10-m intervals in the 50 – 600-m depth range. The Vestmanna VSP was sampled at 5-m intervals in the 50 – 500-m depth range. Attenuation studies based on VSPs from these two wells have previously been published by Shaw (2006) and by Shaw et al. (2008).

Conventional seismic data in the vicinity of Glyvursnes

Conventional seismic reflection profiles from the OF94 *Western Geophysical* conventional survey in the vicinity of Glyvursnes are included in the present study. The data were acquired with a 5280-in^3 airgun array and a 6000-m-long streamer with 480 channels, 12.5-m group interval and 12.5-m group length.

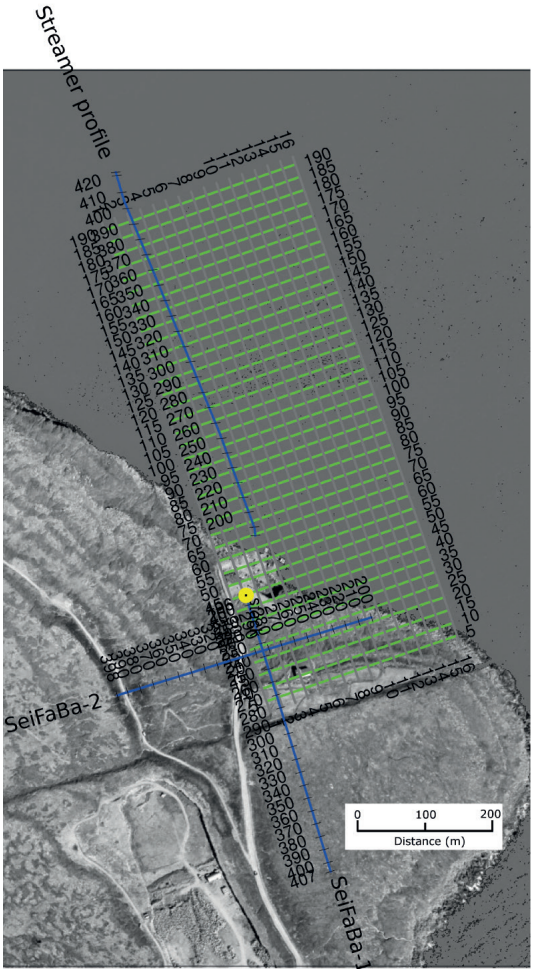

Figure 3
The grid used for the 3D geometry of the airgun-geophone data (every inline and every fifth cross-line is shown); the positions of the 2D airgun-streamer data (Streamer profile) and the two 2D dynamite-geophone lines (SeiFaBa-1 and SeiFaBa-2) are also shown. All positions are common depth points (CDP). The position of the Glyvursnes-1 borehole is marked with the yellow dot.

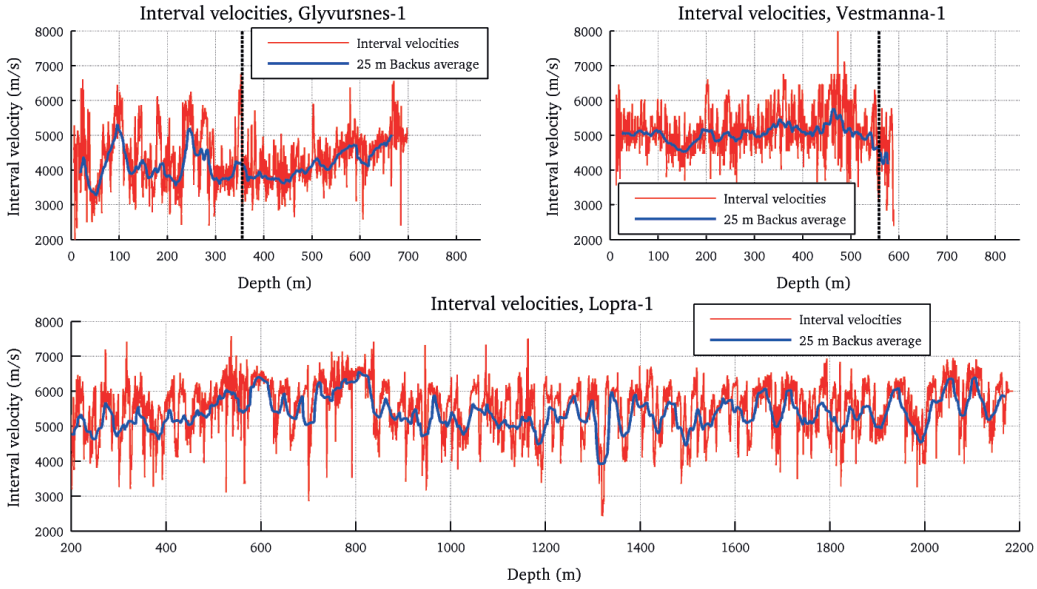

Figure 4

P-wave velocity logs at initial sampling and at 25-m Backus averaging. Well logs for Glyvursnes and Vestmanna are the full-waveform velocity logs processed by the Geological Survey of Denmark and Greenland (GEUS) and the bulk-density logs recalibrated to measurements on core (Waagstein, unpublished data). For Lopra the Lopra-1 SVEL log was used and bulk density log RHOB. The vertical black stippled line on the upper left figure marks the Enni-Malinstindur boundary, the C-horizon, and on the upper right figure it marks the Malinstindur-Beinisvørð boundary, the A-horizon.

Results

Logs

The basalt successions covered by the Lopra, Vestmanna and Glyvursnes wells have attenuation of similar magnitude and V_P/V_S ratios that are not too different (Table 1). On the other hand, the velocity distribution in the Enni and Beinisvørð Fms differs from that of the Malinstindur Fm. Velocity fluctuations within the Enni and Beinisvørð Fms are significantly greater than those in the Malinstindur Fm. This difference is preserved after applying Backus averaging (Backus, 1962) at 25-m intervals (Figure 4). The 25-m interval was chosen because it has been shown to be a representative scale for seismic wave propagation through the basalt succession at Glyvursnes (Petersen et al., 2013).

Backus averaging also computes the horizontal P-wave velocity. At Backus averaging of 25-m intervals, horizontal P-wave velocities are higher than vertical P-wave velocities (Figure 5). For the Enni Fm horizontal P-wave velocities are about 5 – 10% higher, and for the Malinstindur Fm they are about 1 – 4% higher. This is consistent with previous anisotropy analysis on the Vestmanna-1 well logs, where horizontal P-wave velocities are reported to be less than 2.5% higher than vertical P-wave velocities (Bais et al., 2009). Similar calculations on the Lopra-1A well logs, covering a major part of the Beinisvørð Fm, show that horizontal P-wave velocities are ~5% higher than vertical velocities (Christie et al., 2006). In contrast, modelling on a walkaway VSP at Lopra shows ~10% higher vertical velocities in the uppermost 800 m (Kiørboe and Petersen, 1995).

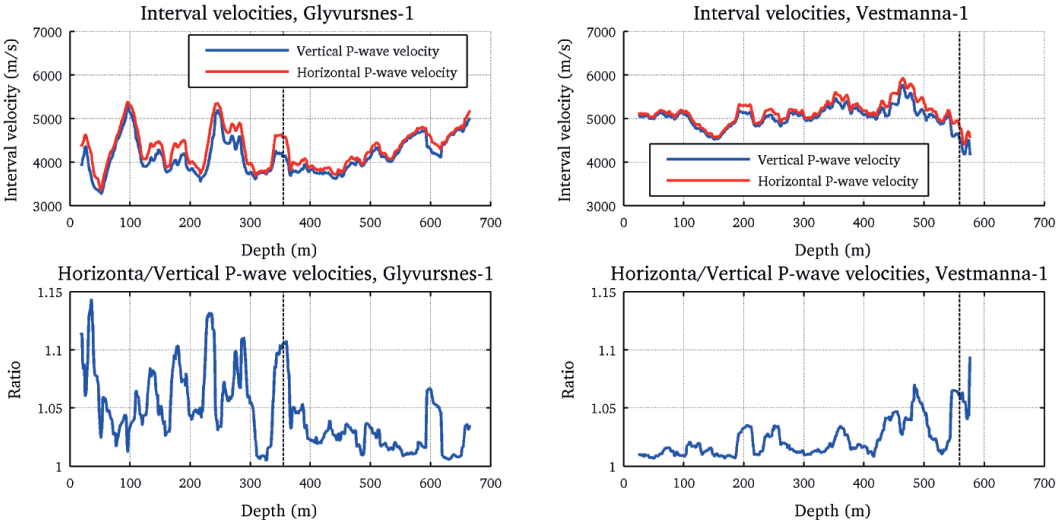

Figure 5

Upper left and right: Vertical and horizontal P-wave velocity for Glyvursnes-1 and Vestmanna-1 calculated by 25-m interval Backus averaging. Lower left and right: Ratio of the horizontal to the vertical P-wave velocity. The vertical black stippled line on the left-hand diagrams marks the Enni-Malinstindur boundary, the C-horizon, and on the right-hand diagrams marks the Malinstindur-Beinisvørð boundary, the A-horizon.

Refraction seismic modelling at Glyvursnes also indicates higher vertical velocities in the uppermost 200 m (Petersen et al., 2013). The latter two conflicting results could possibly be related to the method, i.e. ray-tracing, although it is not clear how.

Figures 6 and 7 show the acoustic impedance and reflectivity of the Enni and Malinstindur Fms and the signature of the C- and A-horizons based on well logs. Both the C-horizon and the A-horizon are located between two reflectors with opposite polarity. In the Glyvursnes log there is a clear difference in reflectivity on either side of the C-horizon. The reflectivity of the Enni Fm is clearly of greater magnitude than that of the underlying Malinstindur Fm. The Vestmanna log covers too little of the Beinisvørð Fm to enable comparison of its properties with those of the Malinstindur Fm.

The model

Joint depth-scale analysis using the continuous wavelet transform (CWT) on the composite log used for the model shows that the Malinstindur Fm appears with much lower amplitude in most of the scale range for the velocity and density logs. This property is preserved for the acoustic impedance while for the reflectivity, the Malinstindur Fm has relatively high amplitudes for the shorter scales. Concentration of energy at certain scales is related to e.g. thicknesses of flow lobes, and flow units, and distance between sedimentary beds of significance. It is worth noting that the differences between the basalt formations that show so clearly on the CWT analysis also are reflected by the visual appearance of exposed basalt sections on hillsides (Figure 8).

Full-waveform modelling

The general seismic response related to the three major basalt formations was modelled using full-waveform modelling. A 2D model was generated based on the composite log. Since the dip of the exposed basalt flows in the investigated area is near-horizontal, about 2° (about 3.5 m vertically per 100 m laterally) with strike oriented to the

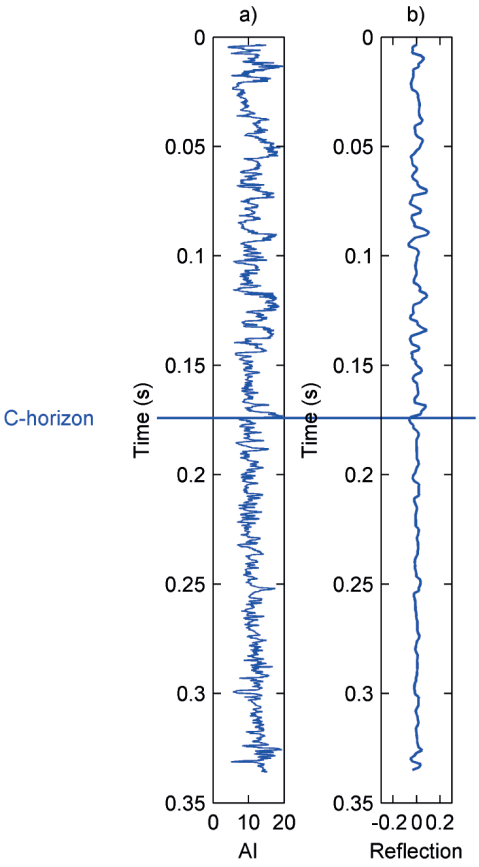

Figure 6
The Glyvursnes well. a) The acoustic impedance, AI. b) The reflectivity calculated with logs resampled to 6.2 m. The location of the C-horizon is taken from Waagstein and Andersen (2003).

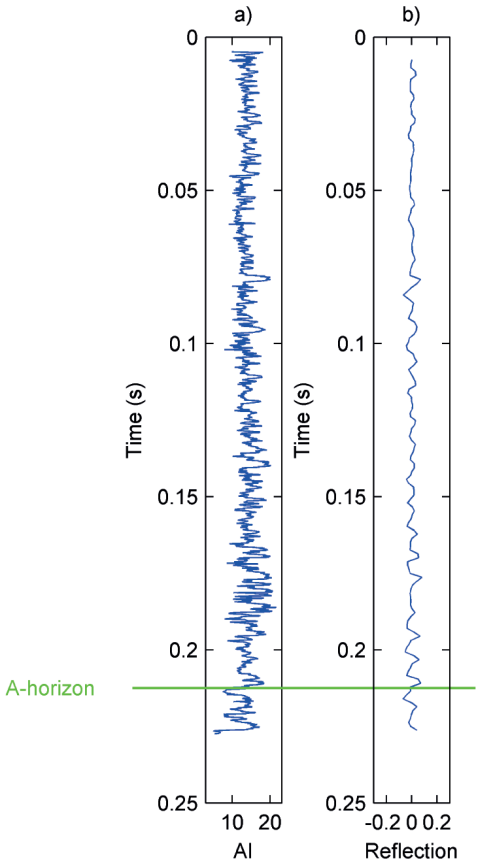

Figure 7
The Vestmanna well. a) The acoustic impedance, AI. b) The reflectivity calculated with logs resampled to 6.2 m. The location of the A-horizon is taken from Waagstein and Andersen (2003).

west-southwest, it was considered adequate to model layers as horizontal thus simplifying the process.

The initially 0.1-m sampled logs were resampled to 3-m intervals and expanded horizontally, thus producing a 2D model. It should be noted that at 3-m sampling intervals the Backus averaging shows no significant difference in horizontal and vertical velocities. The modelling was based on the ELA2D code (Falk, 1996).

The full-waveform data were generated using the same acquisition geometry as for one of the land-seismic profiles and processed to stack with similar processing parameters. The seismic response shows a division in seismic facies that can be related to the Enni, Malinstindur and Beinisvørð Fms, the Malinstindur being much lower in amplitude than the overlying and underlying Enni and Beinisvørð Fms (Figure 9). Applying the CWT to the seismic traces also shows that the characteristics of the logs seen in Figure 8 are preserved in the seismic data. At Glyvursnes it should thus be possible to identify the Malinstindur Fm directly from the seismic facies.

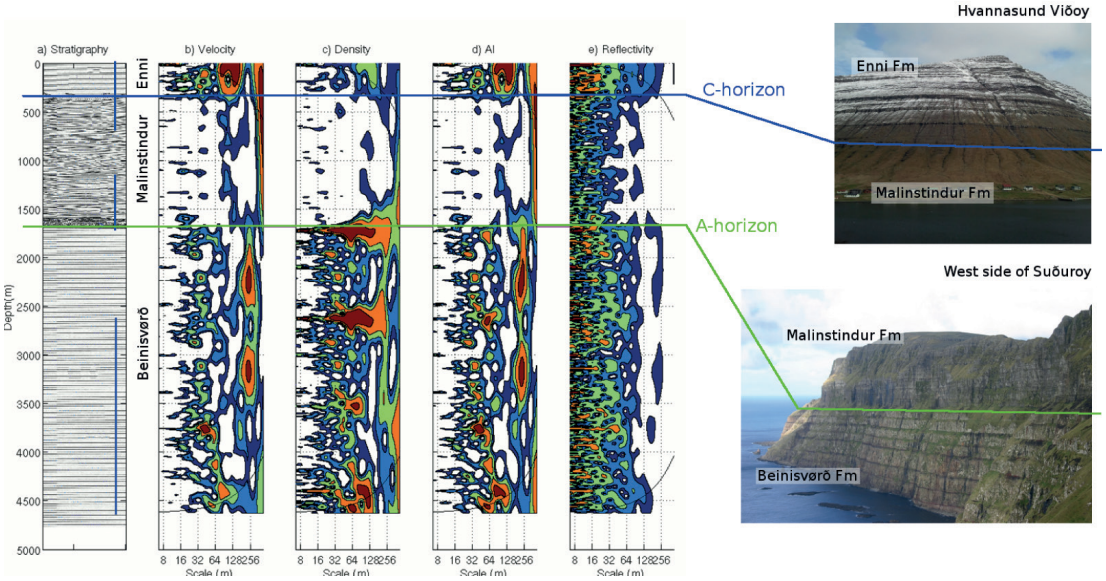

Figure 8
CWT analysis applied on the composite logs of the modelled stratigraphic sequence. Contour levels are logarithmic.

It is less clear to what degree the data are affected by interbed multiples. Comparison of fullwaveform modelling with the synthetic seismograms (primaries-only) shows that in the shallow section there is little difference between the two (Figure 9), but that at depth, below the strong reflection at ~0.6 s, there is a significant difference. Whether this difference originates in the wave-train tail generated in the shallow section or is related to interbed multiples occurring below 0.6 s is not clear.

VSP upgoing wavefield

In our earlier study (Petersen et al., 2006), our interpretation of the A-horizon was more qualitative. In the present paper we present a more quantitative interpretation of this horizon based on the VSP experiments at Glyvursnes and Vestmanna, as well as a further description of properties of the major basalt formations. The 660-m-deep Vestmanna well penetrates the top of a ~3-m-thick sedimentary bed at 555 m depth interpreted to be the A-horizon (Waagstein and Andersen, 2003) and previous studies have associated a high-amplitude reflection with this depth location (Bais et al., 2009).

The extraction of the upgoing wavefield for the Glyvursnes VSP is as follows:

1. Pick first onset for all traces
2. **Amplitude balancing of raw data:** Scale traces by balancing maximum amplitudes from analysis on first arrivals.
3. **Median filter to remove downgoing wave:** After Butterworth bandpass filtering at 14/16 – 150/180 Hz, apply a median filter along the first onset curve with a 7-point window. Then subtract the downgoing wavefield.
4. **Amplitude balancing of the separated upgoing event:** Reverse the scaling of the raw data and then correct for the combined spherical divergence, scattering, and

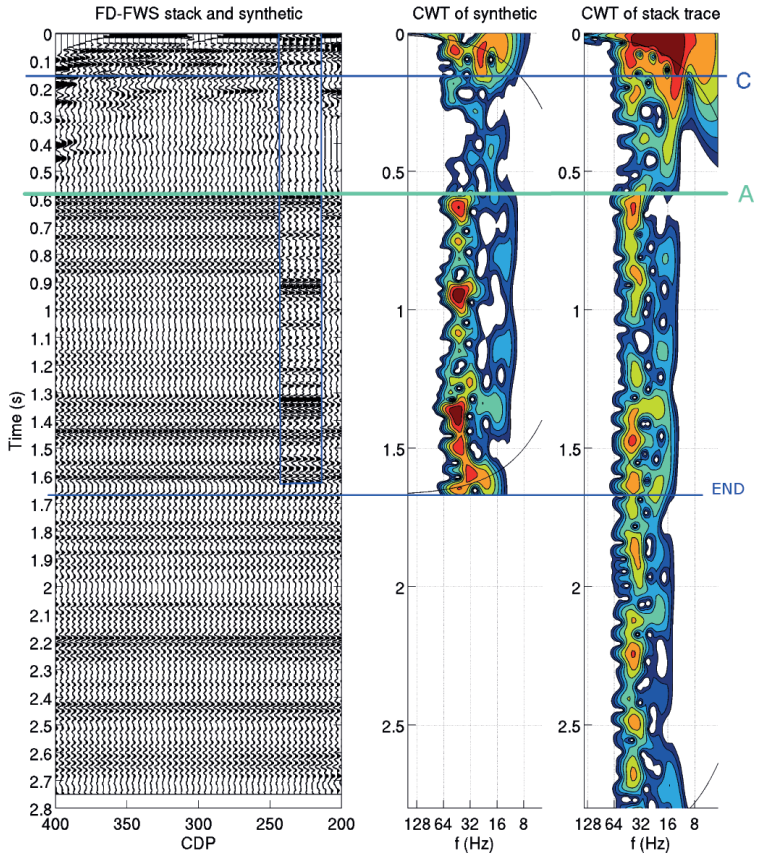

Figure 9
Left: The full-waveform synthetic stacked section. The synthetic seismogram, primaries-only, is spliced in (blue rectangle). Middle: CWT analysis of the synthetic seismogram, primaries-only. Right: CWT analysis of a trace from the stacked section. Horizontal lines show the boundaries between the Enni and Malinstindur Fms, marked C, and the Malinstindur and Beinisvørð Fms, marked A. The blue line „END" marks the base of the model. Below, a homogeneous section is added. No gain, other than correction for spherical divergence, has been applied to the full-waveform synthetic stack.

intrinsic attenuation. Analysis of the resulting maximum amplitudes of first arrivals shows that the combined attenuation correction is represented by travel time to the power 1.6.

5. **Median filter to enhance upgoing event:** Apply a median filter along the reversed curve with a 9-point window.

The extraction of the upgoing wavefield for the Vestmanna VSP was similar to that for the Glyvursnes VSP, expect for two parameters. First this regards step *4* above, where the amplitude analysis gave a power of 1.1 for Vestmanna. This indicates a significant difference in attenuation between Malinstindur and Enni Fms. Shaw et al. (2008) found very similar values for effective *Q* based on VSP data from the Vestmanna and Glyvursnes wells. However, they found significant numerical uncertainty in the Glyvursnes data. And besides, the two wells penetrate different sections with different proportions of the formations (Figure 1 and Table 1). So these two sets of results are not contradictory. Second, this regards step *5*, where a 21-point window was used for the median filter in order to enhance upgoing events.

A synthetic, primaries-only, trace, based on the velocity and density logs (Figures 6 and 7) and the wavelet extracted from the downgoing wavefield, was produced for each of the wells for the establishment of a log-tie with the upgoing wavefield and corridor stack. Zero time of the synthetics and

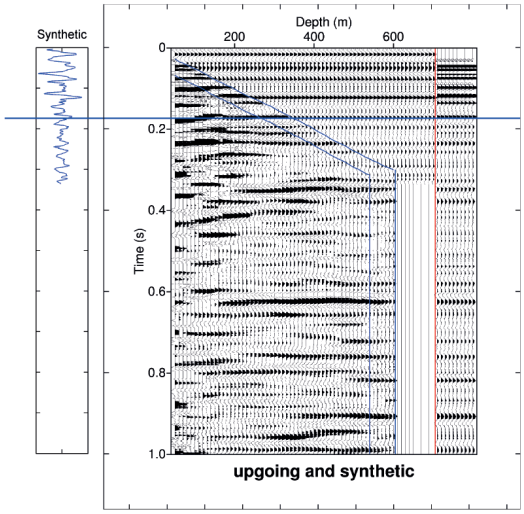

Figure 10
Glyvursnes VSP. To the left: the synthetic seismogram with log tie of the C-horizon (blue horizontal line). To the right: a combination of the VSP upgoing wavefield with the blue polygon marking the corridor used for the stack; the corridor stack (to the right of the red line), and the synthetic spliced in between the two.

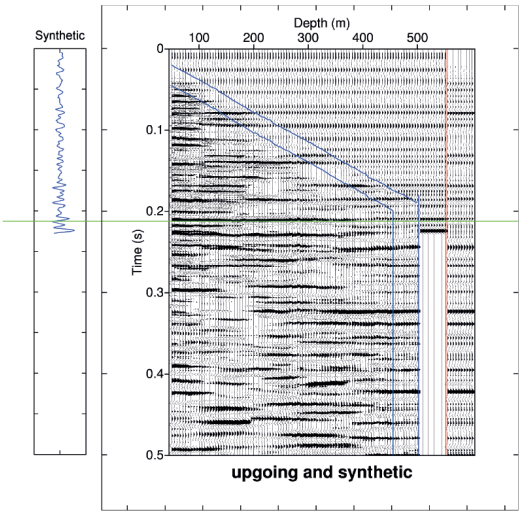

Figure 11
The Vestmanna VSP. To the left: the synthetic seismogram with log tie of the A-horizon (green horizontal line). To the right: a combination of the VSP upgoing wavefield with the blue polygon marking the corridor used for the stack; the corridor stack (to the right of the red line), and the synthetic spliced in between the two.

VSPs is set at the first upward zero crossing (Figures 10 and 11).

The experimental setup of the Vestmanna VSP resulted in a seismic signature quite different to that at Glyvursnes. While the centre frequency for the Glyvursnes VSP is ~30 Hz, it is ~60 Hz for the Vestmanna VSP. In order to compare the Vestmanna and Glyvursnes corridor stacks, the Vestmanna corridor stack was deconvolved with the Vestmanna wavelet and then convolved with the Glyvursnes wavelet, a *wavelet replacement* so to speak. The location of the sedimentary bed defining the A-horizon at Vestmanna is marked on the corridor stack (Figure 12). The upgoing wavefield ties to the surface seismic data and, based on this, the character of the reflection from the A-horizon is established on surface seismic data (Figure 13).

Conventional data

The seismic facies identified in the upgoing VSP wavefield and on surface seismic data at Glyvursnes are expected to show up also on conventional marine seismic data. However, inspection of several profiles of conventional marine seismic data in the vicinity of the Glyvursnes does not show similar facies. The appearance of the profiles makes it plausible to attribute the dissimilar seismic response to seabed multiples and scattered seismic energy.

However, our reprocessing of one profile gave a quite different stack. The OF94 A-A' profile has been reprocessed using stacking velocities generated from the results of refraction seismic modelling, and with the focus on removing seabed multiples and scattered energy by muting near offsets. This produces a distribution of seismic facies similar to that at Glyvursnes, i.e. a threefold depth

division with a high-amplitude section above ~0.3 s and below ~0.7 s and a low-amplitude section between ~0.3 and ~0.7 s (Figure 14). However, the near-offset mute starts at the first seabed multiple and continues downwards. As a consequence, the interpretation at depths of the first seabed multiple must be made with caution, since events at these depths could be artefacts of the processing.

A comparison with the initial 1995 processing of the same line clearly shows that the new processing strategy is more appropriate when it comes to imaging the shallow section. It must be born in mind, however, that the initial processing probably targeted the deeper section and the new processing reveals no more details here.

Based on the interpretation of surface seismic data at Glyvursnes (Figure 13) the A-horizon can be interpreted with confidence on the OF94 A-A' profile (Figure 16). The interpretation of the C-horizon is ambiguous but is expected to be at ~0.27 s based on a comparison of travel times between stacks (Figure 16; note the separate shifted time scale for OF94), i.e. assuming that the thickness of the Malinstindur Fm at the western end of the OF94 A-A' profile is similar to that inferred at Glyvursnes.

The depth to the C-horizon has also been estimated by extrapolation of the surface mapping of the C-horizon on land to the western end of the OF94 A-A' profile. The dip of the C-horizon at southern Eysturoy is 2.5° with a southwest-northeast strike parallel to the seismic profile (Berthelsen et al., 1984, p. 12). The shortest distance to the profile is ~7900 m, which gives a depth of ~345 m below sea level. Time conversion based on two layers (water/basalt) with an estimated basalt velocity of ~4500 m/s gives a two-way time to C-horizon of ~0,235 s, slightly shallower than estimated from the tie to the Glyvursnes data, implying a slight thickening of the Malinstindur Fm towards the western end of the OF94 A-A' line, ~19 km northeast of Glyvursnes.

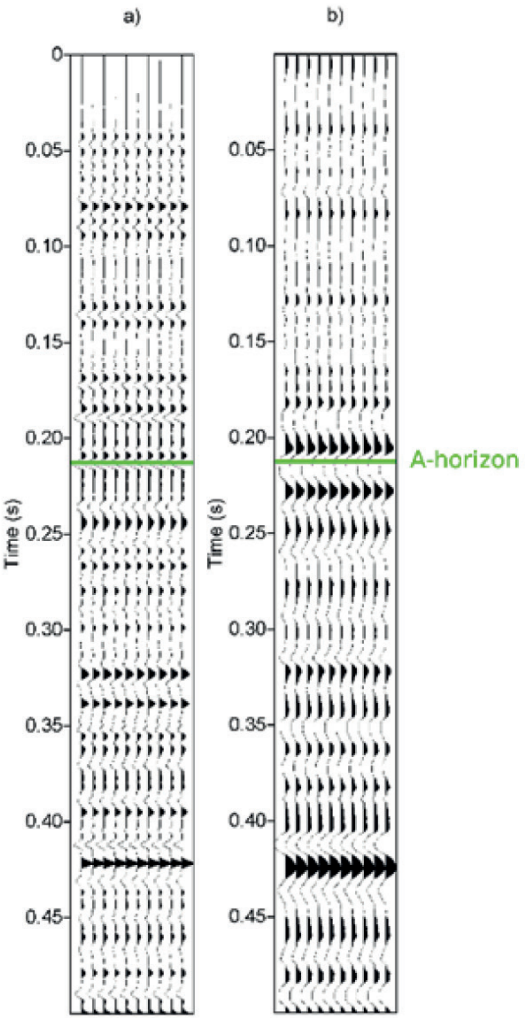

Figure 12
a) Vestmanna corridor stack. b) The same with wavelet replacement. Location of A-horizon is annotated.

TGS reprocessed data

A recent reprocessing of the OF94/OF95 data by TGS (OF94/95RE11) resulted in significant improvement relative to the initial 1995 processing. The data and processing were presented by TGS at the Faroe Island Exploration Conference 2012 (Woodburn et al., 2012). Two main steps in addition to standard processing were applied: *low frequency boost* and *multi-domain noise attenuation*.

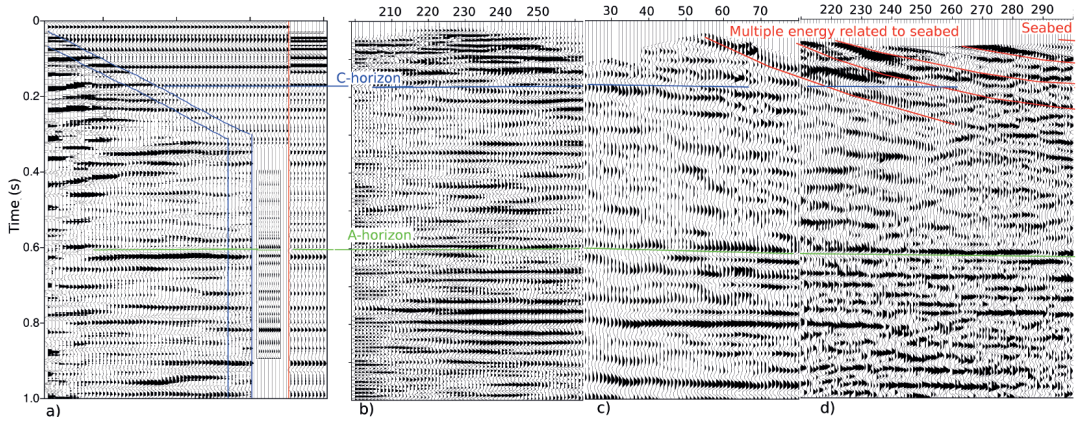

Figure 13

a) Glyvursnes VSP upgoing wavefield with correlated Vestmanna corridor stack and interpreted A-horizon inserted; b) Dynamite-geophone profile, SeiFaBa-2; c) Airgun-geophone profile, Inline-4; d) Airgun-streamer profile. A-horizon (green) interpreted on Vestmanna VSP and C-horizon (blue) interpreted on Glyvursnes VSP. CDP numbers are plotted above profiles. See Figure 3 for location.

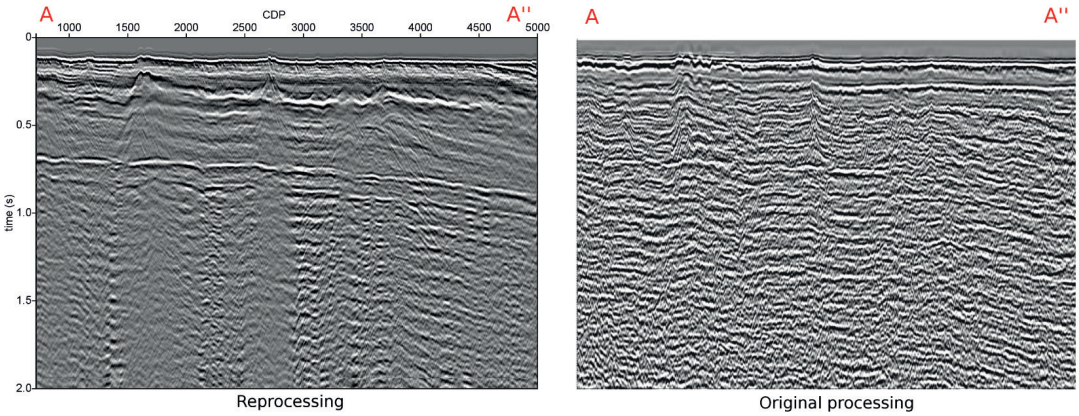

Figure 14

Left: Section of the OF94 A-A' reprocessing. Right: Initial 1995 processing. See location on Figure 15.

In relation to our work it is of special interest that the TGS processed section, although more dominated by low frequencies, show a similar clear image of the A-horizon (Figure 17). The A-horizon can be mapped over the full length of the OF94 A-A' profile (Figure 18) and on all intersecting profiles (e.g. Figure 19). However, the difference between the Malinstindur Fm above the A-horizon and the Beinisvørð Fm below it (Figure 17) is much less pronounced than after our processing (Figure 14, left) probably due to effects of the low-frequency boost and *the multi-domain noise attenuation.*

In fact, inspection of all of the TGS-reprocessed profiles shows that the A-horizon can be picked on most of the profiles surrounding the Faroes. This provides a means for future mapping of this horizon all over the Faroese continental shelf.

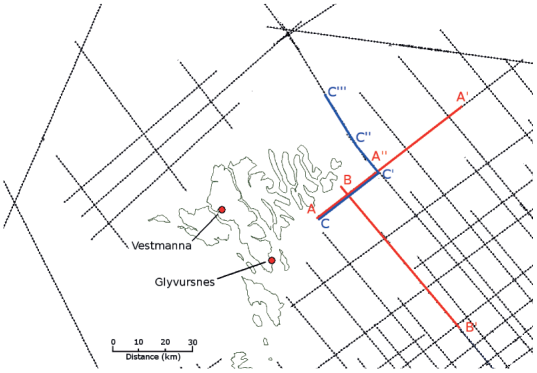

Figure 15
OF94 profile locations. Southwest endpoint of OF94 A-A'', A, is located ~19 km northeast of Glyvursnes.

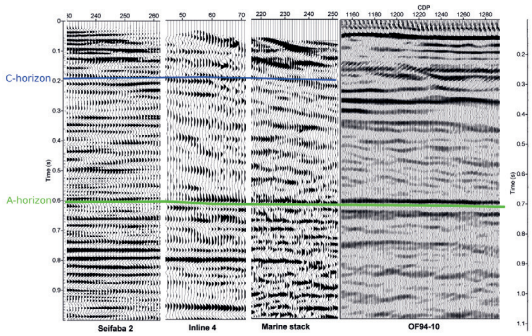

Figure 16
Sections from the composite tie from Figure 13. The interpreted A-horizon and C-horizon are annotated. Timescale to left is for Seifaba-2, Inline-4 and marine stack whilst timescale to right is for OF94 A-A' section.

The composite profile OF94 C-C' shows that the A-horizon dips gently towards the northeast but significantly (~5°) to the southeast (Figure 20).

The mapping of the A-horizon could, for example, be used to estimate the thickness of the Malinstindur Fm offshore close to the Faroe Islands. Extrapolation of the C-horizon from surface mapping onto the southwest end of the OF94 A-A' profile gives an approximate thickness of ~1100 m for the Malinstindur Fm, or slightly greater than the thickness at Glyvursnes (Petersen et al., 2006), while at the northwest end of the OF94 C'-C'' profile there is a significant discordance between the C-horizon (as extrapolated from surface mapping) and the A-horizon. This may suggest a significant thinning of the Malinstindur Fm to the northeast of the Faroes to ~650 m. It must, however, be noted that further to the northeast, crossing profiles indicate that the Malinstindur Fm indeed retains a significant thickness.

Discussion

The data from the Glyvursnes area demonstrate clearly that seismic energy is transmitted through thick basalt complexes. This is for instance demonstrated by the prominent reflection related to the A-horizon at ~1.4 km depth. The main reason that the A-horizon is so distinct at Glyvursnes is due to the transparency of the overlying ~1 km thick Malinstindur Fm. Although the individual basalt flows have the common velocity structure of a high-velocity massive core and a low-velocity porous crust, the difference in the individual seismic facies, of the basalt formations, relates to the configuration of flow thicknesses and interbedded sediments characterising the respective formations.

Velocity variations from well-log analyses establish that there is a difference between the property distribution of the Malinstindur Fm on the one hand and the distributions of the overlying Enni and underlying Beinisvørð Fms on the other hand. The Malinstindur Fm consists mainly of thin flow lobes forming lava flows of compound-braided facies. Volcaniclastic beds are very thin or absent in most of the Malinstindur Fm but increase in number and thickness in the upper part. The overlying Enni Fm consists of a mixture of simple and compound flows with tabular-classic and compound-braided facies architectures respectively, and with a further increase in number and thickness of volcaniclastic beds. The underlying Beinisvørð Fm consists mainly of thick simple

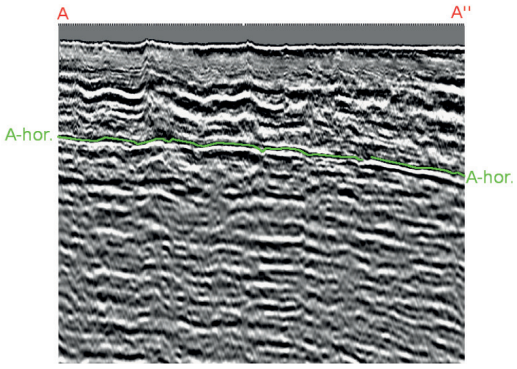

Figure 17
TGS reprocessing of same section as in Figure 14. The interpreted A-horizon is shown in green. For comparison with the left-hand part of Figure 14, notice that neither time migration nor phase correction has been applied to that profile, while time migration and zero-phase correction are applied to the TGS data here. See Figure 15 for location. Courtesy of TGS.

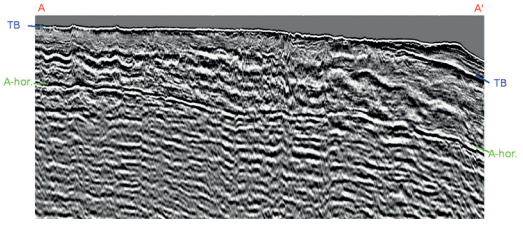

Figure 18
OF94 A-A' profile. The positions of the A-horizon and top-basalt (TB) are shown at the left and right endpoints of the profile. Courtesy of TGS.

flows, presumably tabular lava flows. Volcaniclastics are common in the Beinisvørð Fm (Hald and Waagstein, 1984; Waagstein and Andersen, 2003; Boldreel, 2006). The differences can thus be summarized as „compound flows and minor sedimentary beds" for the Malinstindur and „thick simple flows and sedimentary beds" for the overlying Enni and underlying Beinisvørð Fms, although compound flows are rather common also in the Enni Fm.

The differences in seismic facies are related to velocity contrasts between massive core, porous crust, and sediments. It appears that sedimentary beds are essential for producing the high-amplitude facies of the Enni and the Beinisvørð Fms, although our study does not show whether a combination of simple-flows-only can generate similar high-amplitude facies.

It is clear, however, from full-waveform modelling that the seismic facies are strongly related to the 1D property distributions of the formations, since modelling based on velocity logs expanded laterally as flat layers, i.e. without applying generalized lateral properties of flows like topography of flow-tops and lateral variations in flow thicknesses, reproduces the seismic facies of the three formations closely.

Our log tie to the A-horizon is based on the Vestmanna well, which penetrates the A-horizon at 555 m depth (Waagstein and Andersen, 2003). The tie to the interpreted A-horizon at Glyvursnes is based on the seismic facies of the basalt formations and on the similarity of the seismic signatures of the A-horizon reflection at Vestmanna and the inferred A-horizon reflection at Glyvursnes. It can be questioned if it is valid to extrapolate the seismic signature and seismic facies to 28 km distance. However, inspection of data shows that the seismic signature of the A-horizon can be traced over most of the Faroese continental shelf at distances of hundreds of km. It should be noted that the synthetic seismic signature of the A-horizon at Vestmanna is modelled on a ~3 m thick sedimentary succession directly between the top Beinisvørð flow and base Malinstindur flow; whereas the surface mapping to the south and northwest on the Faroe Islands describes the sedimentary succession to be ~10 m thick overlain by a tuff-agglomerate zone along a presumed northwest-trending eruption fissure (Rasmussen and Noe-Nygaard, 1969).

The fact that the A-horizon can be mapped over most of the Faroese continental shelf makes it a potential marker that can be used to deduce the

Cenozoic evolution on the Faroese continental shelf in more detail (cf. Andersen et al., 2002). While the thickness of the Malinstindur Fm presented in this paper is to some degree speculative due to the long distance of extrapolation of the C-horizon, the mapping of the A-horizon can be used to estimate the total basalt thickness above the A-horizon, i.e. the total volume of syn-breakup lava erupted during the final continental breakup between the Faroes and Greenland (Larsen et al., 1999).

Initially Smythe (1983) suggested that the Beinisvørð Fm extended furthest to the southeast, with the margins of the Malinstindur and Enni Fms progressively 'stepping back' towards the Faroes. However, geochemical and bio-stratigraphic analysis of a large number of dredge hauls on the outer Faroese continental shelf by Waagstein and Heilmann-Clausen (1995) as well as seismic interpretations led to Ritchie et al. (1999) suggesting a reversed structure of the basalt distribution, such that it is the Malinstindur and Enni Fms that reach furthest offshore. Ellis et al. (2002) have a description consistent with that of Ritchie et al. based mainly on seismic interpretation. Contrary to this, Passey and Bell (2007), based on the emplacement mechanisms of compound lava flows, suggest that the compound lava flows of the Malinstindur and Enni Fms occur only locally to the Faroe Islands and may not extend offshore for any significant distance; and Passey and Hitchen (2011) extend this assessment to a distribution similar to that of Smythe (1983), with the Beinisvørð Fm reaching furthest offshore. Recent work by Schofield and Jolley (2013) suggests locally fed lava sequences equivalent to the Malinstindur and Enni Fms to the east and southeast of the Faroes area.

In this context the A-horizon presented in this paper can be used as a significant marker in the interpretation of seismic profiles, and thus to map the distribution of pre- and syn-breakup basalts. The few profiles presented in this paper establish that to the northeast and to the east the syn-breakup basalts extend to a significant distance offshore, on the order of hundreds of km. The profiles presented here offer the prospect of confident interpretation of syn-breakup basalts on the Faroese continental shelf.

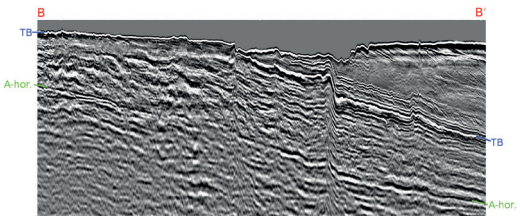

Figure 19
OF94 B-B' profile. At the endpoints of the profile the A-horizon and top-basalt (TB) are annotated. See Figure 15 for location. Courtesy of TGS.

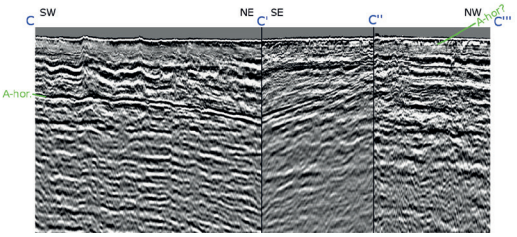

Figure 20
Composite profile OF94 C-C'-C''-C'''. Top-basalt is at seabed. The A-horizon is annotated, but notice that the crossing at seabed is only suggested due to low data quality close to seabed. See Figure 15 for location. Courtesy of TGS.

Conclusions

We have shown that the seismic response of the Malinstindur Fm differs essentially from the mutually similar responses of the Enni and Beinisvørð Fms, and that this difference can be directly related to the Malinstindur Fm being composed of compound flows with few, very thin, volcaniclastic beds.

We have tied the A-horizon as logged in the Vestmanna well to its presumed reflection event on our SeiFaBa stacked seismic data. But we suspect that the A-horizon seismic response will be

influenced far more by the contrast in properties of the overlying and underlying Malinstindur and Beinisvørð Fms than by those of the very thin sediments of the A-horizon.

Processing of seismic data using seismic velocities generated by modelling of known geological structure of the basalts produce imaging of the basalt succession with the potential for interpretation of stratigraphic horizons. Notably, as a result of our work, the A-horizon may be used as a marker horizon. We have traced it throughout significant parts of the Faroes area on reprocessed OF94/95 data.

Our distinction between subaerial basalt formations characterised by different lava morphology is a tool for the interpretation of seismic facies of volcanic sequences.

And finally, our processing shows that when focusing on intrabasalt seismic response, a simple processing sequence might be beneficial.

Acknowledgements

This paper is based on data acquired in connection with the SeiFaBa project 2002 – 2006. We also would like to thank TGS for allowing us to include examples of their reprocessing of the OF94/95RE11 data in our paper. Finally we wish to thank Regin Waagstein for his critical review with several suggestions for improving the final manuscript.

References

Andersen, M. S., Sørensen, A. B., Boldreel, L. O., and Nielsen, T. 2002. Cenozoic evolution of the Faroe Platform: comparing denudation and deposition. *In:* A. G. Doré, J. A. Cartwright, M. S. Stoker, J. D. Turner and N. White (Eds.) *Exhumation of the North Atlantic Margin: Timing, Mechanisms and Implications for Petroleum Exploration*. Geological Society, London, 196, Special Publications: 291-311.

Backus, G. E. 1962. Long-wave elastic anisotropy produced by horizontal layering. *Journal of Geophysical Research, 67*/11: 4427-4440.

Bais, G., White, R. S., Worthington, M. H., Andersen, M. S., and The SeiFaBa Group. 2009. *Seismic properties of Faroe basalts from borehole and surface data*. Paper presented at the Faroe Island Exploration Conference: Proceedings of the 2nd Conference, Tórshavn, Faroe Islands.

Berthelsen, O., Noe-Nygaard, A., and Rasmussen, J. 1984. *The Deep drilling project 1980-1981 in the Faeroe Islands*: Annales Sociatatis Scientiarum Færoensis.

Boldreel, L. O. 2006. Wire-line log-based stratigraphy of flood basalts from the Lopra-1/1A well, Faroe Islands. *In:* J. A. Chalmers and R. Waagstein (Eds.) *Scientific results from the deepened Lopra-1 borehole, Faroe Islands*, Geological Survey of Denmark and Greenland bulletin, 9: 7-22.

Chalmers, J. A., and Waagstein, R. (Eds.). 2006. *Scientific results from the deepened Lopra-1 borehole, Faroe Islands*. Geological Survey of Denmark and Greenland bulletin 9, 156 pp.

Christie, P. A. F., Gollifer, I. D., and Cowper, D. 2006. Borehole seismic studies of a volcanic succesion from the Lopra-1/1A borehole in the Faroe Islands, northern North Atlantic. *In:* J. A. Chalmers and R. Waagstein (Eds.) *Scientific results from the deepened Lopra-1 borehole, Faroe Islands*. Geological Survey of Denmark and Greenland Bulletin, 9: 23–40.

Ellis, D., Bell, B. R., Jolley, D. W., and O'Callaghan, M. 2002. The stratigraphy, environment of eruption and age of the Faroes Lava Group, NE Atlantic Ocean. *In:* D. W. Jolley and B. R. Bell (Eds.) *The North Atlantic Igneous Province: Stratigarphy, Tectonic, Volcanic and Magmatic Processes*. The Geological Society, London, Special Publications, 197: 253-269.

Falk, J. 1996. Ela2d. *University of Hamburg. http://www.agg.dkrz.de/soft/.*

Fruehn, J., Fliedner, M. M., and White, R. S. 2001. Integrated wide-angle and near-vertical subbasalt study using large-aperture seismic data from the Faeroe-Shetland region. *Geophysics, 66*/5: 1340–1348.

Gallagher, J. W., and Dromgoole, P. W. 2008. Seeing below the basalt - offshore Faroes.

Geophysical Prospecting, 56/1: 33-45.

Hald, N., and Waagstein, R. 1984. Lithology and chemistry of a 2-km sequence of Lower Tertiary tholeiitic lavas drilled on Suðuroy, Faeroe Islands (Lopra-1). *In:* O. Berthelsen, A. Noe-Nygaard and J. Rasmussen (Eds.) *The deep drilling project 1980-1981 in the Faeroe Islands*. Føroya Fróðskaparfelag, Tórshavn: 15-38.

Japsen, P., Andersen, C., Andersen, H. L., Andersen, M. S., Boldreel, L. O., Mayko, G., Mohammed, N. G., Pedersen, J. M., Petersen, U. K., Rasmussen, R., Shaw, F., Springer, N., Waagstein, R., White, R. S., and Worthington, M. 2005. Preliminary results from investigations of seismic and petrophysical properties of Faroes basalts in the SeiFaBa project. *In:* A. G. Doré and B. A. Vining (Eds.) *Petroleum Geology: North-West Europe and Global Perspectives—Proceedings of the 6th Petroleum Geology Conference*. Geological Society, London: 1461-1470.

Japsen, P., Andersen, M. S., Boldreel, L. O., Waagstein, R., White, R. S., Worthington, M., and The SeiFaBa Group 2006. *Seismic and petrophysical properties of Faroes basalts (the SeiFaBa project Final Report)*. Geological Survey of Denmark and Greenland Report 29.

Kiørboe, L., and Petersen, S. A. 1995. Seismic investigation of the Faeroe basalts and their substratum. *In:* R. A. Scrutton, G. B. Shimmield and A. W. Tudhope (Eds.) *The Tectonics, Sedimentation and Palaeoceanography of the North Atlantic Region*. Geological Society, London, Special Publication, 90: 111–122.

Larsen, L. M., Waagstein, R., Pedersen, A. K., and Storey, M. 1999. Trans-Atlantic correlation of the Palaeogene volcanic successions in the Faeroe Islands and East Greenland. *Journal of the Geological Society, 156*: 1081-1095.

Maresh, J., White, R. S., Hobbs, R. W., and Smallwood, J. R. 2006. Seismic attenuation of Atlantic margin basalts: Observations and modeling. *Geophysics, 71*/6: B211–B221.

Nielsen, P. H., Stefánsson, V., and Tulinius, H. 1984. Geophysical logs from Lopra-1 and Vestmanna-1. *In:* O. Berthelsen, A. Noe-Nygaard and J. Rasmussen (Eds.) *The deep drilling project 1980-1981 in the Faeroe Islands*. Føroya Fróðskaparfelag, Tórshavn: 115 - 135.

Passey, S. R., and Bell, B. R. 2007. Morphologies and emplacement mechanisms of the lava flows of the Faroe Islands Basalt Group, Faroe Islands, NE Atlantic Ocean. *Bulletin of Volcanology, 70*: 139-156.

Passey, S. R., and Hitchen, K. 2011. Cenozoic (igneous). *In:* J. D. Ritchie, H. Ziska, H. Johnson and D. Evans (Eds.) *Geology of the Faroe–Shetland Basin and adjacent areas*. British Geological Survey and Jarðfeingi.

Passey, S. R., and Jolley, D. W. 2009. A revised lithostratigraphic nomenclature for the Palaeogene Faroe Islands Basalt Group, NE Atlantic Ocean. *Earth and Environmental Science Transactions of the Royal Society of Edinburgh, 99*: 127-158.

Petersen, U. K. 2014. *Propagation and scattering of reflection seismic waves in a basalt succesion*. (Thesis PhD), University of The Faroe Islands, Tórshavn. (NVDRit 2014:01)

Petersen, U. K., Andersen, M. S., White, R. S., and the SeiFaBa Group. 2006. Seismic imaging of basalts at Glyvursnes, Faroe Islands: hunting for future exploration methods in basalt covered areas. *First Break, 24*/March.

Petersen, U. K., Brown, R. J., and Andersen, M. S. 2013. P-wave velocity distribution in basalt flows of the Enni Formation in the Faroe Islands from refraction seismic analysis. *Geophysical Prospecting, 61*: 168-186.

Planke, S., Alvestad, E., and Eldholm, O. 1999. Seismic characteristics of basaltic extrusive and intrusive rocks. *The Leading Edge, 18*/3: 342-348.

Planke, S., Symonds, P. A., Alvestad, E., and Skogseid, J. 2000. Seismic volcanostratigraphy of large-volume basaltic extrusive complexes on rifted margins. *Journal of Geophysical Research-Solid Earth, 105*/B8: 19335–19351.

Rasmussen, J., and Noe-Nygaard, A. 1969.

Beskrivelse til Geologiske kort over Færøerne. København: Geological Survey of Denmark.

Rasmussen, J., and Noe-Nygaard, A. 1970. *Geology of the Faeroe Islands*. København: C. A. Reitzels Forlag.

Richardson, K. R., White, R. S., England, R. W., and Fruehn, J. 1999. Crustal structure east of the Faroe Islands: mapping sub-basalt sediments using wide-angle seismic data. *Petroleum Geoscience, 5*/2: 161–172.

Ritchie, J. D., Gatliff, R. W., and Richards, P. C. 1999. Early Tertiary magmatism in the offshore NW UK margin and surrounds. *In:* A. J. Fleet and S. A. R. Boldy (Eds.) *Petroleum Geology of Northwest Europe: Proceedings of the 5th Conference*. Geological Society, London: 573-584.

Schofield, N., and Jolley, D. W. 2013. Development of intra-basaltic lava-field drainage systems within the Faroe-Shetland Basin. *Petroleum Geoscience, 19*/3: 273-288.

Shaw, F. 2006. *Seismic properties of Faroe Island basalts*. (DPhil), University of Oxford, Oxford.

Shaw, F., Worthington, M. H., White, R. S., Andersen, M. S., Petersen, U. K., and The SeiFaBa Group. 2008. Seismic attenuation in Faroe Islands basalts. *Geophysical Prospecting, 56*/1: 5-20.

Smythe, D. K. 1983. Faeroe-Shetland Escarpment and continental margin north of the Faroes. *In:* M. H. P. Bott, S. Saxov, M. Talwani and J. Theide (Eds.) *Structure and Development of the Greenland-Scotland Ridge: new Methods and Concepts*. Plenum Press, New York: 109-119.

Sørensen, A. B. 2003. Cenozoic basin development and stratigraphy of the Faroes area. *Petroleum Geoscience, 9*: 189-207.

Spitzer, R., White, R. S., and Christie, P. A. F. 2008. Seismic characterization of basalt flows from the Faroes margin and the Faroe-Shetland basin. *Geophysical Prospecting, 56*/1: 21–31.

Waagstein, R. 1988. Structure, composition and age of the Faeroe Basalt plateau. *In:* A. C. Morton and L. M. Parson (Eds.) *Early Tertiary Volcanism and the opening of the NE Atlantic*. Geological Society London, Special Publication, 39: 225-238.

Waagstein, R., and Andersen, C. 2003. *Well completion report: Glyvursnes-1 and Vestmanna-1, Faroe Islands*. Geological survey of Denmark and Greenland Report 99.

Waagstein, R., and Hald, N. 1984. Structure and petrographyof a 660 m lava sequence from the Vestmanna-1 drill hole, lower and middle basalt series, Faeroe Islands. *In:* O. Berthelsen, A. Noe-Nygaard and J. Rasmussen (Eds.) *The deep drilling project 1980-1981 in the Faeroe Islands*. Føroya Fróðskaparfelag, Tórshavn: 39 - 70.

Waagstein, R., and Heilmann-Clausen. 1995. Petrography and biostratigraphy of Paleogene volcaniclastic sediments dredged from the Faeroes shelf. *In:* R. A. Scrutton, M. S. Stoker, G. B. Shimmield and A. W. Tudhope (Eds.) *The Tectonics, Sedimentation and Palaeoceanography of the North Atlantic Region*. Geological Society, London, Special Publication, 90: 179-197.

White, R. S., Smallwood, J. R., Fliedner, M. M., Boslaugh, B., Maresh, J., and Fruehn, J. 2003. Imaging and regional distribution of basalt flows in the Faeroe-Shetland Basin. *Geophysical Prospecting, 51*/3: 215–231.

Woodburn, N., Hardwick, A., and Travis, T. 2012. *Enhanced low frequency signal processing for sub-basalt imaging on the Faroese Continental Shelf*. Paper presented at the Faroe Islands Exploration Conference 2012, Tórshavn, Faroe Islands.

Ziolkowski, A., Hanssen, P., Gatliff, R., Jakubowicz, H., Dobson, A., Hampson, G., Li, X. Y., and Liu, E. R. 2003. Use of low frequencies for sub-basalt imaging. *Geophysical Prospecting, 51*/3: 169-182.